AD-A052 435 SYSTEMS TECHNOLOGY INC MOUNTAIN VIEW CALIF F/G 1/2
SIMULATION AND ANALYSIS OF WIND SHEAR HAZARD.(U)
DEC 77 J M LEHMAN, R K HEFFLEY, W F CLEMENT NAS2-8889
UNCLASSIFIED STI-TR-1063-3 FAA/RD-78/7 NL

1 OF 2
ADA
052435

Report No.FAA-RD-78-7

(12)

SIMULATION AND ANALYSIS OF WIND SHEAR HAZARD

John M. Lehman Robert K. Heffley Warren F. Clement

SYSTEMS TECHNOLOGY, INC.
2672 Bayshore-Frontage Road
Mountain View, CA 94043

December 1977

FINAL REPORT

Prepared for

U.S. DEPARTMENT OF TRANSPORTATION
FEDERAL AVIATION ADMINISTRATION
Systems Research & Development Service
Washington, D.C. 20590

NOTICE

This document is disseminated under the sponsorship of the Department of Transportation in the interest of information exchange. The United States Government assumes no liability for its contents or use thereof.

(18) FAA/RD (19) 78/7

Technical Report Documentation Page

1. Report No.	2. Government Accession No.	3. Recipient's Catalog No.
FAA-RD-78-7		

4. Title and Subtitle
(16) SIMULATION AND ANALYSIS OF WIND SHEAR HAZARD.

5. Report Date
(11) Dec[redacted]77

6. Performing Organization Code

(12) 157p.

8. Performing Organization Report No.
(14) STI-TR-1063-3

7. Author(s)
(10) John M. Lehman, Robert K. Heffley
Warren F. Clement

9. Performing Organization Name and Address *
Systems Technology, Inc.
2672 Bayshore-Frontage Road
Mountain View, CA 94043

10. Work Unit No. (TRAIS)

11. Contract or Grant No.
(15) NAS2-8889

13. Type of Report and Period Covered
(9) Final Report.
Jun[redacted]76 - Oct[redacted]977,

12. Sponsoring Agency Name and Address
U.S. Department of Transportation
Federal Aviation Administration
Systems Research and Development Service
Washington, D.C. 20590

14. Sponsoring Agency Code

15. Supplementary Notes

* Under contract to: National Aeronautics and Space Administration
Ames Research Center
Moffett Field, CA 94035

16. Abstract

The results of an unmanned simulation and an analysis of wind shear hazard are presented. The study involved the application of mathematical models of four diverse passenger aircraft types ranging from a small STOL commuter aircraft to a jumbo jet and of pilot models appropriate to each flight situation. The hazard to each aircraft was evaluated for both approach and takeoff in three severe wind shear profiles. The effects of varying operational techniques and propulsion system features were investigated and explained with the aid of a simplified linear analysis. No direct correspondence was found between wind shear hazard and aircraft size or type, per se. Instead, the main factors affecting sensitivity to wind shear were shown to be airspeed, flight path regulation, and airspeed regulation. Also, the shear dependency as modeled in the simulation was found to be important.

17. Key Words		18. Distribution Statement
Wind Shear	STOL Aircraft	Document is available to the U.S. public through the National Technical Information Service, Springfield, Virginia 22161.
Hazard Definition	Commercial Aircraft	
Landing Simulation		
Mathematical Pilot Model		

19. Security Classif. (of this report)	20. Security Classif. (of this page)	21. No. of Pages	22. Price
UNCLASSIFIED	UNCLASSIFIED	164	

Form DOT F 1700.7 (8-72) Reproduction of completed page authorized

409 136 JOB

METRIC CONVERSION FACTORS

Approximate Conversions to Metric Measures

Symbol	When You Know	Multiply by	To Find	Symbol
		LENGTH		
in	inches	*2.5	centimeters	cm
ft	feet	30	centimeters	cm
yd	yards	0.9	meters	m
mi	miles	1.6	kilometers	km
		AREA		
in^2	square inches	6.5	square centimeters	cm^2
ft^2	square feet	0.09	square meters	m^2
yd^2	square yards	0.8	square meters	m^2
mi^2	square miles	2.6	square kilometers	km^2
	acres	0.4	hectares	ha
		MASS (weight)		
oz	ounces	28	grams	g
lb	pounds	0.45	kilograms	kg
	short tons (2000 lb)	0.9	tonnes	t
		VOLUME		
tsp	teaspoons	5	milliliters	ml
Tbsp	tablespoons	15	milliliters	ml
fl oz	fluid ounces	30	milliliters	ml
c	cups	0.24	liters	l
pt	pints	0.47	liters	l
qt	quarts	0.95	liters	l
gal	gallons	3.8	liters	l
ft^3	cubic feet	0.03	cubic meters	m^3
yd^3	cubic yards	0.76	cubic meters	m^3
		TEMPERATURE (exact)		
°F	Fahrenheit temperature	5/9 (after subtracting 32)	Celsius temperature	°C

*1 in = 2.54 (exactly). For other exact conversions and more detailed tables, see NBS Misc. Publ. 286, Units of Weights and Measures, Price $2.25, SD Catalog No. C13.10:286.

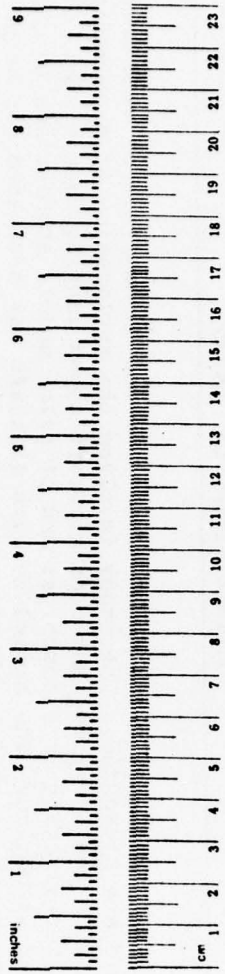

Approximate Conversions from Metric Measures

Symbol	When You Know	Multiply by	To Find	Symbol
		LENGTH		
mm	millimeters	0.04	inches	in
cm	centimeters	0.4	inches	in
m	meters	3.3	feet	ft
m	meters	1.1	yards	yd
km	kilometers	0.6	miles	mi
		AREA		
cm^2	square centimeters	0.16	square inches	in^2
m^2	square meters	1.2	square yards	yd^2
km^2	square kilometers	0.4	square miles	mi^2
ha	hectares (10,000 m^2)	2.5	acres	
		MASS (weight)		
g	grams	0.035	ounces	oz
kg	kilograms	2.2	pounds	lb
t	tonnes (1000 kg)	1.1	short tons	
		VOLUME		
ml	milliliters	0.03	fluid ounces	fl oz
l	liters	2.1	pints	pt
l	liters	1.06	quarts	qt
l	liters	0.26	gallons	gal
m^3	cubic meters	35	cubic feet	ft^3
m^3	cubic meters	1.3	cubic yards	yd^3
		TEMPERATURE (exact)		
°C	Celsius temperature	9/5 (then add 32)	Fahrenheit temperature	°F

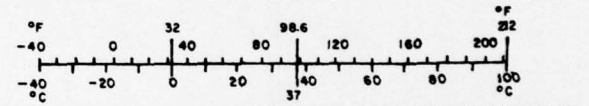

FOREWORD

The research reported here was done under NASA Contract NAS2-8889 as part of a joint NASA/FAA program. The NASA Contract Technical Monitor was John Stewart and the FAA Project Manager was Barry C. Scott. The Systems Technology, Inc., Project Engineer was initially Robert L. Stapleford, then Robert K. Heffley. The work was accomplished in the period between June 1976 and October 1977.

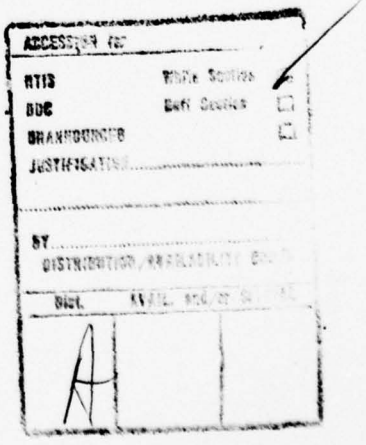

TABLE OF CONTENTS

LIST OF FIGURES

LIST OF TABLES

LIST OF SYMBOLS

cg	Vehicle center of gravity
C_D	Non-dimensional drag coefficient
C_L	Non-dimensional lift coefficient
C_{L_α}	$\partial C_L/\partial\alpha$ lift curve slope (1/rad or 1/deg)
C_m	Non-dimensional pitching moment coefficient
EPR	Engine pressure ratio (dimensionless)
EPR_c	Commanded engine pressure ratio
EPR_{ic}	Initial trimmed engine pressure ratio
g	Gravitational acceleration (ft/sec^2)
G_H	Crossfeed upper threshold limit (deg)
G_L	Crossfeed lower threshold limit (deg)
GPIP	Glide path intercept point
h	Altitude (ft)
K_d	Pilot model glide slope displacement gain in flight path compensation (deg/ft or percent/ft)
K_D	Pilot model displacement gain in Y_θ (dimensionless)
K_I	Pilot model integral (trim) gain in Y_θ (sec)
K_R	Pilot model rate gain in Y_θ (sec)
K_u	Pilot's airspeed gain compensation (1/sec or deg/kt)
K_{δ_T}	Pilot's acceleration-to-throttle command scaling factor (EPR/kt/sec)
K_{ϵ_c}	STOL pilot model glide slope-to-throttle command scaling factor (dimensionless)
K_θ	Pilot model gain in Y_θ: $K_D + K_I$ (dimensionless)

K_{θ_T}	Crossfeed gain (-32.2 ft/sec^2-deg)
m	Aircraft mass
R	Aircraft range from glide slope transmitter (ft)
R_o	"Critical" aircraft range (= 5280 ft)
s	Laplace transform operator
S	Reference wing area (ft^2)
T_D	Pilot model glide slope loop lead time constant (sec)
T_{eff}	Effective neuromuscular and transport lag in Y_θ (sec)
T_E	Effective lag time constant of engine thrust response to throttle (sec)
T_{L_1}	Larger pilot model lead time constant in Y_θ: $K_D T_2/(K_D + K_I)$ (sec)
T_{L_θ}	Smaller pilot model lead time constant in Y_θ: K_R/K_D (sec)
T_u	Closed-loop time constant of airspeed control mode: $\doteq 1/\omega_{c_u}$ (sec)
T_2	Pilot model lag time constant in Y_θ (sec)
u_a	Aircraft airspeed (kt)
u_{aic}	Initial aircraft trim airspeed (kt)
$\dot{u}_c$	Pilot's airspeed commanded acceleration (ft/sec^2)
u_g	Longitudinal or horizontal gust velocity (ft/sec)
$\dot{u}_g$	$\partial u_g/\partial t$, longitudinal or horizontal gust acceleration (ft/sec^2) or shear rate
U_H	Pilot's airspeed upper threshold (kt)
U_L	Pilot's airspeed lower threshold (kt)
U_o, V_a, V	Aircraft trimmed airspeed (kt or ft/sec)
V_y	Airspeed for maximum rate of climb (kt)
w_g	Normal or vertical gust velocity (ft/sec)
W	Aircraft gross weight (lb)
X	Longitudinal force
X_u	$\frac{1}{m}\frac{\partial X}{\partial u}$ (1/sec)

X_w	$\frac{1}{m}\frac{\partial X}{\partial w}$ (1/sec)
X_α	$U_o X_w$ (ft/sec^2)
X_{δ_T}	$\frac{1}{m}\frac{\partial X}{\partial \delta_T}$ (ft/sec^2-rad)
Y_θ	Pilot model pitch attitude compensation (dimensionless)
Z	Normal force
Z_u	$\frac{1}{m}\frac{\partial Z}{\partial u}$ (1/sec)
Z_w	$\frac{1}{m}\frac{\partial Z}{\partial w}$ (1/sec)
Z_α	$U_o Z_w$ (ft/sec^2)
Z_{δ_T}	$\frac{1}{m}\frac{\partial Z}{\partial \delta_T}$ (ft/sec^2-rad)
$1/T_{\theta_1}$	Low frequency zero of θ/δ_e numerator (1/sec)
$1/T_{\theta_2}$	High frequency zero of θ/δ_e numerator (1/sec)
α	Angle of attack (rad or deg)
γ	Flight path angle (rad or deg)
δ_e	Elevator deflection (rad or deg)
δ_{e_c}	Commanded elevator deflection (deg)
$\delta_{T_{max}}$	Maximum throttle limit (EPR or percent)
$\delta_{T_{min}}$	Minimum throttle limit (EPR or percent)
Δh	Aircraft height (altitude) change (ft)
Δh_{max}	Maximum altitude excursion below the nominal flight path (ft)
$\Delta\theta$	Aircraft attitude change (deg)
ϵ_{GS}	Glide slope error (rad)
ζ_d	Closed-loop damping ratio of height control mode (dimensionless)
θ	Aircraft pitch attitude (rad or deg)

θ_{ic}	Initial aircraft trim attitude (deg)
θ_{max}	Upper limit on aircraft pitch attitude (deg)
θ_{min}	Lower limit on aircraft pitch attitude (deg)
ρ	Air density (slugs/ft^3)
ω_{c_d}	Glide slope loop crossover frequency (rad/sec)
ω_{c_u}	Airspeed loop crossover frequency ($\doteq 1/T_u$) (rad/sec)
ω_d	Closed-loop natural frequency of height control mode (rad/sec)

SECTION I

INTRODUCTION

A. BACKGROUND

The current high interest in the effect of wind shears on aircraft has prompted several studies (Refs. 1, 2, and 3) in an attempt to discover and quantify these effects.

Wind shear encounters can produce catastrophic results by introduction of conditions which exceed the capability of the pilot/vehicle combination. Recent examples have included large commercial jet transports in both takeoff and landing flight phases.

The purpose of this study was to explore the hazard imposed by wind shear on different classes of passenger aircraft and to consider the effects of varying operational techniques and design parameters.

Two techniques were used to study the problem. First, an unmanned simulation was conducted to obtain flight profiles in wind shear conditions. Second, an analysis was performed of the key features of the aircraft, the pilot's actions, and the shears themselves. This second step involved appropriate linearization of pilot/vehicle mathematical models.

The unmanned simulation was an important aspect of the program. The mathematical model which took the role of the real pilot was, in some respects, superior. If we assume the mathematical model to be valid, it eliminated pilot variability in run-to-run comparisons, it prevented learning of specific shears, and it was less expensive than using real pilots.

The crucial question is, of course, how valid is the mathematical model pilot? This is discussed in Section II, where the mathematical pilot model is justified as being representative of a large class of human pilots. The pilot model was not designed to duplicate exactly a specific pilot, but instead, to approximate "typical" human pilot responses. To help to insure

that this was the case, the pilot model used in this study was checked against and "fine-tuned" with data involving human pilots. Additionally, studies were made of the effect of variations in the pilot model parameters to check for any overly sensitive aspects.

This study specifically involved a comparison of

- Four specific aircraft
  - (i) A twin engine light jet transport (referred to as the "light transport")
  - (ii) A wide-bodied jumbo jet transport (referred to as the "jumbo")
  - (iii) A light twin engine jet (referred to as the "business jet"), and
  - (iv) A STOL commuter aircraft (referred to as the "STOL commuter")
- Three specific wind shears
  - (i) A nighttime stable boundary layer shear
  - (ii) A frontal passage shear
  - (iii) A thunderstorm cold air outflow shear
- Both approach and takeoff cases
- Variation in key aircraft performance and controllability parameters and all pilot model parameters.

Only the longitudinal degrees of freedom were simulated since it was believed that these were most critical in determining shear hazard and aircraft safety.

B. REPORT ORGANIZATION

The report is organized into the following five sections and 3 appendices. Section II contains a description of the pilot model, the aircraft models, the shear models, and the simulation procedure. Section III contains a description of the linear analysis methods and procedures. Section IV

contains the results from the approach cases. Section V contains the results from the takeoff cases. Section VI presents conclusions and recommendations based on this simulation. The appendices contain background information concerning the pilot, aircraft, and shear models used in the study.

SECTION II

SIMULATION DESCRIPTION

The simulation conducted in this program was routine except for one important feature — the pilot consisted of a mathematical model. In the following pages the rules used to define the model pilot's control strategy are defined and discussed. This is followed by descriptions of the airplane model, the wind shear profiles, and the simulation procedure.

A. PILOT MODEL

Three distinct forms of the pilot model were used. These were:

(i) A Conventional Takeoff and Landing (CTOL) form for use with the light transport, jumbo, and business jet aircraft in the approach flight phase,

(ii) A Short Takeoff and Landing (STOL) form for use with the STOL commuter aircraft in the approach flight phase, and

(iii) A takeoff form used for all aircraft in the takeoff flight phase.

In the following subsections each of the three pilot model forms will be described in general; however, the pitch attitude loop which is common to all three forms will be described only in connection with the CTOL pilot model. Appendix A presents the details of the CTOL pilot model. Each subsection also discusses how the pilot model was fine-tuned to match better the results from piloted simulations.

1. The CTOL Pilot Model

An overall block diagram of the CTOL pilot model is given in Fig. II-1, the key features of which include:

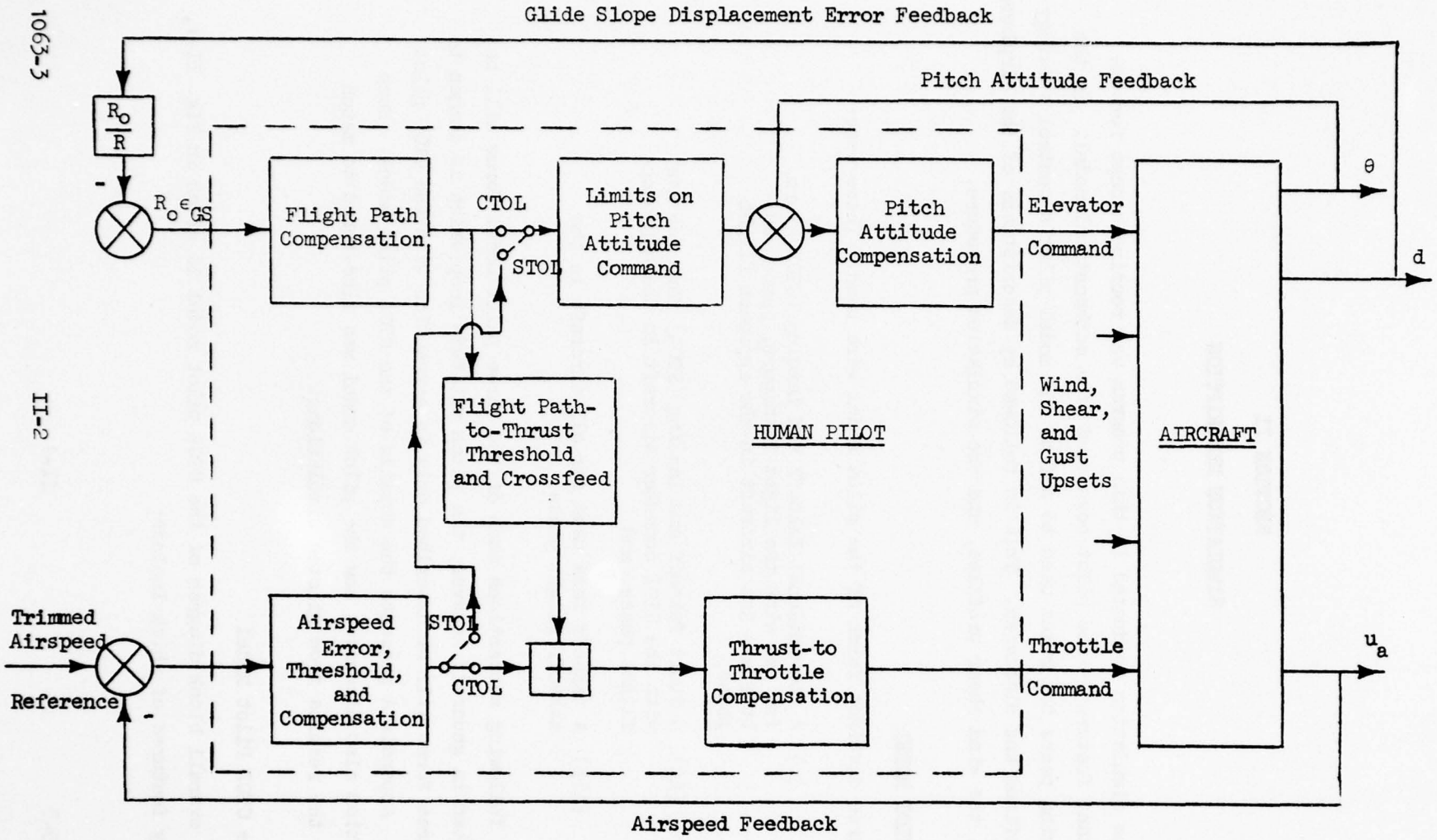

Figure II-1. Block Diagram of Pilot Model in the Context of Manual Approach Control Illustrating Differences in Technique for CTOL and STOL

- Regulation of pitch attitude with elevator command via control column,
- Regulation of glide slope error with a commanded pitch attitude,
- Regulation of airspeed error with throttle with a 5 kt threshold of indifference, and
- Crossfeed from pitch command to throttle for large attitude commands.

These four key features are based on the quasi-linear pilot models for compensatory multiloop systems described in Ref. 4. The first two features have been extensively analyzed in Refs. 5-8 in the absence of significant throttle activity. Validating measurements of pilot describing functions representing the first two features have been reported in Refs. 9-11, again, in the absence of significant throttle activity.

The basis for the two latter features are not nearly as well documented or validated in the literature on the subject of airspeed regulation and control for CTOL, e.g., Ref. 5. The pilot normally inhibits throttle activity for the purpose of airspeed regulation with a $\pm$ 5 kt threshold of indifference to disturbance-induced airspeed variations about the desired trimmed airspeed. If the aircraft heave damping-airspeed product ($U_o Z_w$) is moderate to large (e.g., as in the cases of CTOL/jet transports) then only small transient angle of attack changes need be provided by pitching control in order to regulate glide slope deviation. As a result of the small angle of attack changes, the drag fluctuates only slightly and the accompanying airspeed variations are usually small. In contradistinction, if $U_o Z_w$ is small, the aircraft can experience great variations in speed. The pilot, however, will limit his commanded variations in angle of attack (via limits on commanded pitch attitude) and will cross-feed throttle commands as a function of his desired flight path angle correction in order to assist his otherwise compensatory airspeed regulation via throttle (Ref. 5).

The downside pitch attitude limit, θ_{min}, in the pilot model (Fig. II-1 and Fig. A-1) was set at a value which would give the pilot model a sufficient amount of nose down capability but would not allow it to generate

unrealistically large negative θ values. Since the shear profiles used primarily drive the aircraft low and slow and result in a positive $\Delta\theta$, θ_{min} was not a critical parameter and, indeed, was never exceeded during the runs. However, the upper pitch attitude limit, θ_{max}, was felt to be an important parameter since hitting this limit caused the pilot model to apply and hold full power, i.e., to essentially abort the approach and initiate a go-around.

It should be noted that the function of the θ_{max} limit was to prohibit the pilot model from placing the aircraft in a pitch attitude that was unrealistically large, i.e., a pitch attitude that a human pilot would be reluctant to use. The reasoning behind having the pilot model apply and hold full power if θ_{max} was exceeded was that the pilot, having used all of his available pitch authority, would then use the only other control available, thrust, in an attempt to extricate himself from the situation.

Several methods of setting θ_{max} were considered. The method finally used was to set θ_{max} equal to the steady state pitch attitude which would be achieved at the designated approach speed with maximum thrust.

The CTOL pilot model was fine-tuned by comparing its responses for the light transport with two manned simulator approaches until the responses of the pilot model compared favorably prior to and throughout the recovery (past the peak airspeed and altitude deviations) from the wind shear upset. The timing and magnitudes of the responses of the aircraft controlled by the pilot model were acceptably similar to those from the manned cases.

2. The STOL Pilot Model

The STOL pilot model (Fig. II-2) is conceptually similar to the CTOL version (Fig. II-1) except that the STOL version incorporates

- A glide slope error to throttle feedback without a threshold
- An airspeed error to pitch attitude feedback with a 5 kt threshold
- No crossfeeds.

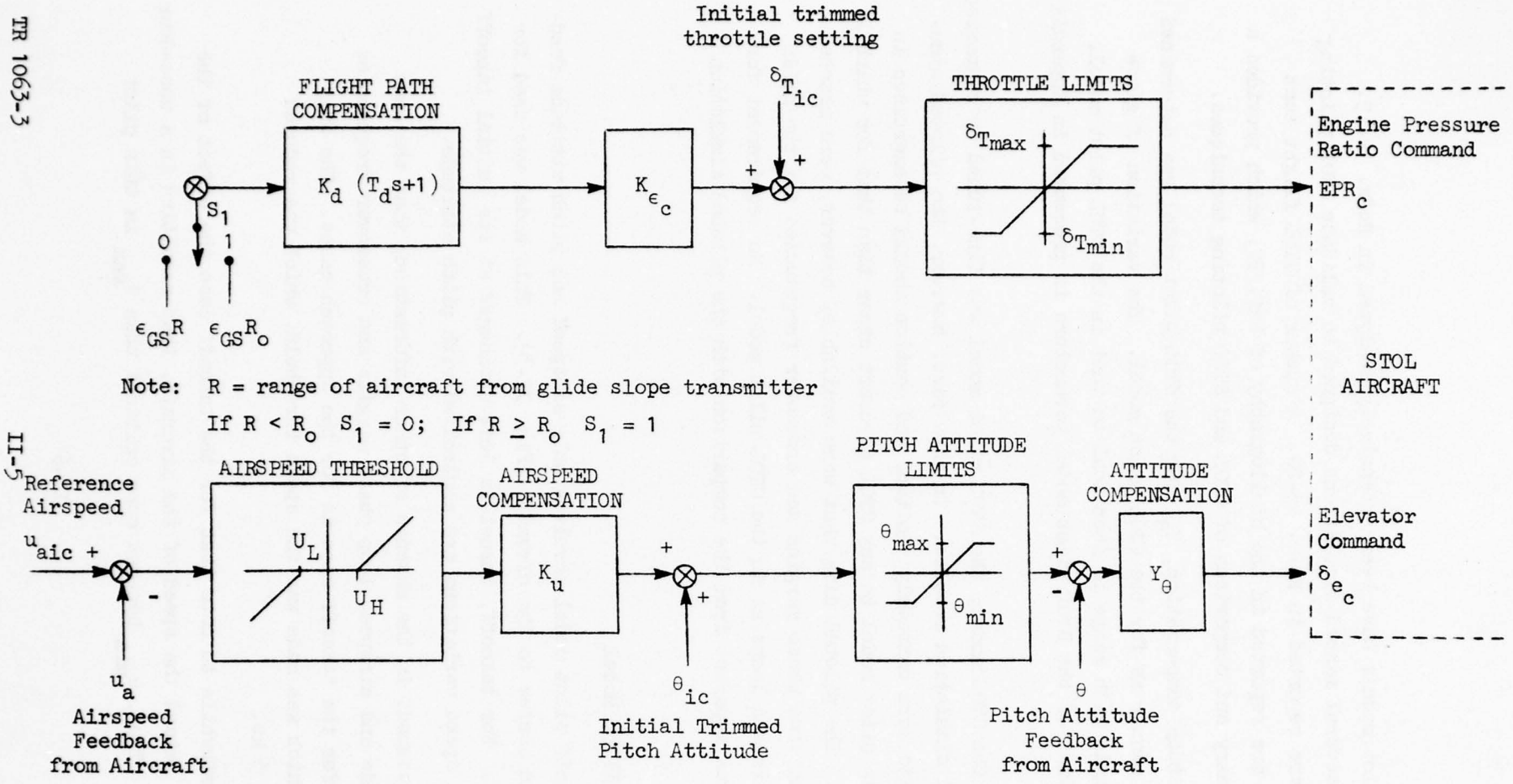

Figure II-2. STOL Pilot Model

STOL pilot models have been extensively analyzed in Refs. 12-15. Results of several manned simulations designed to validate STOL piloting techniques are reported in Refs. 15-20. A number of STOL flight test validations are reported in the bibliography of Ref. 20, which provides a concise summary and comparison of CTOL and STOL piloting techniques.

The attitude compensation, Y_θ, for the STOL pilot model was determined in the same manner as for the CTOL pilot model. The variation of glide slope loop gain with range is identical to that in the CTOL pilot model. A detailed list of the STOL pilot model parameters is presented in Appendix A, Table A-1.

As with the CTOL model, the STOL pilot model was fine-tuned by comparison with piloted simulation results. In this case, however, the piloted simulation results were extremely limited, and caution should be exercised in applying this pilot model to any STOL aircraft other than that for which it was adapted. The piloted data that were available, however, were matched utilizing the same phase margins and crossover frequencies for the glide slope and airspeed loops as in the CTOL pilot model. No requirement for crossfeeds was apparent from the comparison with the piloted simulation results.

3. Takeoff Pilot Model

The takeoff pilot model involves only airspeed and pitch attitude feedback loops in series to the elevator (Fig. II-3). This model was used for all aircraft. For takeoff, thrust is left unchanged at its initial takeoff setting, and speed variations are controlled with pitch attitude.

It was assumed, in the absence of other information, that the same pitch attitude and airspeed loop phase margins and crossover frequencies would apply for the takeoff case as for the approach cases. The only alteration which was made was the speed threshold, which was reduced from 5 kt to 3 kt.

It is worthwhile to note that for the takeoff case the effect of the shears is to retard the speed of the aircraft, thus resulting in a nose-down pitch input. Thus, θ_{min} becomes more critical than θ_{max} in this pilot

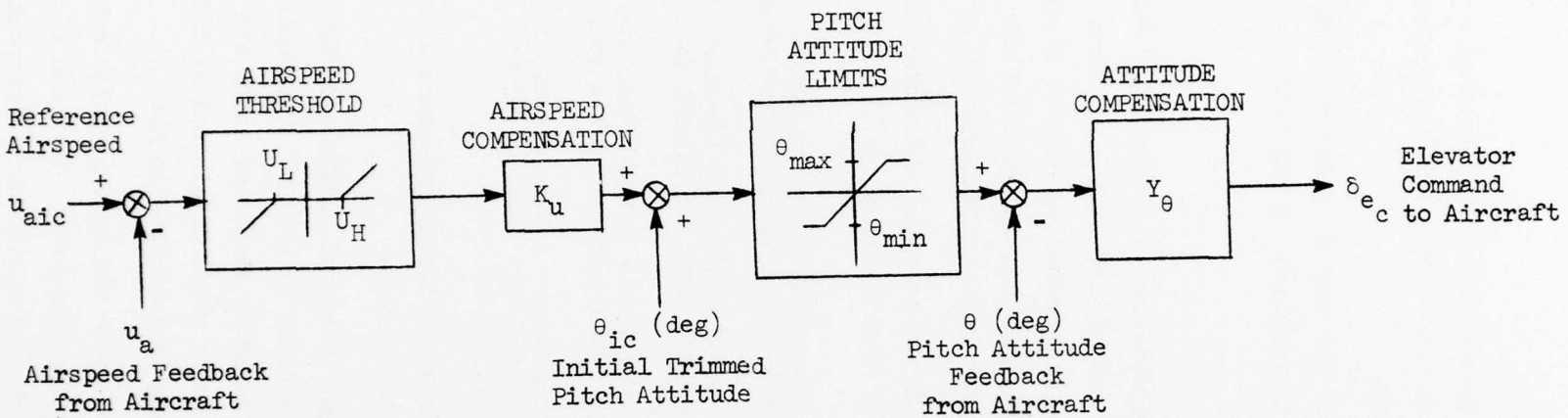

Note: No height control loop

Figure II-3. Takeoff Pilot Model (All Aircraft)

model. No rational justification for choosing a θ_{min} other than pilot reluctance to lower the nose further was suggested, and a θ_{min} of -10 deg was chosen arbitrarily.

A detailed list of the takeoff pilot model parameters for the cases and aircraft tested is presented in Appendix A, Table A-2.

B. AIRCRAFT MODELS

To facilitate the modeling of a variety of different aircraft for this simulation, a simple generic aircraft model form was devised. The simplicity of this model allowed rapid modeling of each aircraft and decreased the time required to check each aircraft, yet retained the important aerodynamic, control system, and propulsion characteristics of each individual aircraft.

Four aircraft, each representing a distinct class of commercial transports, were simulated. The aircraft are described briefly below:

- The light transport — A twin-engine, low-wing, light jet transport with a takeoff gross weight of 110,000 lb.
- The jumbo — A four-engine, low-wing, jumbo jet with a takeoff gross weight of 733,000 lb.
- The business jet — A twin-engine, light, swept-wing, business jet with a takeoff gross weight of 12,500 lb.
- The STOL commuter — A twin-engine, turbo prop, commuter airline STOL aircraft with a takeoff gross weight of 11,579 lb.

Each model has been used previously in manned simulator experiments at NASA Ames Research Center (ARC).

The jumbo and light transport models were developed by their manufacturer based on the data from Refs. 21 and 22. The business jet model was originally developed by STI for a vortex encounter study and is described in Ref. 23. Finally, the STOL commuter model originated at NASA ARC for guidance and navigation research and is described in Ref. 24.

Each of the above models utilizes a table look-up scheme for basic aerodynamic and propulsion features. Lift and pitching moment are described to a point beyond stall, and engine thrust response varies appropriately

with thrust level. Control system descriptions include servo lags and limits on surface rate and displacement.

Basic aircraft design features are summarized in Table II-1 and in the general arrangement drawings in Fig. II-4. Stability derivatives and transfer functions are listed in Appendix B using the notation defined in Ref. 25.

C. SHEAR MODELS

Three different wind shear models were provided by NASA for use in this study. They are identified as:

- Boundary layer shear
- Logan shear
- Kennedy shear.

Each is defined in terms of a "look-up"* table of wind velocity (horizontal and vertical components) versus altitude, although a range dependency was also contrived for the latter two shears. (The dependency aspect is discussed fully at the beginning of Section IV.) The three shears are summarized in Fig. II-5.

One shear represents a nighttime stable boundary layer shear corresponding to a low level temperature inversion overlayed by fairly strong winds immediately above the inversion. The simulated velocity profile is given in Table II-2.

The Logan shear represents a shear caused by a frontal passage. It consists of a 33 kt tailwind at 1600 ft which changes gradually to a 14 kt headwind at 200 ft then rapidly to a 4 kt tailwind at 20 ft. The altitude and velocity breakpoints are given in Table II-3. The critical aspect of this shear is the decreasing headwind below 200 ft. Nominally, the altitude dependent version of this shear should cause greater aircraft problems than

---

* A "look-up" table implies the use of an interpolation algorithm in the computer simulation.

TABLE II-1

SUMMARY OF AIRCRAFT MODEL CHARACTERISTICS

	JUMBO	LIGHT TRANSPORT	BUSINESS JET	STOL COMMUTER
Wing Area (ft^2)	5,500	980	231.77	420
Wing Aspect Ratio	6.96	8.83	5.46	10.06
Landing				
Weight (lb)	570,000	95,000	12,500	11,000
Flap Deflection (deg)	30	40	40	40
$C_{L_{max}}$	2.44	3.0	1.61	2.75
Takeoff				
Weight (lb)	733,000	110,000	12,500	11,579
Flap Deflection (deg)	10	5	20	20
$C_{L_{max}}$	1.86	2.0	1.48	2.53

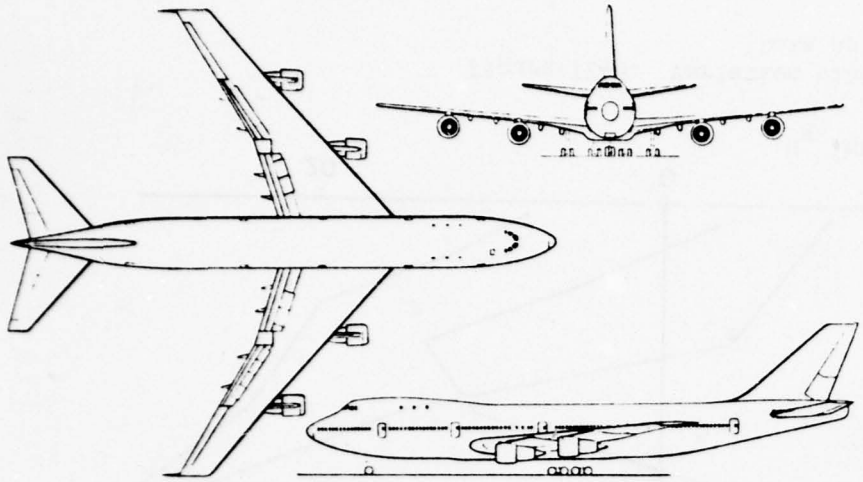

JUMBO

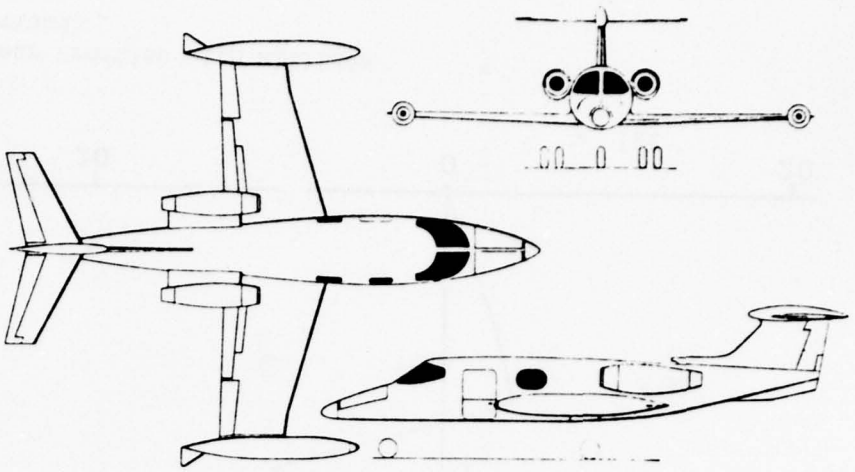

BUSINESS JET

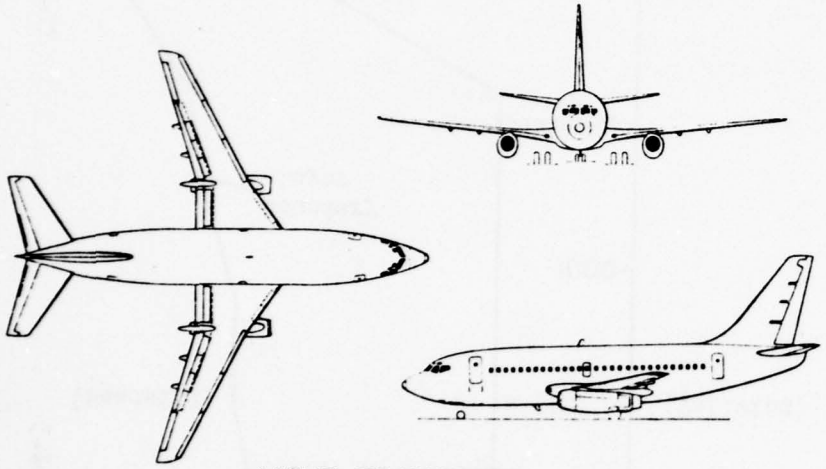

LIGHT TRANSPORT

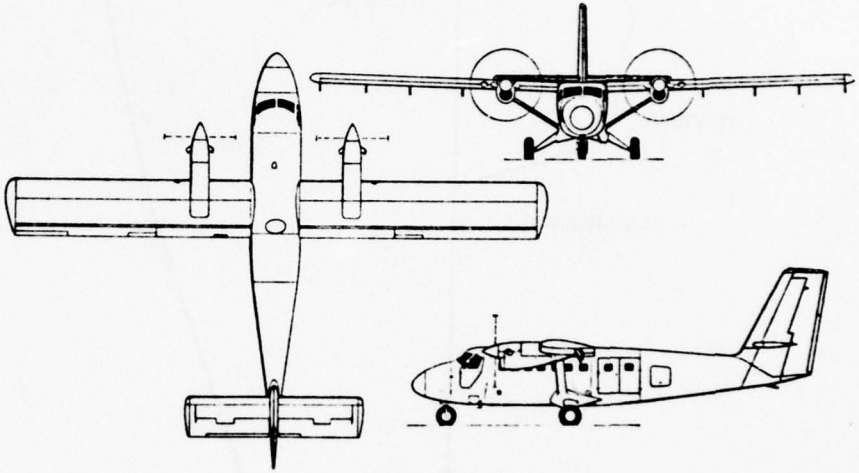

STOL COMMUTER

Figure II-4. General Arrangements of Aircraft Studied

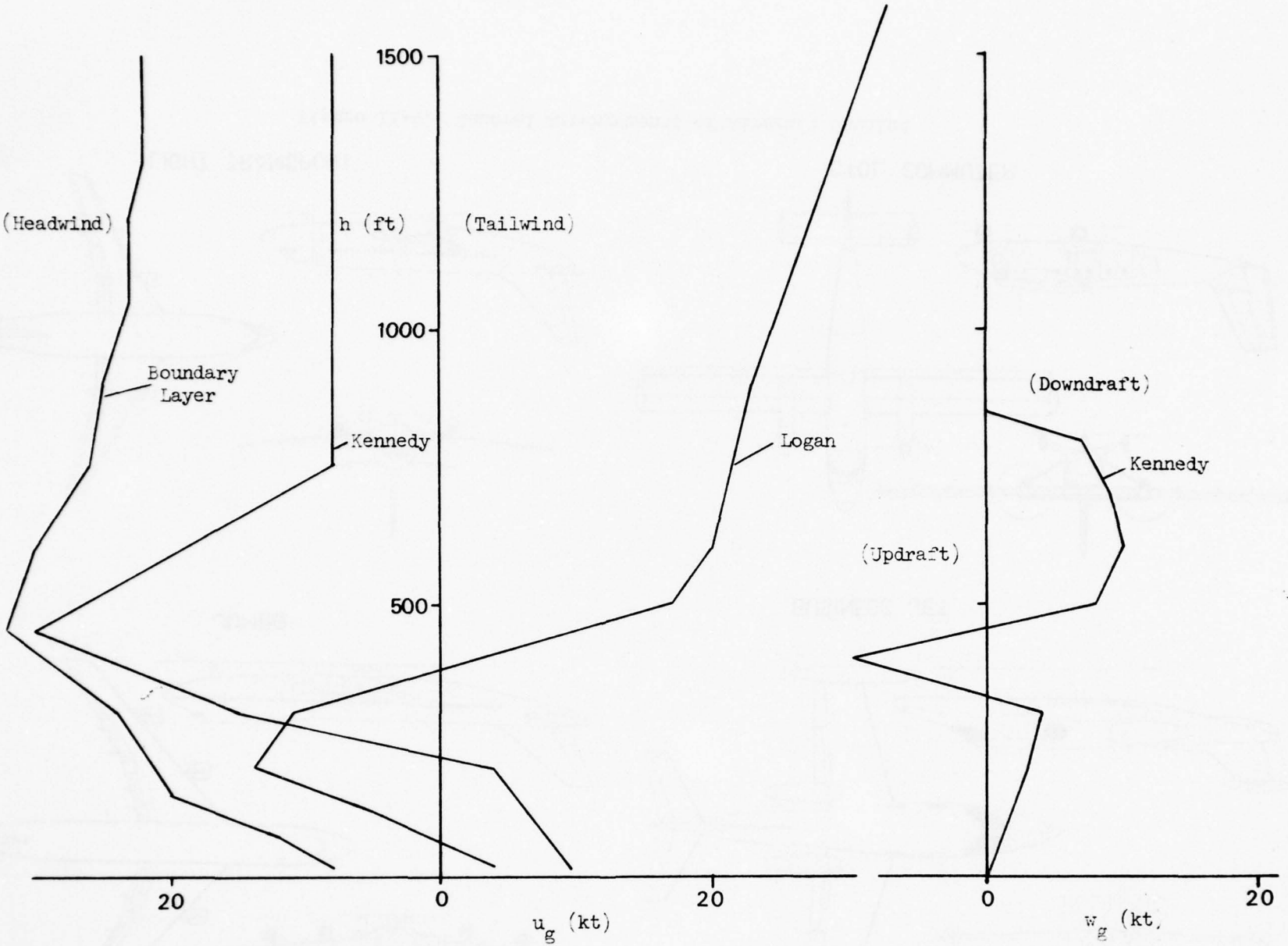

Figure II-5. Variation Wind Shear Profiles with Altitude
(Data as Provided)

TABLE II-2

BOUNDARY LAYER SHEAR

ALTITUDE, h (ft)	HORIZONTAL WIND VELOCITY, u_g* (kt)
1500	-22
1300	-22
1200	-23
1050	-23
900	-25
750	-26
600	-30
450	-32
300	-24
150	-20
75	-12
20	-8

* A positive u_g corresponds to a tailwind.
The vertical gust component, $w_g \equiv 0$.

TABLE II-3

LOGAN SHEAR

ALTITUDE, h (ft)	HORIZONTAL WIND VELOCITY, u_g* (kt)
1600	33
1100	26
900	23
800	22
700	21
600	20
500	17
400	2
300	-11
200	-14
120	-5
20	4
0	4

* A positive u_g corresponds to a tailwind. The vertical gust component, $w_g = 0$.

the range-dependent version, since the shear causes the aircraft to go low and slow which, for an altitude-dependent shear, causes further decrease in headwind.

The Kennedy shear is the most complex of the shears with both horizontal and vertical components. The shear is representative of the conditions due to a thunderstorm cold air outflow and was derived from an analysis of the conditions encountered by Eastern Airlines Flight 066 near John F. Kennedy Airport in June 1975. The wind profiles are shown in Table II-4. Initially the aircraft encounters a mild headwind. As the aircraft descends, it encounters a simultaneous increase in headwind and a downdraft (near 800 ft). Near 450 ft the headwind starts to decrease and the downdraft changes briefly to an updraft. The winds become particularly adverse around 300 ft where there is a downdraft and a very rapidly decreasing headwind.

The Logan and Kennedy shears were investigated from both range-dependent and altitude-dependent points of view for reasons we shall discuss at the beginning of Section IV. For the altitude-dependent shears, the wind velocity look-up table was entered with the vehicle altitude, h_A, while for the range-dependent shears, the look-up table was entered with the altitude of the glide slope, h_{GS}, corresponding to the vehicle's ground range from the glide path intercept point (GPIP) sketched in Fig. II-6. The differences between the range- and altitude-dependent versions of a shear are small if the aircraft stays close to the glide slope, but can be significant if large deviations from the glide slope occur. The mechanization of the shears indicated above was used for both the approach and takeoff flight phases. For the takeoff the nominal flight path angle used to compute the wind velocities for range-dependent shears was 3 deg. For the altitude-dependent shears the height of the aircraft's cg was used.

Since the aircraft normally had a takeoff climb gradient greater than 3 deg, the altitude-dependent cases usually caused more rapid changes in the wind velocity than did the range-dependent cases. However, if the shears caused the climb gradient to be less than 3 deg, the altitude-dependent cases would cause less rapid wind changes than the range-dependent cases.

TABLE II-4

KENNEDY SHEAR

Horizontal Component

ALTITUDE, h (ft)	WIND VELOCITY, u_g* (kt)
1500	8
750	8
450	30
300	15
200	-4
0	-10

Vertical Component

ALTITUDE, h (ft)	WIND VELOCITY, w_g* (kt)
850	0
800	7
700	9
600	10
500	8
400	-10
300	4
250	3.5
200	3
0	0

* A positive u_g corresponds to a tailwind and a positive w_g, a downdraft.

D. SIMULATION PROCEDURE

The standard procedure used to initiate a simulated approach run was to position the aircraft at an altitude of 1600 ft on speed and on glide slope. For the CTOL aircraft a 3 deg glide slope was used. The STOL commuter aircraft was nominally flown on a 6 deg glide slope, but some runs also were made with a 3 deg glide slope. The aircraft, initially trimmed, was then allowed to fly, under the control of the pilot model, down the glide slope and through the shear. The run was automatically terminated whenever the aircraft hit the ground or overflew the glide slope transmitter. The values for the nominal approach speeds, sink rates, flight path angles, and landing weights for the aircraft are given in Table II-5.

For the takeoff tests, the aircraft heading relative to the horizontal wind was reversed. The aircraft would be positioned at an altitude of 30 ft at a longitudinal position that would place the aircraft outbound on a 3 deg glide slope, regardless of the actual takeoff climb angle of the aircraft (see Fig. II-7). This was done so that, regardless of the initial climb angle of the aircraft being investigated, the wind conditions at the 30 ft trim point would be identical for the range- and altitude-dependent versions of a given shear.

The aircraft was trimmed at this initial position in the presence of the appropriate winds at a particular speed and power setting. It then proceeded to fly, under the guidance of the pilot model, through the shear. The nominal takeoff speeds, climb rates, flight path angles, and takeoff weights for each aircraft are listed in Table II-6.

As the aircraft proceeded along its flight through the shear, the following variables were recorded on strip charts:

- Aircraft cg height above ground
- Glide slope error
- Sink rate
- Vertical deviation from glide slope
- Horizontal wind component

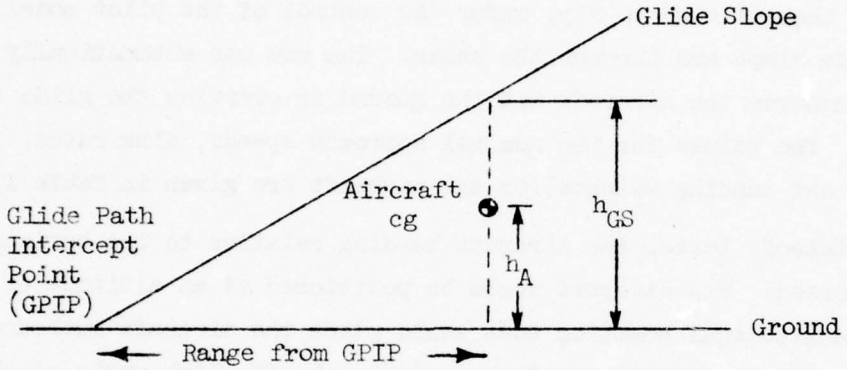

Figure II-6. Entry Altitudes for Wind Velocity Tables

TABLE II-5

NOMINAL APPROACH CONDITIONS

AIRCRAFT	APPROACH SPEED (kt)	SINK RATE (ft/sec)	FLIGHT PATH ANGLE (deg)	LANDING WEIGHT (lb)
Jumbo	142	-12.6	-3	570,000
Light Transport	130	-11.5	-3	95,000
Business Jet	125	-11.0	-3	12,500
STOL Commuter	70	-12.4	-6	11,000

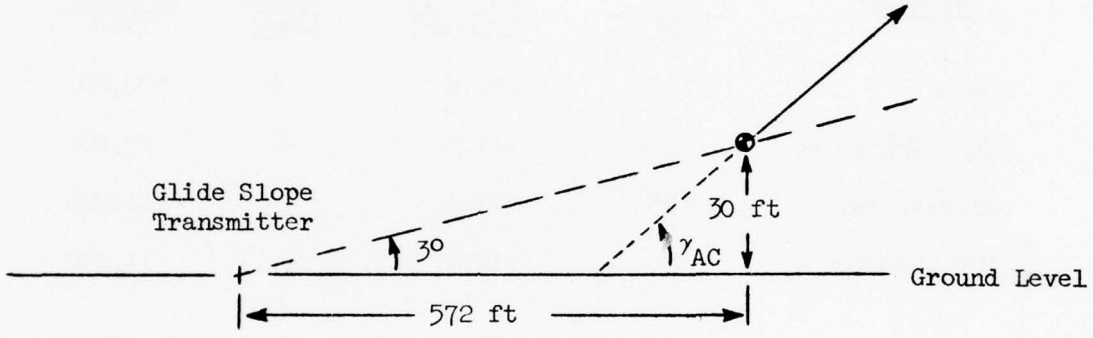

γ_{AC} = aircraft climb angle

Figure II-7. Takeoff Initial Conditions

TABLE II-6

NOMINAL TAKEOFF CONDITIONS

AIRCRAFT	TAKEOFF SPEED (kt)	CLIMB RATE (ft/sec)	FLIGHT PATH ANGLE (deg)	TAKEOFF WEIGHT (lb)
Jumbo	187	38.5	7.0	733,000
Light Transport	161	37.4	7.9	110,000
Business Jet	135	62.5	15.9	12,500
STOL Commuter	78	21.3	9.3	11,579

- Throttle position
- Engine thrust, lb
- Pitch attitude
- Vertical wind component
- Engine thrust, % max
- Elevator position
- Angle of attack
- Velocity error
- Aircraft range from glide slope transmitter
- Various internal pilot model signals and flags indicating the internal pilot status.

In addition to the above strip chart variables, the digital computer was programmed to monitor eight variables and record the maximum and minimum value of each variable, along with the time and altitude at which the maximum and minimum values occurred. These eight variables were:

- Rate of climb
- Pitch angle
- Angle of attack
- Engine pressure ratio
- Column position
- Glide slope error (angular)
- Vertical distance from glide slope
- Velocity.

Examples of typical digital output are given in Table II-7.

TABLE II-7

TYPICAL DIGITAL OUTPUT

CIVIL TRANSPORT SHEAR STUDY

RUN NUMBER: 7 DATE: 19:15 OCT 14,'76 AIRCRAFT ID: LEAR-LDG

IWIND: 1 ISHEAR: 3 HGS ICTOL: 1

XIC = -17981.0 FT HIC = 1800.0 FT VEQIC = 125.00 KT

GAMVIC = -3.00 DEG WAITIC = 12499. LBS CG = .25 %

ZIE = -1.50 FT ALTHGSB = .00 FT

QUANTITY	MAXIMUM	HEIGHT	TIME	MINIMUM	HEIGHT	TIME
RATE OF CLIMB	3.75 FT/SEC	386.22 FT	57.90 SEC	-20.82 FT/SEC	699.73 FT	23.76 SEC
PITCH ANGLE	7.51 DEG	414.09 FT	46.51 SEC	.15 DEG	369.74 FT	67.50 SEC
ANGLE OF ATTACK	7.89 DEG	160.40 FT	79.38 SEC	4.38 DEG	814.41 FT	17.51 SEC
ENGINE PRESSURE RATIO	1.54 N-D	132.22 FT	81.62 SEC	1.25 N-D	999.31 FT	.09 SEC
COLUMN POSITION	.50 DEG	796.39 FT	18.74 SEC	-4.37 DEG	159.12 FT	79.46 SEC
GLIDE SLOPE ERROR	.17 DEG	382.09 FT	66.35 SEC	-2.98 DEG	-.30 FT	98.74 SEC
VERT DIST FROM G. S.	20.60 FT	383.68 FT	66.18 SEC	-127.55 FT	466.40 FT	39.82 SEC
VELOCITY	125.39 KT	379.95 FT	55.97 SEC	116.26 KT	196.26 FT	77.18 SEC

HIT GROUND?: YES HIT XCG = 541.8 FT HIT TIME = 98.74 SEC

PILOT MODEL QUANTITIES

XKD = .1006 DEG/FT TDGS = .00 SEC THTCMIN = -10.0 DEG THTCMAX = 25.0 DEG

XKTH = -.851 N-D TAUL = .0100 SEC TAUEFF = .3333 SEC

DCMIN = -30.0 DEG DCMAX = 30.0 DEG

GL = -3.0 DEG GH = 3.0 DEG XKTHTT = .3333 KT/DEG-SEC

UL = -5.0 KT UH = 5.0 KT XKU = .214 1/SEC XKEPR = .112 SEC/KT

EPRMIN = .00 N-D EPRMAX = 2.00 N-D GSR0 = 5280.0 FT

SECTION III

LINEAR ANALYSIS

A. BACKGROUND

The pilot and aircraft models used in the simulation effort included nonlinearities. The pilot model involved thresholds and limiters while the aircraft models incorporated nonlinear aerodynamic, control system, and propulsion system effects. These nonlinearities may be required in a simulation to achieve a valid and reasonable correlation with real world results, but they tend to obscure key effects and parameters. To counter this problem, linearized models were developed to simplify the pilot and vehicle and reveal the essential features of both.

The use of linear small perturbation aircraft models allows the expression of vehicle dynamic characteristics with a minimum number of essential parameters. Additionally, the linear models contain explicitly the vehicle stability derivatives which have a key effect on aircraft behavior. Expressed in this way, the key dynamic parameters of the model are more clearly partitioned. The stability derivatives have the additional benefit that each one is easily derived from, or associated with, an aerodynamic or geometric characteristic of the aircraft.

In the following pages we shall define the linear models used in our analysis and proceed to use these models in exposing dominant wind shear effects. We shall end this section by presenting a simplified view of the mechanism of wind shear acting on the piloted aircraft. This will serve as a background for the subsequent presentation of simulation results.

B. LINEARIZED PILOT AND AIRCRAFT MODELS

The pilot models were linearized by removing the thresholds and limits from all pilot models and by removing the crossfeed term from the CTOL approach pilot model. Figures III-1, III-2, and III-3 show block diagrams of the linear pilot models for the CTOL approach, STOL approach, and takeoff,

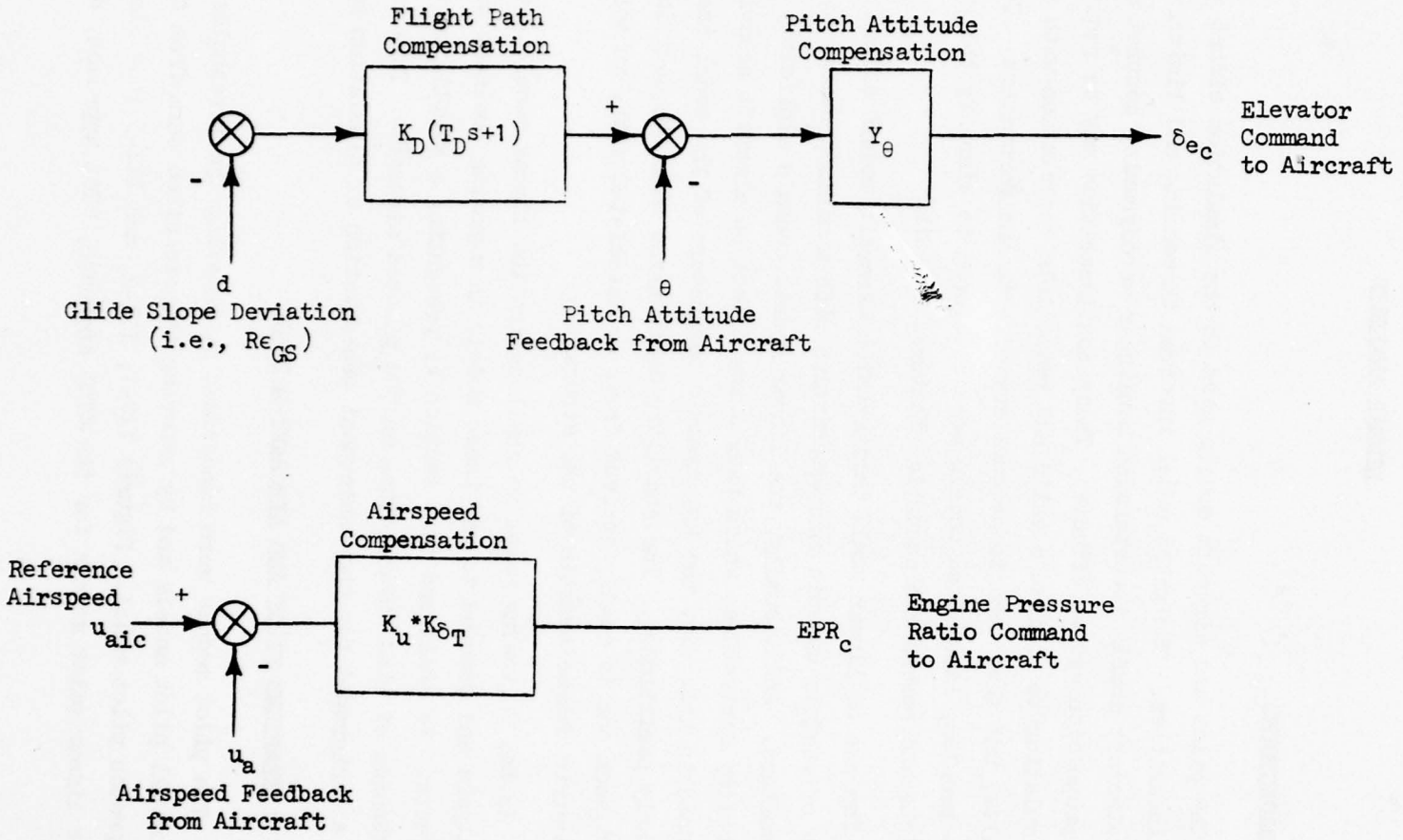

Figure III-1. Linearized CTOL Approach Pilot Model

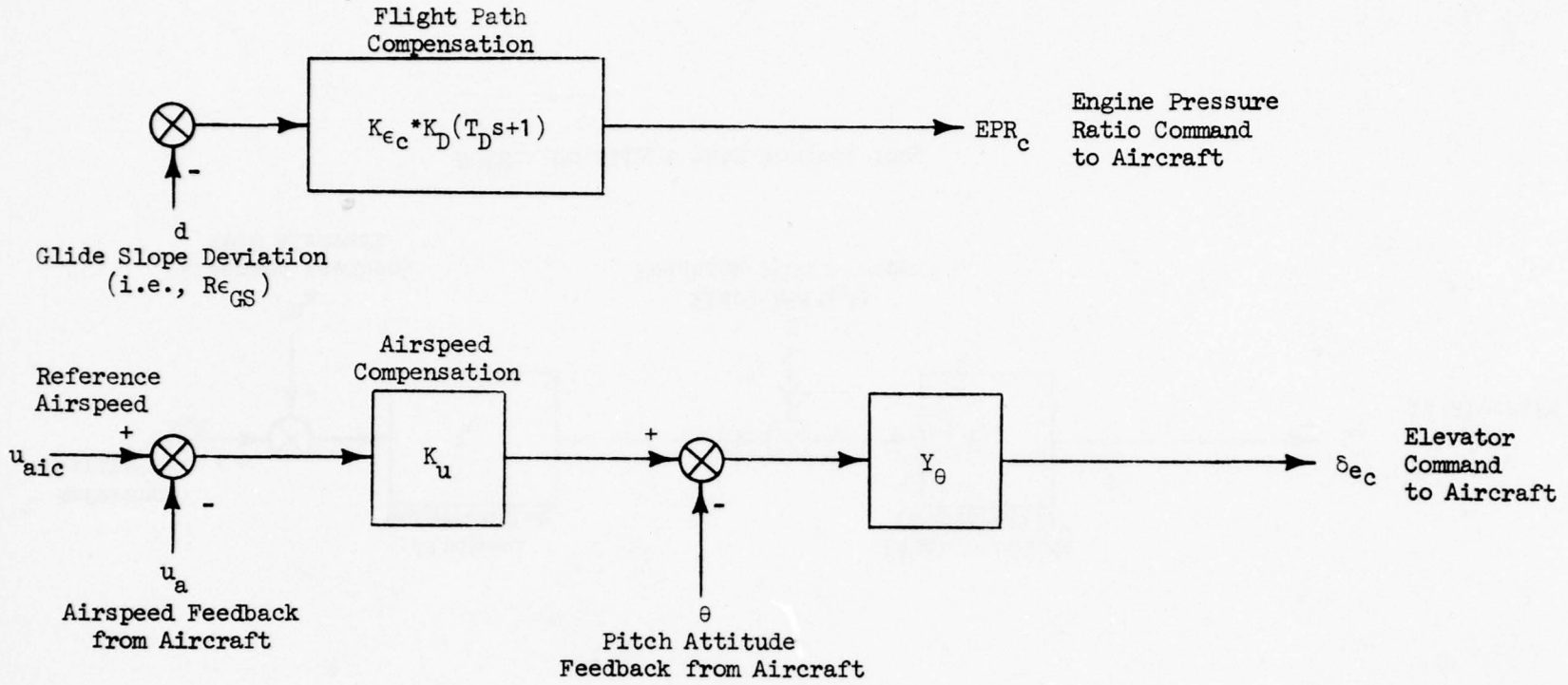

Figure III-2. Linearized STOL Approach Pilot Model

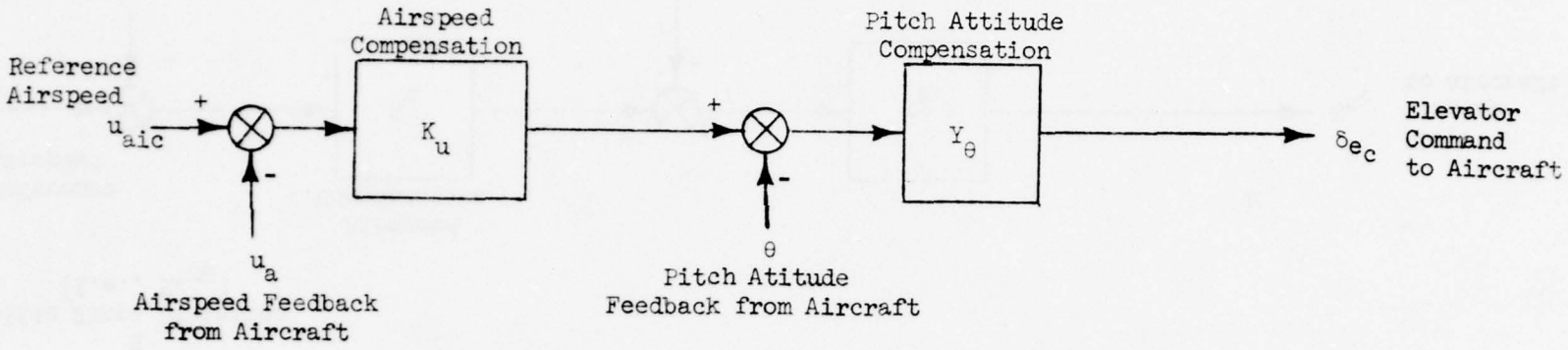

NOTE: No flight path control loop

Figure III-3. Linearized Takeoff Pilot Model

respectively. The numerical values of transfer functions correspond to those of the non-linear model (see Appendix A).

The aircraft models were linearized by the conventional methods of small perturbations about a nominal trim point and expressed in terms of dimensional stability derivatives in a body-fixed stability axis system. Both the aircraft aerodynamic and propulsion system characteristics were treated in this matter. Reference 25 may be consulted for details of the equations of motion. The stability derivatives for the models at baseline conditions are given in Appendix B.

The linearized descriptions of pilot and aircraft dynamics can be directly utilized by formulating closed loop transfer functions of aircraft motion due to applied gust disturbances. As we shall discuss in Section IV, one of the most significant motion quantities is altitude excursion. Hence, it is instructive to consider the transfer functions:

$$\frac{\Delta h}{u_g} \quad \text{and} \quad \frac{\Delta h}{w_g}$$

Two examples of the above transfer functions are shown in Figs. III-4 and III-5 for the light transport and in Figs. III-6 and III-7 for the STOL commuter. The light transport is representative of all the CTOL types considered in this study. Some important general observations can be made from these figures. First, the frequency response characteristics for both types of aircraft are comparable, although the STOL response is not as well damped as the CTOL response. The pilot-vehicle combination acts as a band pass filter to horizontal gust velocity and as a low pass filter to vertical gust velocity. (We can also characterize the horizontal gust response as a low pass filter for horizontal gust acceleration or rate of shear, i.e., $\dot{u}_g$.) One of the main features of the figures is that closed-loop pitch response modes which are characteristically above 1 rad/sec are well attenuated. The predominant aircraft response occurs in the spectral range below 1 rad/sec. Further, by neglecting the pitch response and

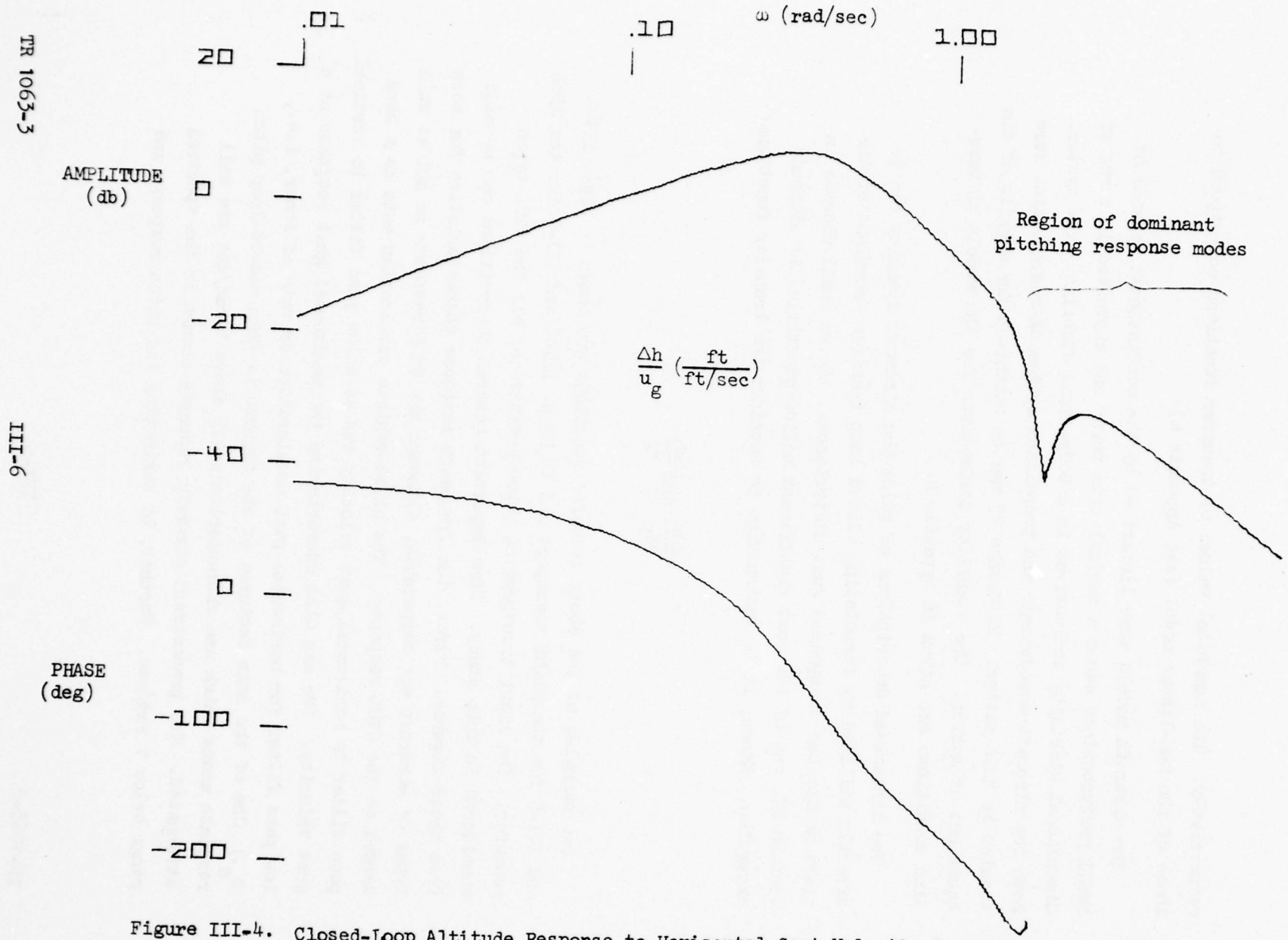

Figure III-4. Closed-Loop Altitude Response to Horizontal Gust Velocity Component (Light Transport, Approach)

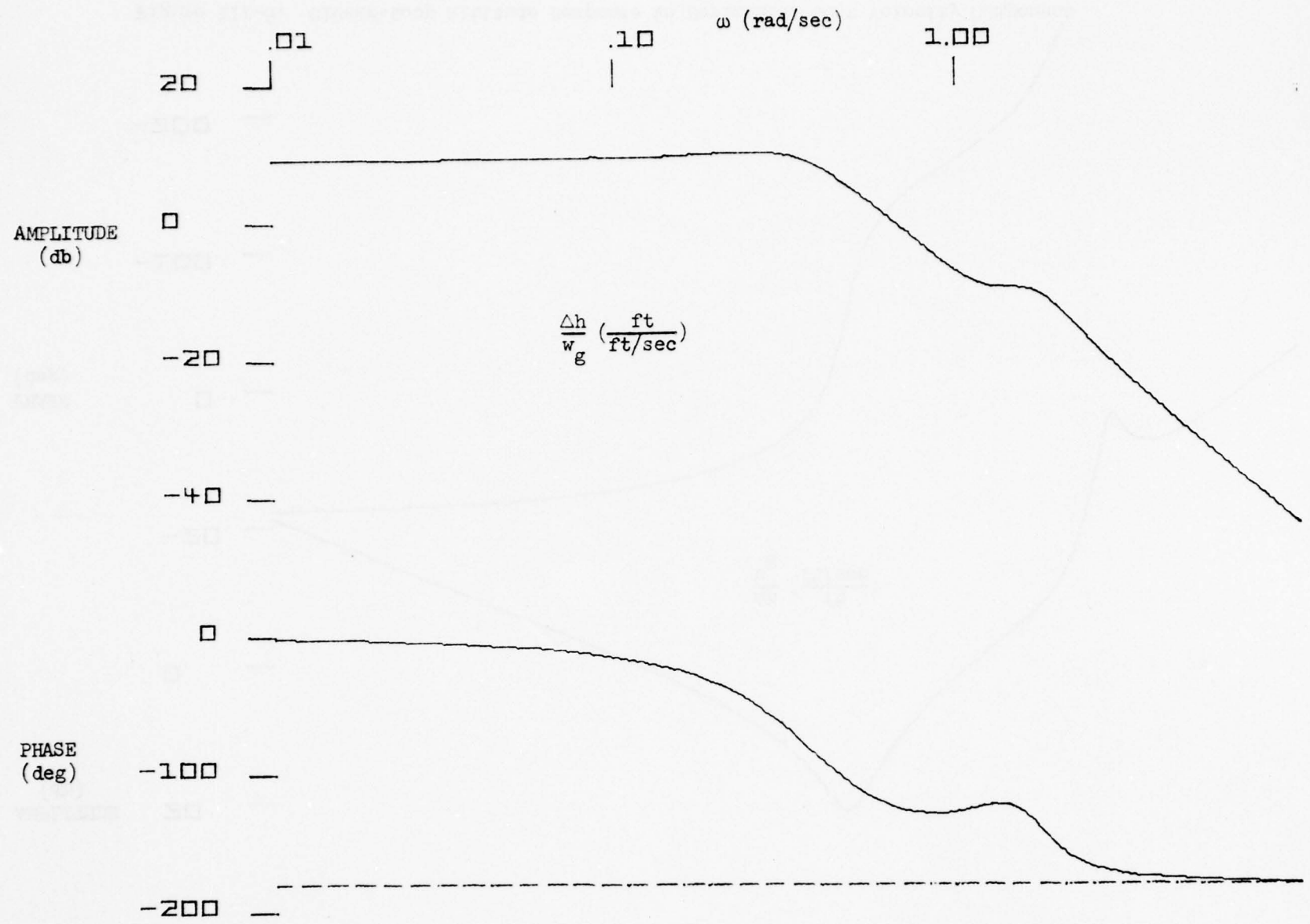

Figure III-5. Closed-Loop Altitude Response to Vertical Gust Velocity Component (Light Transport, Approach)

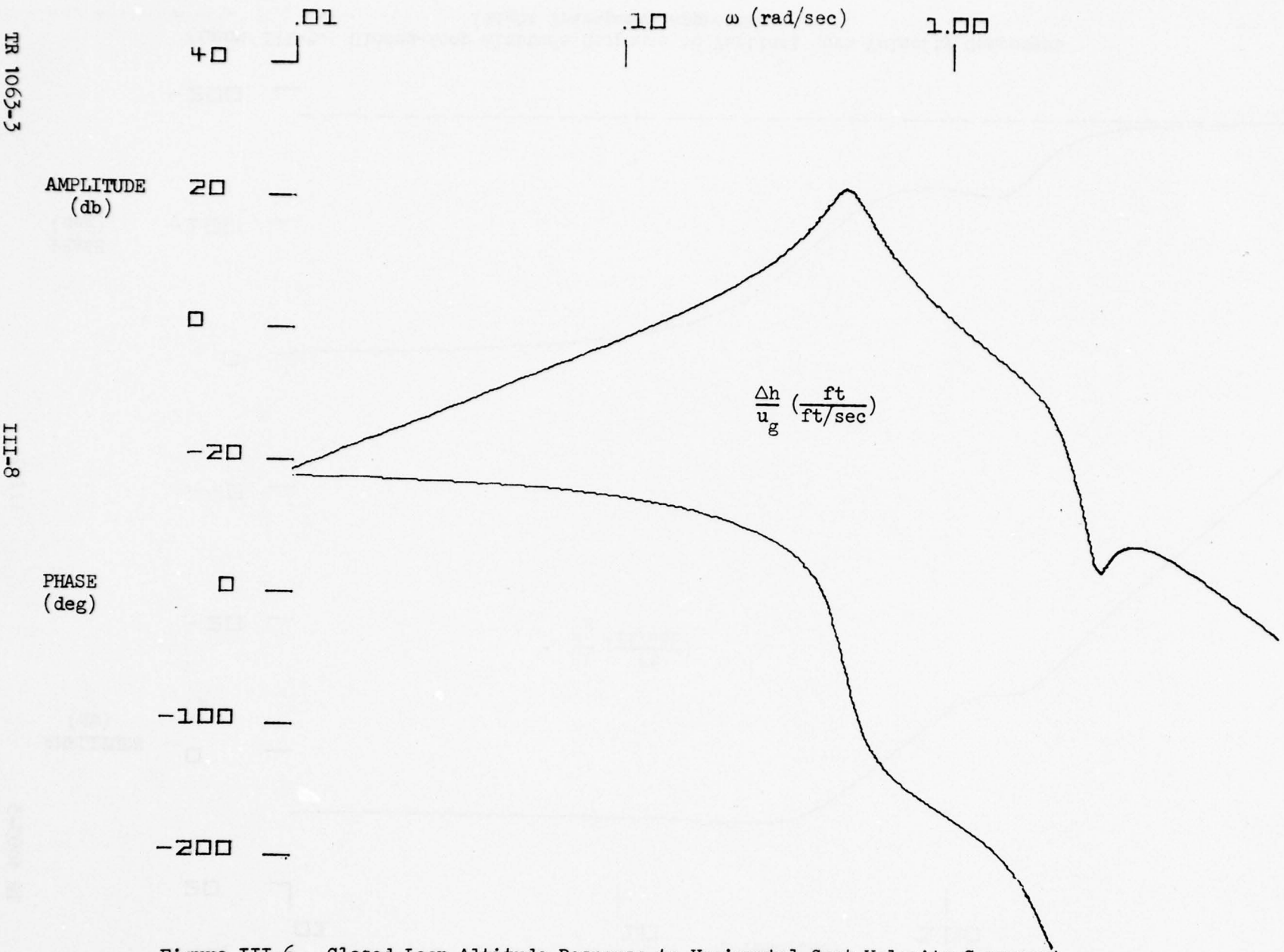

Figure III-6. Closed-Loop Altitude Response to Horizontal Gust Velocity Component (STOL Commuter, Approach)

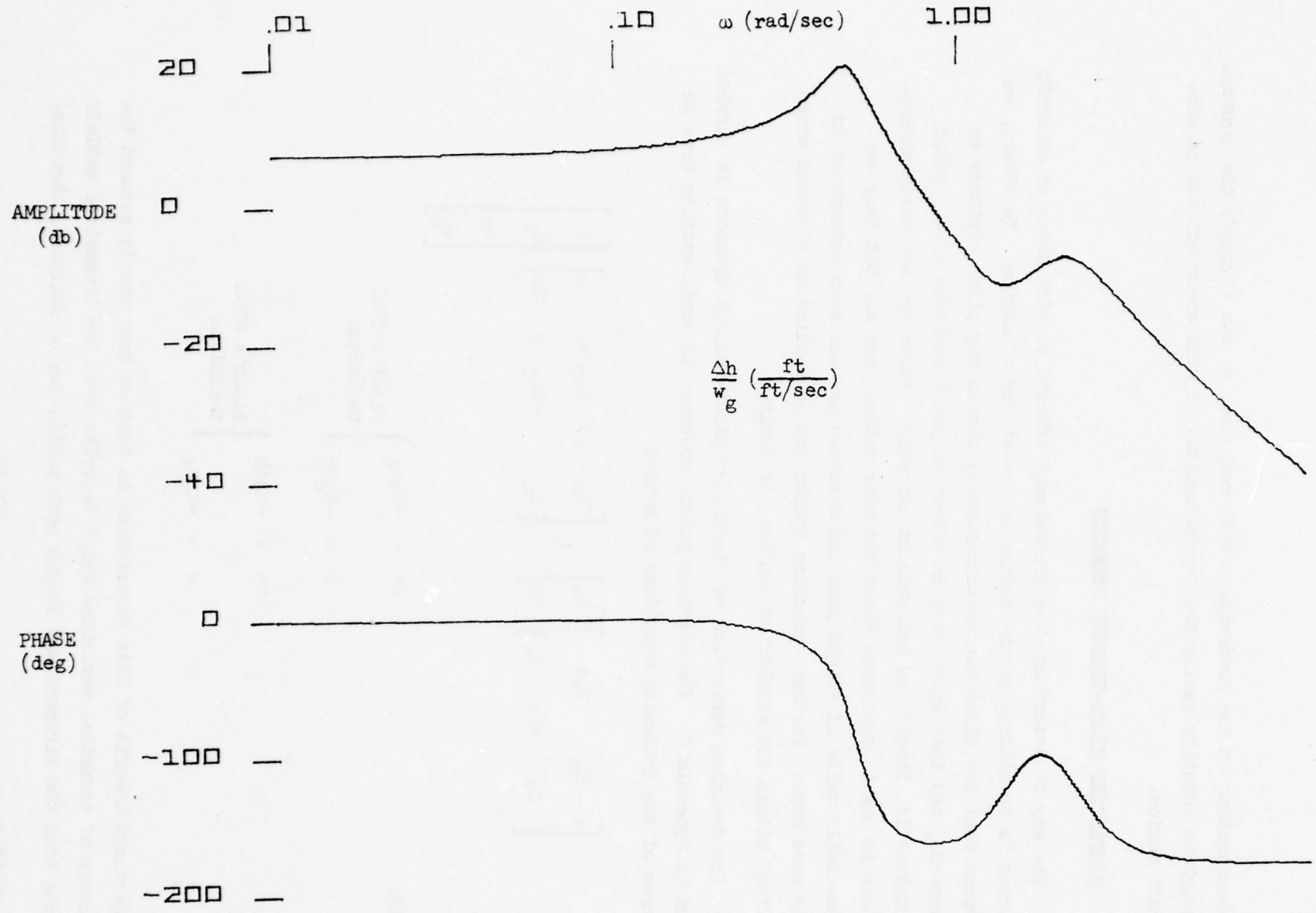

Figure III-7. Closed-Loop Altitude Response to Vertical Gust Velocity Component (STOL Commuter, Approach)

concentrating on the predominant path response, we can simplify the dynamics enough to identify easily the key mechanisms of wind shear effects on aircraft motion.

C. SIMPLIFIED PILOT-VEHICLE DYNAMICS

The key to describing the predominant effects of wind shear on aircraft motion is to utilize pitch-constrained equations of motion. In effect, we assume that the pilot can instantaneously obtain any pitch attitude he commands, and that gusts have no effect on pitch attitude (i.e., pitch attitude is, itself, an independent control). These are not valid assumptions if one is concerned about pitching motion, per se, but they are reasonably valid if flight path and airspeed are the main concern as in the case here. Further, pitching motion can be handled as a second order effect within the simplified context, if desired.

The detailed derivation of simplified pilot-vehicle dynamics is carried out in Appendix C. The starting point, however, is worth stating here in terms of the following equations of motion:

$$\begin{bmatrix} s - X_u & X_w s \\ Z_u & s(s - Z_w) \end{bmatrix} \begin{bmatrix} u_a \\ \Delta h \end{bmatrix} \doteq \begin{bmatrix} (X_\alpha - g) & X_{\delta_T} - s & -X_w \\ -Z_\alpha & -Z_{\delta_T} & 0 & Z_w \end{bmatrix} \begin{bmatrix} \theta \\ \delta_T \\ u_g \\ w_g \end{bmatrix}$$

with

$$\left.\begin{aligned} \delta_T &= -K_u u_a \\ \theta &= -K_{\dot{q}} \Delta h \end{aligned}\right\} \text{Pilot's CTOL technique}$$

or

$$\left.\begin{aligned} \delta_T &= -K_{\dot{q}} \Delta h \\ \theta &= -K_u u_a \end{aligned}\right\} \text{Pilot's STOL technique}$$

The first benefit of this description is that we have vastly reduced the number of essential variables which describe even the linearized vehicle. Note that the airspeed and flight path motion due to attitude, throttle,

horizontal gusts, and vertical gusts is dependent only upon the six parameters X_u, X_w, Z_u, Z_w, V, and $X_{\delta_T}/Z_{\delta_T}$ ($X_\alpha = V\,X_w$ and $Z_\alpha = V\,Z_w$). Each of these is easily estimated as demonstrated in Ref. 20. Two pilot parameters are involved, K_u and K_d. These are set directly in proportion to their respective control loop tightness as expressed by crossover frequencies, ω_{c_u} and ω_{c_d}. For the CTOL case;

$$K_u X_{\delta_T} \doteq \omega_{c_u}$$

and

$$-K_d Z_\alpha \doteq \omega_{c_d}$$

The altitude response due to horizontal and vertical gusts can be expressed in the following generic forms:

$$\frac{\Delta h}{u_g} \doteq \frac{-\frac{2g}{V}\,s}{(s + \frac{1}{T_u})(s^2 + 2\zeta_d\omega_d s + \omega_d^2)}$$

or

$$\frac{\Delta h}{\dot{u}_g} \doteq \frac{-\frac{2g}{V}}{(s + \frac{1}{T_u})(s^2 + 2\zeta_d\omega_d s + \omega_d^2)}$$

and

$$\frac{\Delta h}{w_g} \doteq \frac{Z_w(s + \frac{1}{T_u} - X_u + \frac{X_w}{Z_w} Z_u)}{(s^2 + 2\zeta_d\omega_d s + \omega_d^2 s)(s + \frac{1}{T_u})}$$

$$\doteq \frac{Z_w^*}{(s^2 + 2\zeta_d\omega_d s + \omega_d^2 s)}$$

where

$$\frac{1}{T_u} \doteq \omega_{c_u}$$

$$\omega_d^2 \doteq \omega_{c_d}^2\left[1 + \frac{Z_u(X_\alpha - g)}{\omega_{c_u} Z_\alpha}\right]$$

and

$$2\zeta_d\omega_d \doteq -X_u - Z_w$$

---

*Z_w represents heave damping and is equal to $\frac{-\rho g C_{L_\alpha} V}{W/S}$

These expressions can be sketched in terms of amplitude response to horizontal gust velocity, u_g, horizontal gust acceleration or rate of shear, $\dot{u}_g$, and vertical gust velocity, w_g, as shown in Fig. III-8. Accordingly, altitude response to horizontal wind shear is inversely proportional to:

- Airspeed
- Airspeed loop tightness (ω_{c_u})
- Square of flight path loop tightness (ω_{c_d})

for the spectral region extending out to the flight path regulation mode at frequency ω_d. Altitude response to vertical gust velocity is proportional to:

- Airspeed
- Lift curve slope, C_{L_α}

and inversely proportional to:

- Wing loading
- Square of flight path loop tightness (ω_{c_d}).

These results will be useful for aiding in the interpretation of simulation results to be presented in the next section.

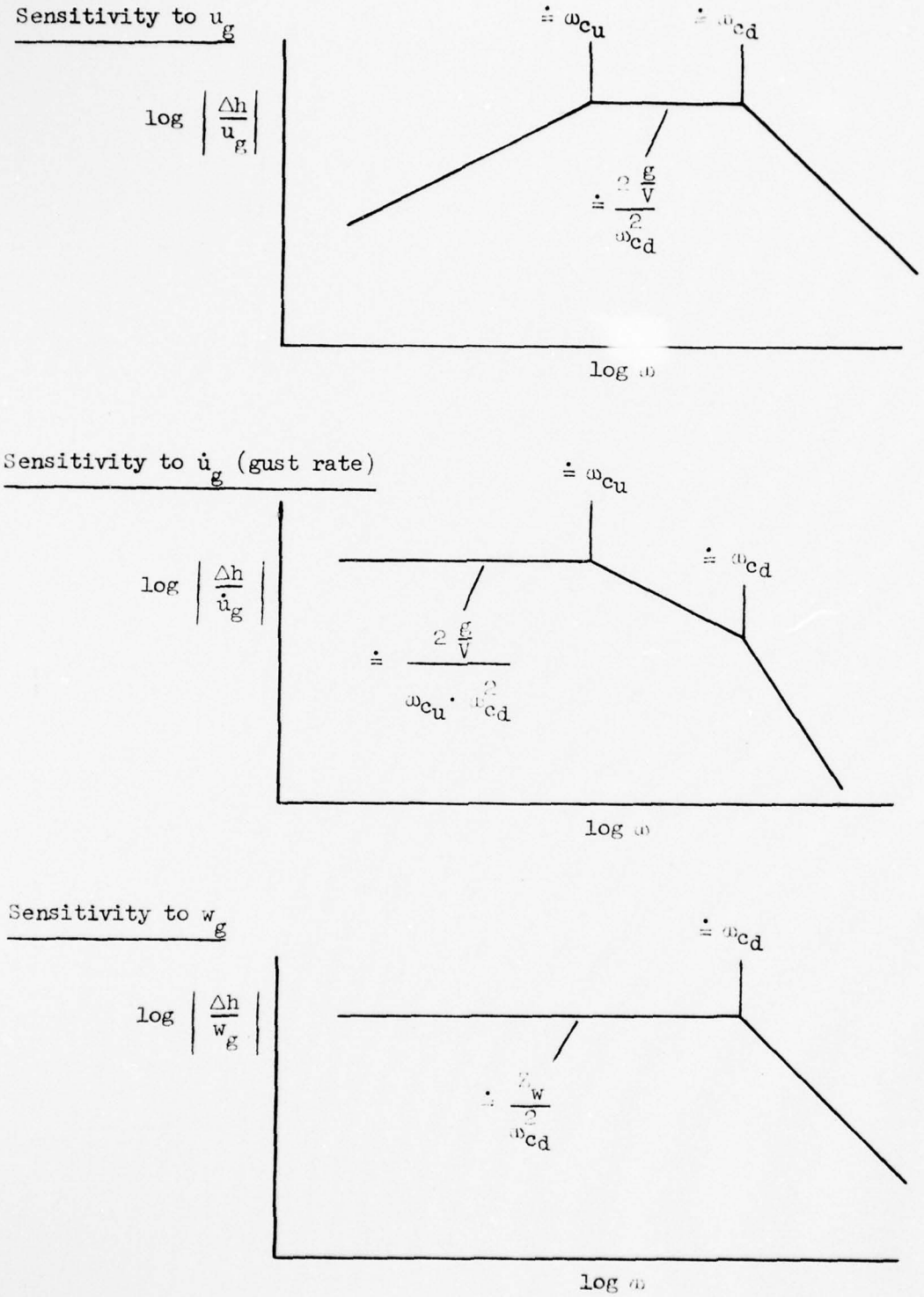

Figure III-8. Sketches of Altitude Amplitude Response Asymptotes

SECTION IV

APPROACH RESULTS

A. BACKGROUND

The presentation of wind shear hazard results for the approach flight phase is divided into three parts with:

- Baseline aircraft and pilot models
- Variation of operational techniques which affect shear hazard
- Variation of propulsion system features which affect shear hazard.

Prior to discussing these three parts of the results, however, it is important to define the metric used to describe wind shear hazard and certain aspects of modeling wind shear which impact the interpretation of the results.

Several metrics were considered including airspeed loss and minimum altitude reached prior to recovery from the disturbance. The most direct and, we believe, the most meaningful proved to be maximum vertical excursion below the glide slope or nominal flight path. This is illustrated in Fig. IV-1.

Initially, airspeed loss was considered as a candidate, and although airspeed loss was frequently substantial, its use was ultimately discarded for two reasons. First, airspeed loss is mainly a function of shear abruptness. The features which would have the most direct impact on airspeed loss are the convective (or speed damping) tendency of the bare airframe and the speed regulation abilities of the pilot. This relationship can be easily expressed as:

$$\frac{-u_a}{u_g} \doteq \frac{s}{s + \frac{1}{T_u}}$$

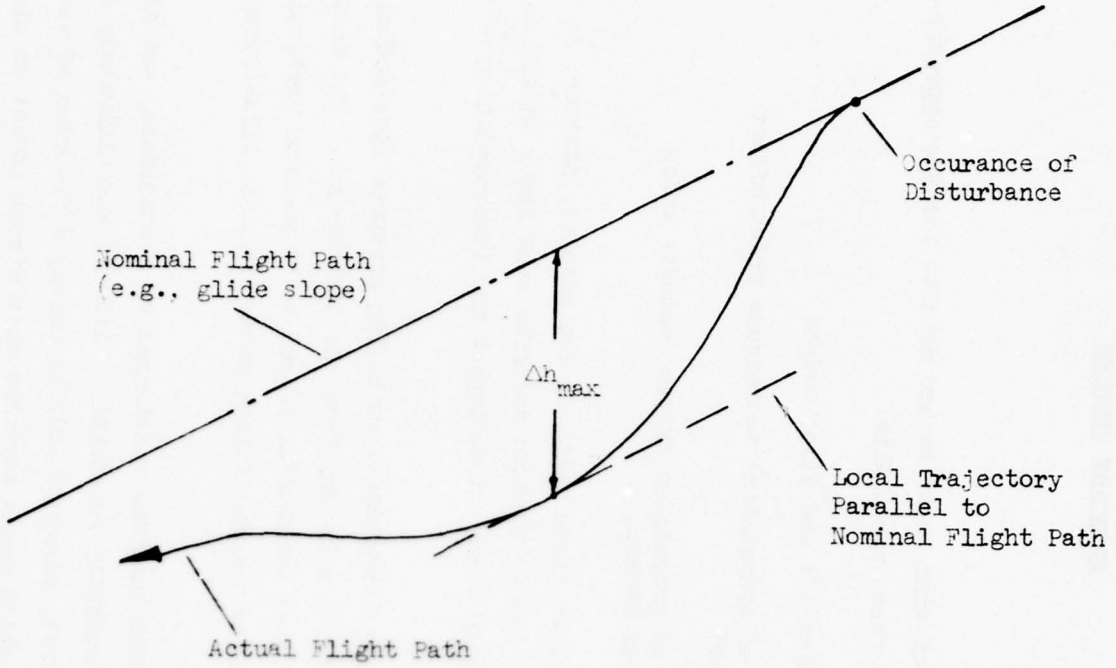

Figure IV-1. Δh_{max} Shear Hazard Metric

where $-u_a \triangleq$ airspeed loss

$u_g \triangleq$ tailwind increase

$T_u \triangleq$ time constant representing the aircraft's convective tendency and/or the pilot's speed regulation ability

The above relationship implies that airspeed loss matches the tailwind increase for a period nearly equal to T_u. At best, T_u includes time to recognize an airspeed change, to take effective control action, and for the control itself to produce a longitudinal acceleration. This could typically be 5 to 10 seconds based on observations from manned simulations. Nevertheless, the airspeed loss, per se, is directly tied to the shear itself.

The second shortcoming of airspeed loss as a metric is its indirect relation to angle of attack. Airspeed loss does not directly result in a large angle of attack increase. During horizontal shear encounters, the angle of attack remains relatively constant as the airspeed decreases, with only 3 to 5 deg changes in α observed. Also, during vertical shear encounters, the sink rate increases without any change in airspeed.

While we recognize the value of airspeed and angle of attack as legitimate safety margin indicators, we claim that the ultimate metric of hazard should be a precursor of ground contact itself. Hence, we are forced to consider an altitude-related quantity.

One example of an altitude metric is the absolute minimum altitude encountered during recovery from a shear disturbance. This is meaningful, however, only if a local minimum occurs in altitude (it may not occur) and if the excursion is tied to an absolute altitude of shear onset. Such a set of conditions is unnecessarily restrictive. Thus, we return to the simple yet effective Δh_{max} metric defined in Fig. IV-1.

Another matter which requires discussion prior to the presentation of results is the way the wind shear is modeled. Despite the use of actual wind shear encounters as the basis of this study, the results can vary depending upon how one implements the shear profiles.

An actual shear profile is a function of spatial position (i.e., range and altitude) and time. Wind shear measurements based upon a single trajectory through an air mass cannot have the full dimensionality required, and an arbitrary dependency must be assigned. It is important to recognize that shear profiles with differing kinds of dependencies will produce different simulator results. This is illustrated in Fig. IV-2.

Let us further consider one of the kinds of shear dependencies. Figure IV-3 shows the effect of an altitude-dependent horizontal wind shear on an attitude-stabilized pilot-vehicle combination. If the wind shear is approximately linear with altitude, a linear feedback occurs. In the case of a decreasing headwind the effect is destabilizing. In fact if the change in headwind with altitude is approximately greater than g/V the total pilot-vehicle-shear combination is unstable.

Range-dependent shears create a similar but far weaker closed loop effect. Time-dependent shears are essentially open loop (i.e., independent) disturbances.

In view of the foregoing, we therefore studied the effects of wind shear using both an altitude-dependent and a range-dependent model of the Kennedy and Logan shears. However, only an altitude-dependent boundary layer shear was used.

It will be apparent that the altitude-dependent shears are usually more severe than their range-dependent counterpart. In view of the insufficient knowledge of the real shear dependency, we can only speculate that the true degree of severity is somewhere between the range-dependent and altitude-dependent solutions.

B. RESULTS FOR BASELINE AIRCRAFT AND PILOT MODELS

Figure IV-4 depicts the maximum deviation below the glide slope, Δh_{max}, for the four aircraft during encounters with the boundary layer shear and the altitude-dependent versions of the Logan and Kennedy shears. (Note that the boundary layer shear was used only with the light transport and STOL commuter.) The data for the range-dependent Logan and Kennedy shears are presented in Fig. IV-5. The data indicate that, for all aircraft, the shears can be rated in order of increasing hazard:

TIME DEPENDENT SHEAR

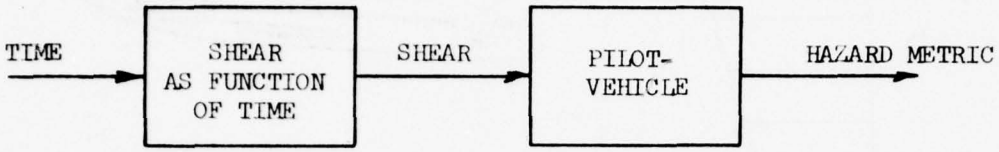

(Open loop interaction between shear and pilot-vehicle)

RANGE DEPENDENT SHEAR

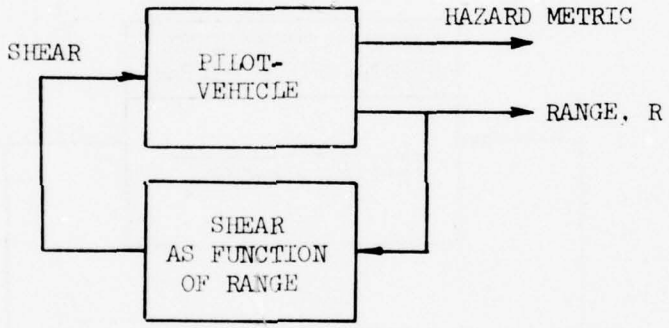

(Closed loop interaction between shear and pilot-vehicle)

ALTITUDE DEPENDENT SHEAR

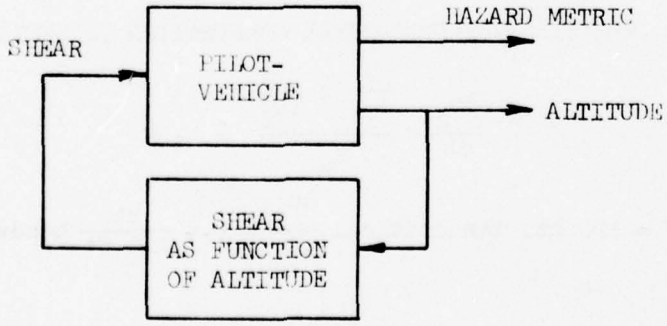

(Closed loop interaction between shear and pilot-vehicle)

Figure IV-2. Varieties of Interactions Between Wind Shear and Pilot-Vehicle

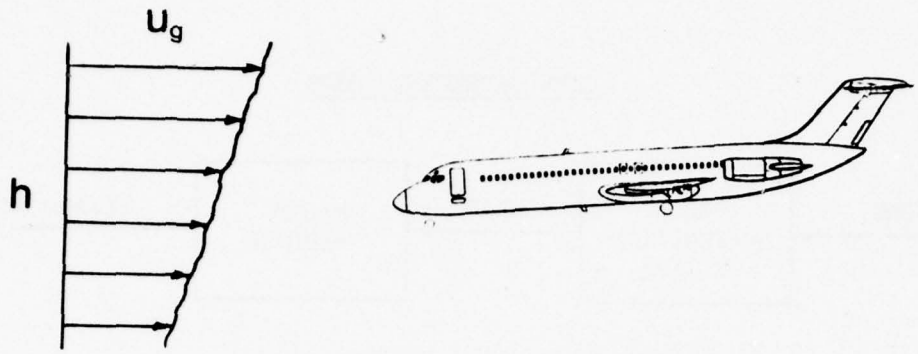

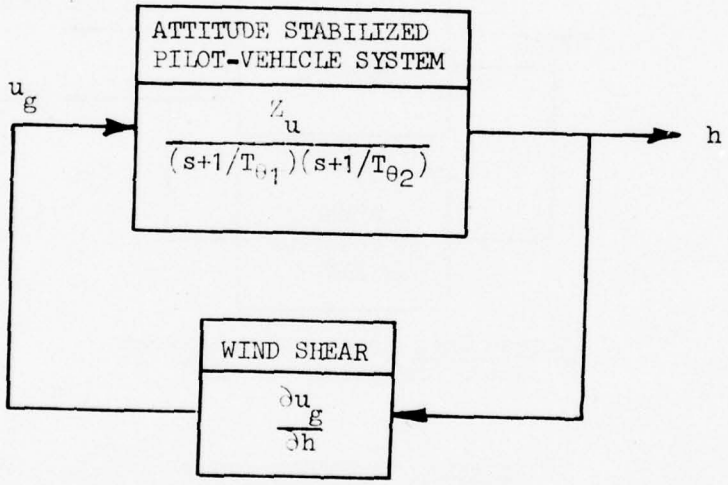

NOTE: THE PILOT-VEHICLE-SHEAR COMBINATION IS UNSTABLE FOR

$$\frac{\partial u_g}{\partial h} < \frac{\frac{1}{T_{\theta_1}} \cdot \frac{1}{T_{\theta_2}}}{Z_u} \doteq -\frac{g}{V}$$

(e.g., if V = 120 kt, the critical $\frac{\partial u_g}{\partial h} = 9.4 \frac{\text{kt}}{100 \text{ ft}}$ headwind-to-tailwind)

Figure IV-3. The Effect of an Altitude-Dependent Horizontal Wind Shear on the Attitude-Stabilized Pilot-Vehicle Combination

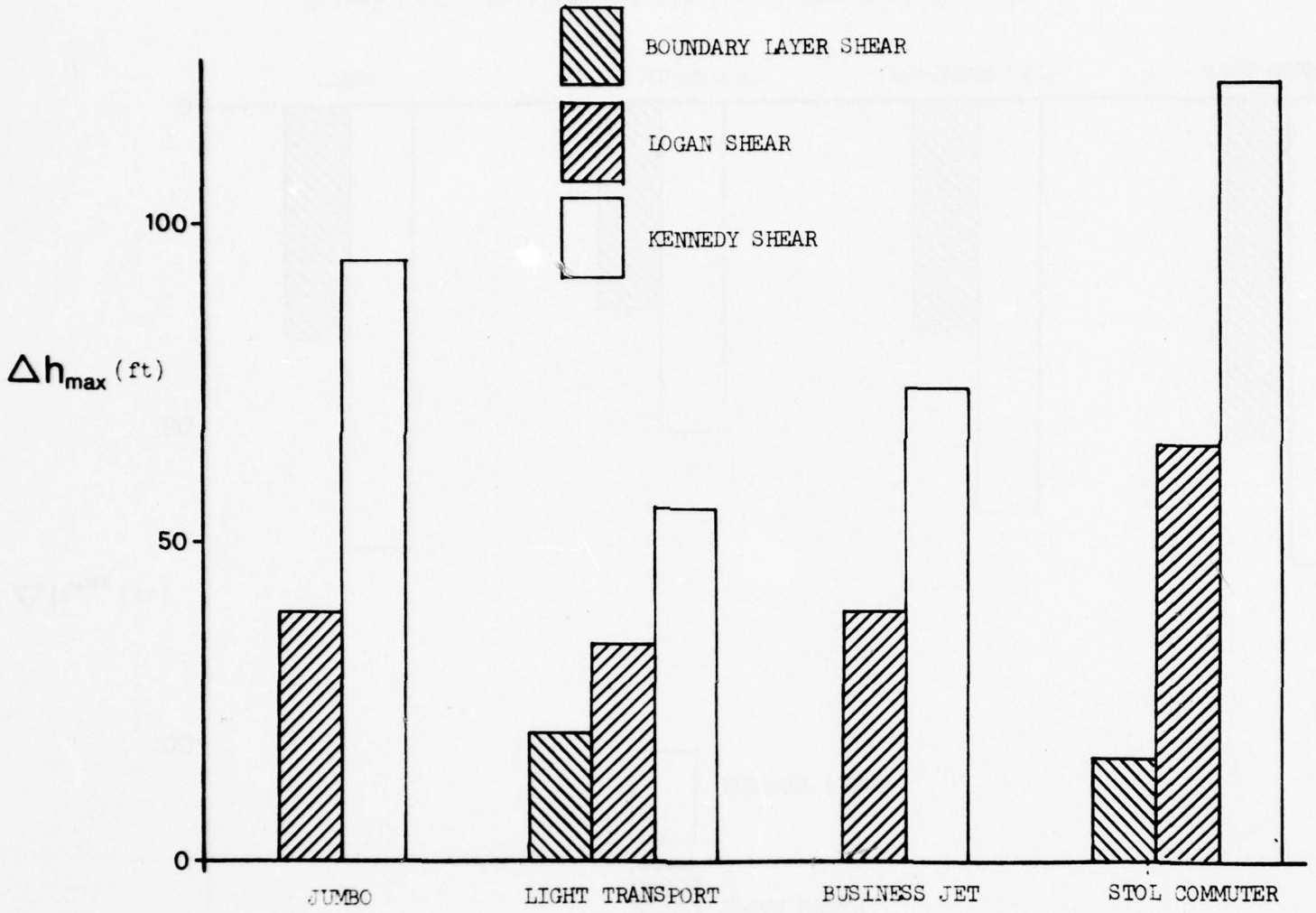

Figure IV-4. Baseline Results (Altitude-Dependent Shears)

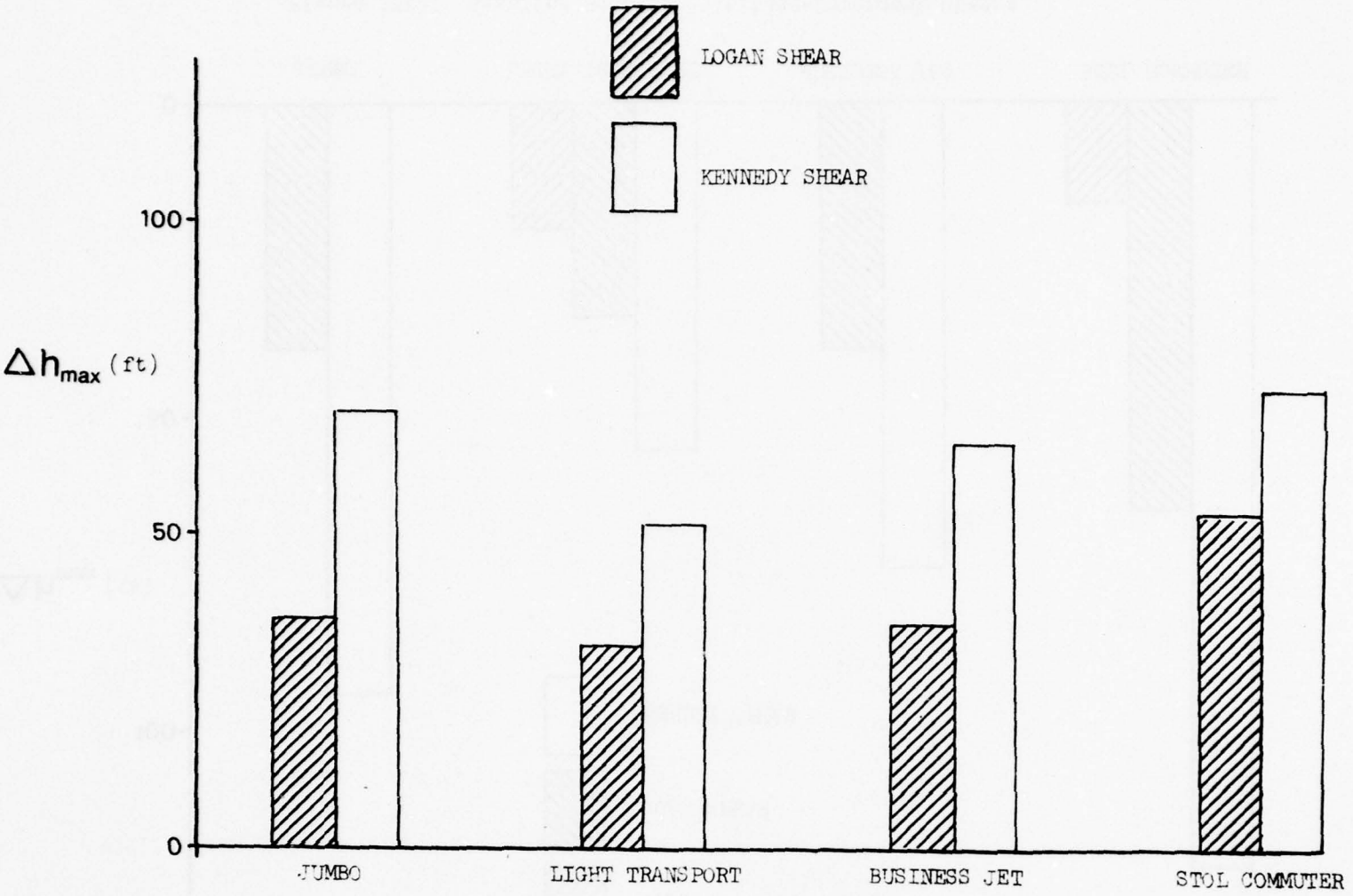

Figure IV-3. Baseline Results (Range-Dependent Shears)

- Boundary layer shear
- Logan shear (range- and altitude-dependent versions present approximately the same hazard)
- Range-dependent Kennedy shear
- Altitude-dependent Kennedy shear.

There are obvious differences in the effect any one shear has on the various aircraft types. We shall, however, discuss individual aircraft differences subsequently in Subsections C and D. At this point let us consider one vehicle, the light transport, and address each shear profile in turn.

A time history of the light transport encountering the boundary layer shear is given in Fig. IV-6. It can be seen that the shear rate ($\partial u_g/\partial t$) is relatively small even below 200 ft altitude and the overall effect on the aircraft is relatively mild. Note also that a speed loss of approximately 8 kt near the end of the run does not cause any large angle of attack change. This is due to the fact that the aircraft was in accelerated (less than 1 g) flight at this point.

A similar time history of the light transport encountering the range-dependent Logan shear is given in Fig. IV-7. Notice that the aircraft initially gets high and fast and that both factors tend to alleviate the seriousness of the shear at lower altitude. At approximately 200 ft (the altitude at which the final abrupt decreasing headwind portion of the shear begins) the aircraft is on the glide slope but 5 kt fast. In this case the aircraft ends up getting 10 kt slow and 35 ft below the glide slope. It is also noticeable that the excursion below the glide slope is arrested chiefly because the shear rate goes to zero rather than because of the action of the pilot model.

The time history for the light transport encountering the range-dependent Kennedy shear is shown in Fig. IV-8. The initial wind encountered by the aircraft is a combination of a downdraft and an increasing headwind. The effect of the downdraft is to drive the aircraft below the glide slope, while the effect of the increasing headwind is to drive the aircraft above the glide slope. The initial result in this case is to drive the aircraft fast and below the glide slope.

LONG	SHORT
250 ALTITUDE ~ ft (cyclic) 0	2.5 GLIDE SLOPE ERROR ~ deg -2.5
25 SINK RATE ~ ft/sec -25	NOT USED
125 GLIDE SLOPE DEVIATION ~ ft -125	Tailwind 50 HORIZONTAL WIND ~ kt Headwind 50
2.5 ENGINE PRESSURE RATIO 0	50,000 THRUST (ALL ENGINES) ~ lb 0
25 PITCH ATTITUDE ~ deg -25	Downdraft 25 VERTICAL WIND ~ kt Updraft 25
12.5 COLUMN POSITION ~ in 12.5	-5000 x-POSITION ~ ft 0
25 ANGLE OF ATTACK ~ deg -25	2000 ALTITUDE ~ ft 0
25 AIRSPEED DEVIATION ~ kt -25	20,000 AIRCRAFT RANGE ~ ft 0

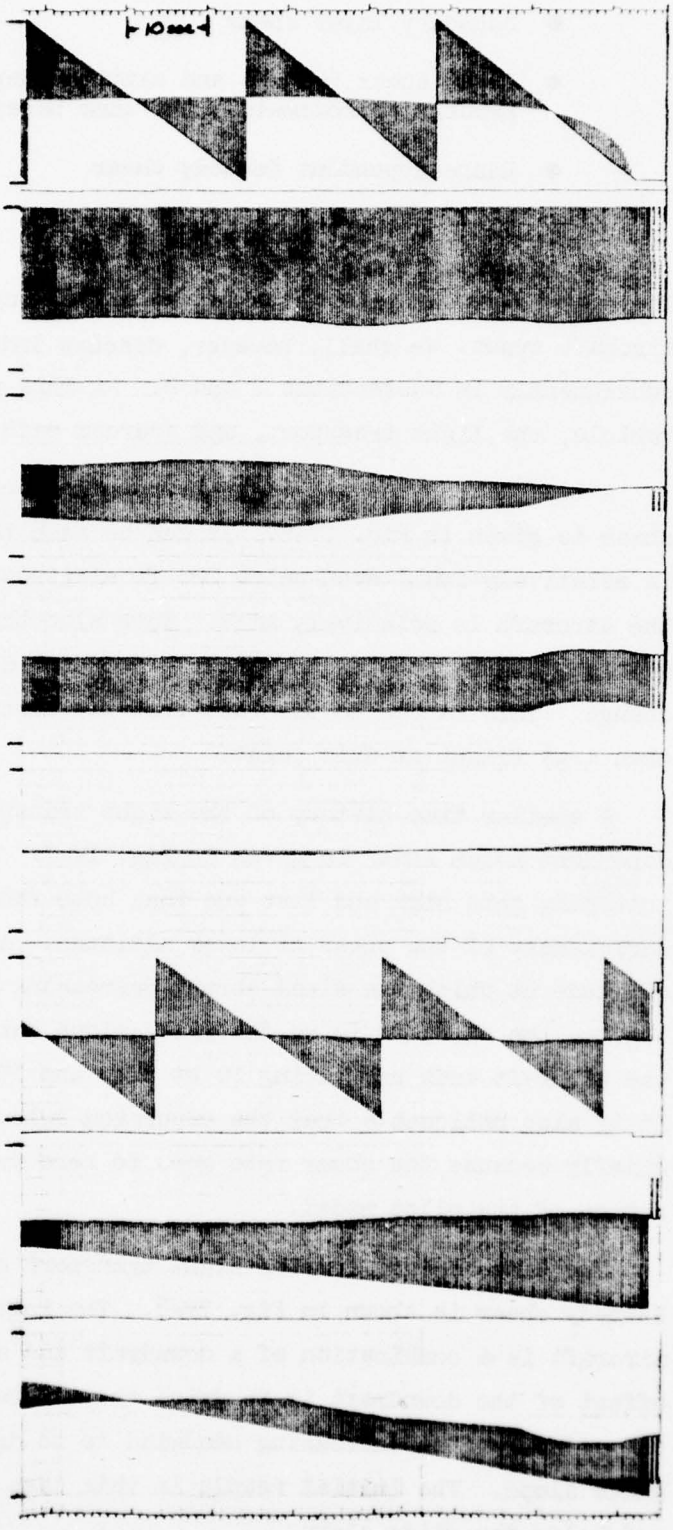

Figure IV-6. Time Histories for the Light Transport in the Boundary Layer Shear (Altitude-Dependent)

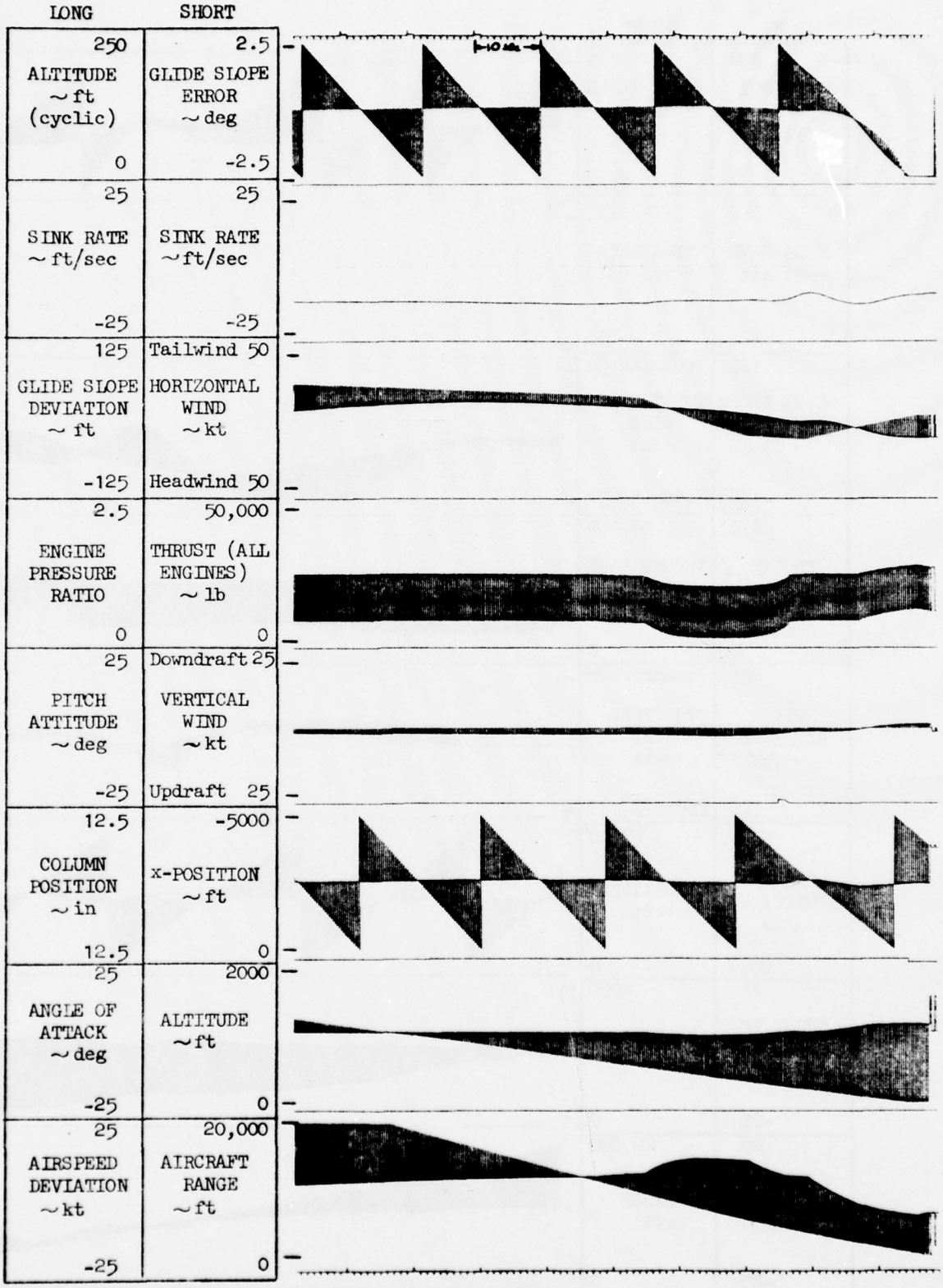

Figure IV-7. Time Histories for the Light Transport in the Logan Shear (Range-Dependent)

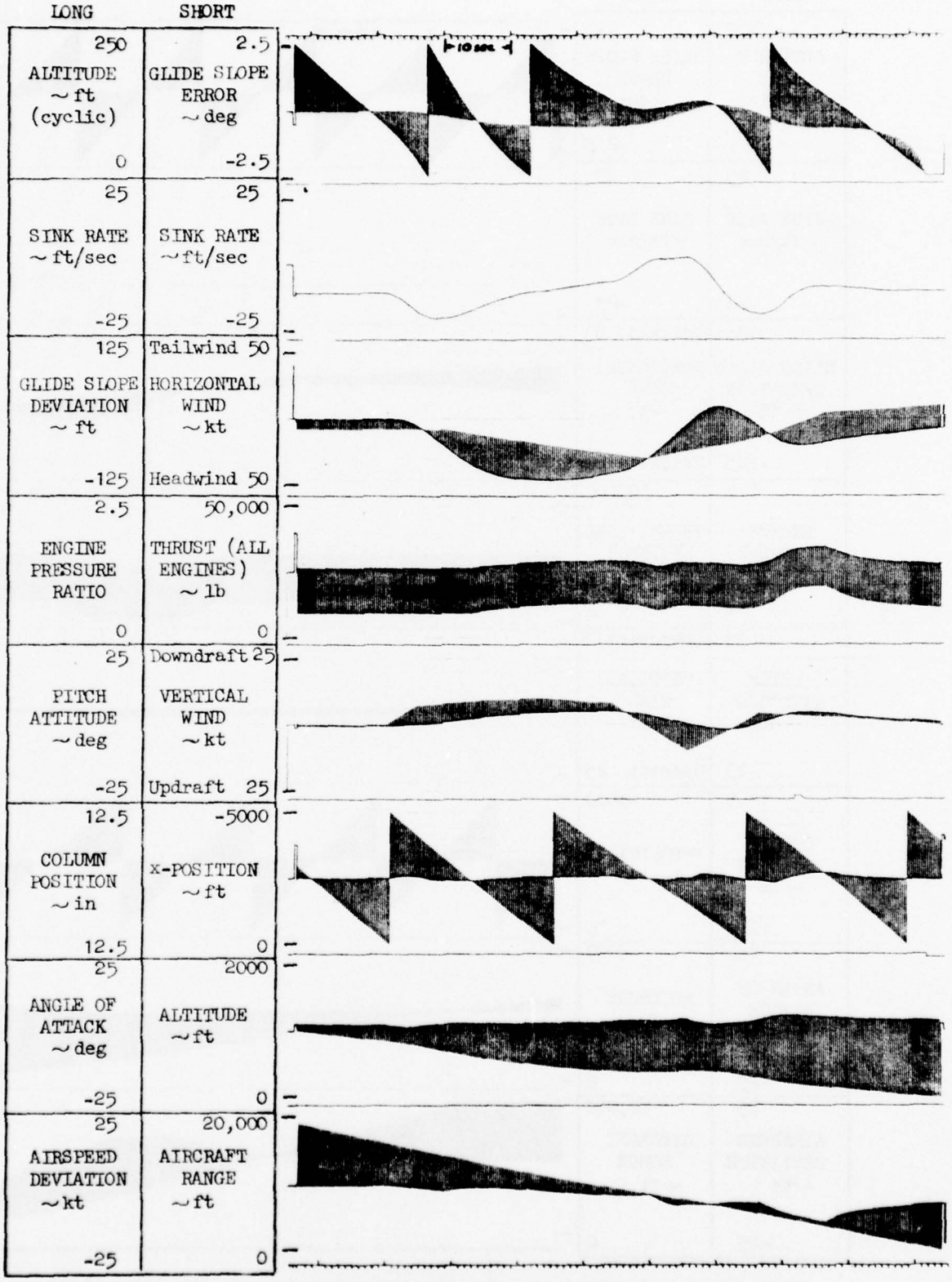

Figure IV-8. Time Histories for the Light Transport in the Kennedy Shear (Range-Dependent)

The next phase of the shear encounter has the downdraft turning into an updraft, while the headwind decreases very gradually. The updraft effect predominates in this phase and the aircraft ends up above the glide slope while being very near to its desired speed.

The final phase of the shear encounter finds the updraft changing again to a downdraft, and the headwind rapidly decreasing to a tailwind. Both of these effects tend to drive the aircraft below the glide slope. The maximum glide slope deviation occurs at roughly 200 ft altitude, and it is this final deviation that is used as a measure of the hazard. The maximum speed error is only 16 kt slow.

It should be noted that although Δh goes to a maximum value at approximately 500 ft, this value is not used in our results. This is because at the altitude and range at which this peak occurs, the pilot model has a lower glide slope gain per foot of glide slope deviation than it does at a lower altitude. The result of this is to make the value of the first excursion very dependent upon the value of the pilot model parameter R_o (range at which the pilot regulates distance from glide slope rather than angle). Increasing R_o would make the second Δh peak the larger one. Under these conditions, the realism of the first peak is perhaps questionable, but the second peak should be realistic.

Time histories for the light transport encountering the altitude-dependent Logan and Kennedy shears are shown in Figs. IV-9 and IV-10, respectively. The general trend of aircraft behavior is similar to that in the range-dependent encounters, although the details vary due to the shear/vehicle interaction of the altitude-dependent shears. Thus in the altitude-dependent Kennedy shear encounter, a 10 kt headwind decrease occurs in 10 sec near 300 ft; while in the range-dependent Kennedy shear, the same 10 kt headwind decrease requires almost 20 sec. This higher shear rate is typical of the effects that occur in the altitude-dependent shears, and is the cause of the greater deviation from the glide slope for all four aircraft for these shears.

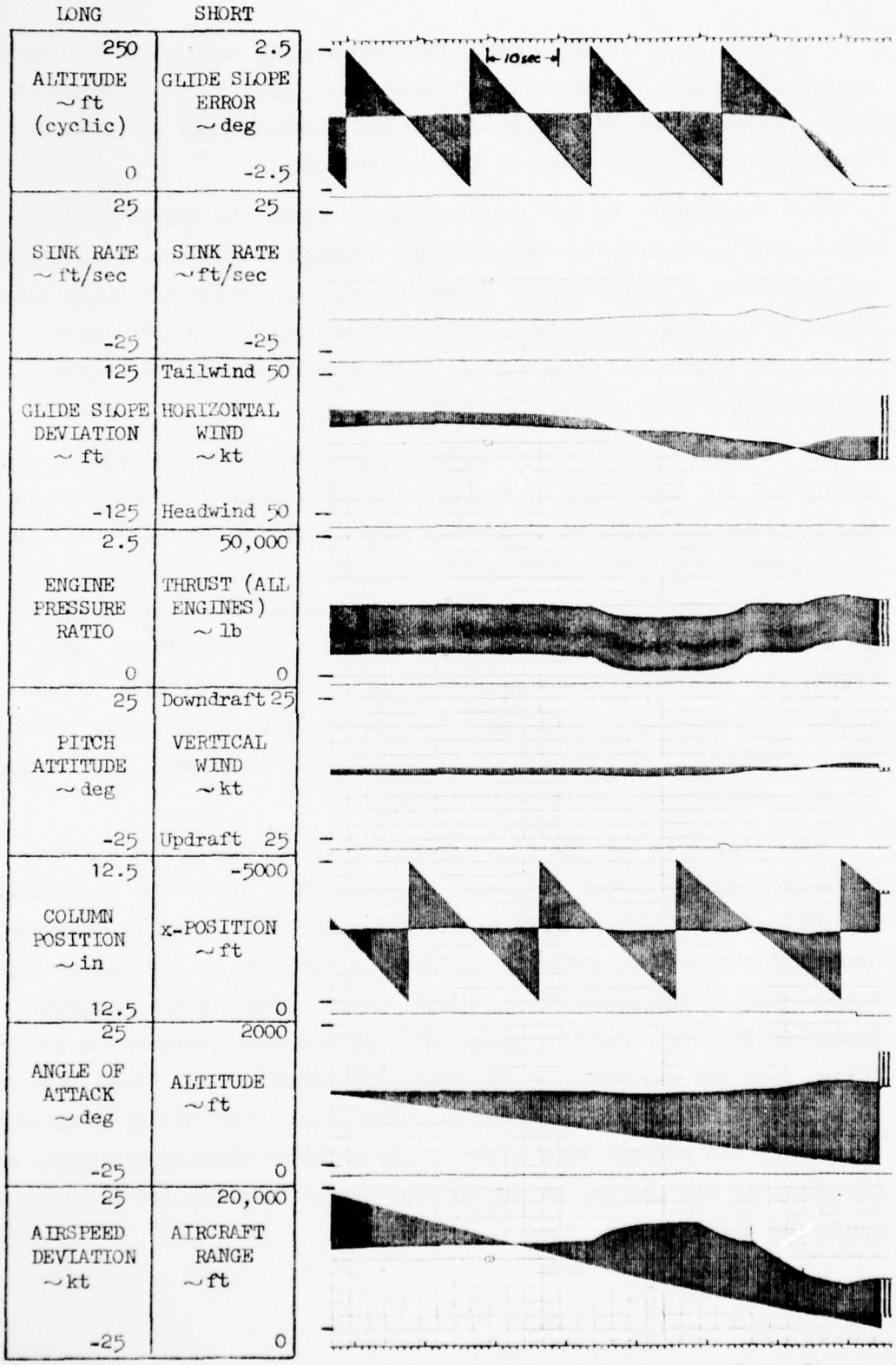

Figure IV-9. Time Histories for the Light Transport in the Logan Shear (Altitude-Dependent)

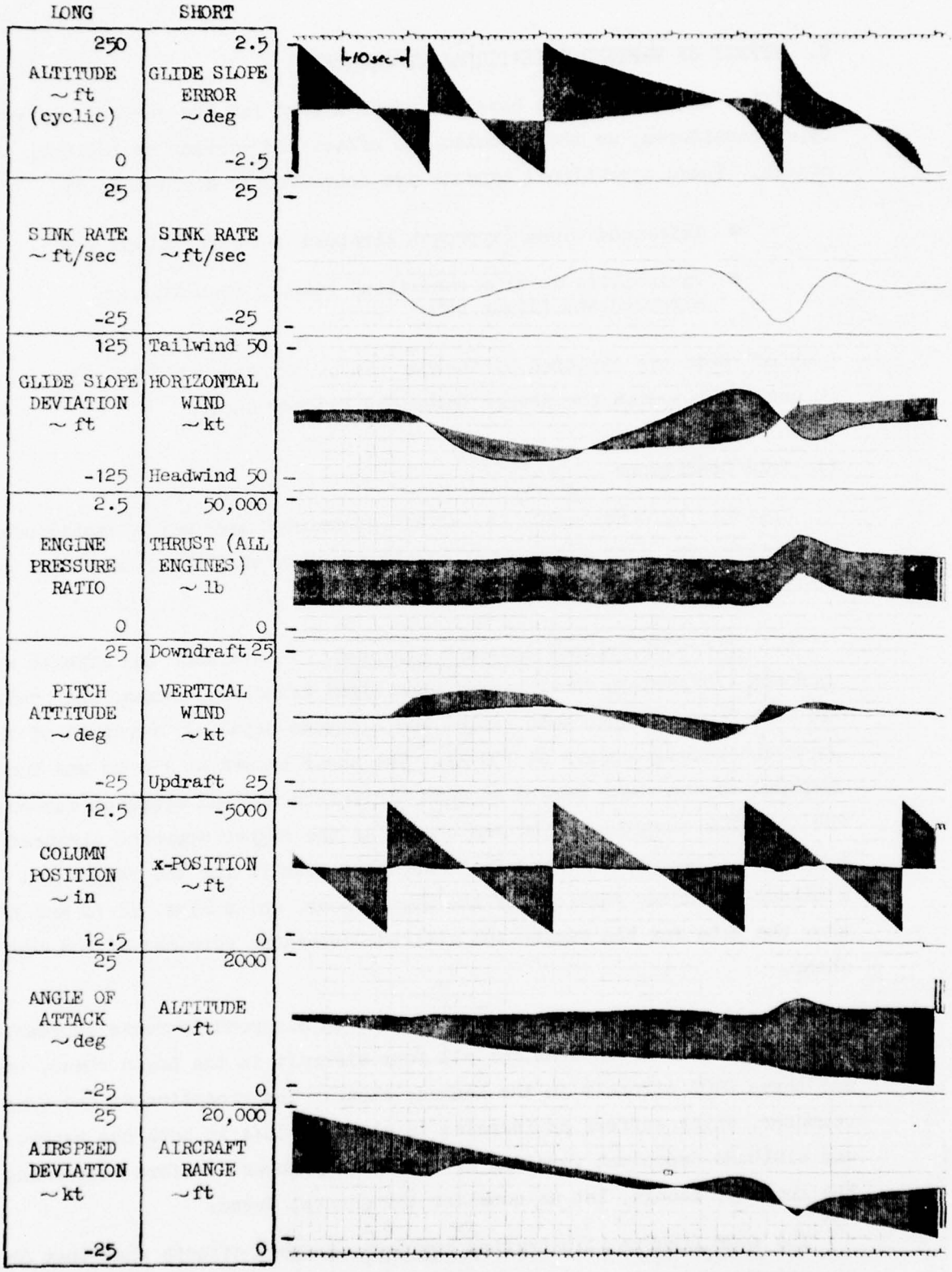

Figure IV-10. Time Histories for the Light Transport in the Kennedy Shear (Altitude-Dependent)

C. EFFECT OF VARYING OPERATIONAL TECHNIQUES

After determining the baseline shear hazard for the various aircraft types considered, we then studied the effects of varying operational techniques. These operational aspects are conveniently divided into:

- Trim conditions (approach airspeed and glide slope angle)
- Variability in trim conditions (manual regulation of airspeed and flight path)

Both of these are explored by further use of the shear hazard metric Δh_{max} in conjunction with the severe Logan and Kennedy shears.

1. Trim Conditions

We begin by considering the effect of trimmed approach airspeed because it involves the most fundamental relationship to wind shear hazard as we shall explain.

a. Effect of Trimmed Approach Airspeed. To evaluate the effects of approach airspeed on shear hazard, the light transport, jumbo, and business jet were flown through both range- and altitude-dependent versions of the Logan and Kennedy shears at 150 kt. The shear hazard at 150 kt was then compared to the shear hazard at each aircraft's nominal approach airspeed. For the STOL commuter, 80 kt was chosen as the higher approach airspeed to evaluate. Figures IV-11 and IV-12 show the results for the range- and altitude-dependent versions of the Logan shear, while Figs. IV-13 and IV-14 show the data for the range- and altitude-dependent versions of the Kennedy shear.

For all but one case the trend is that an airspeed increase decreases shear hazard. This is true for all four aircraft in the Logan shear, and all three CTOL aircraft in the Kennedy shear. The exception is the STOL commuter, which suffers an increase in altitude loss in both the range- and altitude-dependent versions of the Kennedy shear. Before addressing the anomaly, though, let us consider the general trend.

The four figures illustrating approach airspeed effects show that Δh_{max} for all the aircraft generally falls along an inverse speed trend line. To

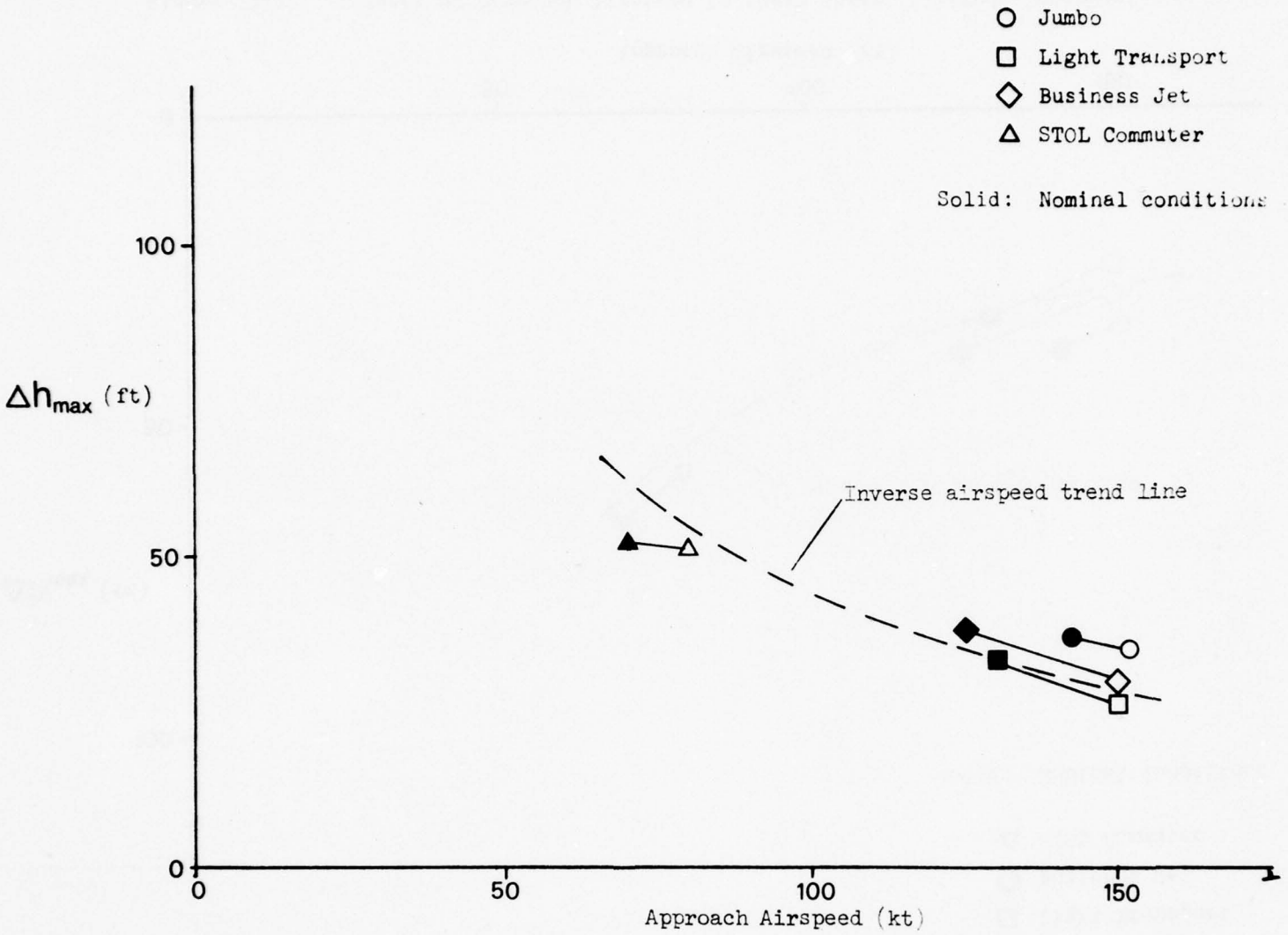

Figure IV-11. Effects of Approach Airspeed in Logan Shear (Range-Dependent)

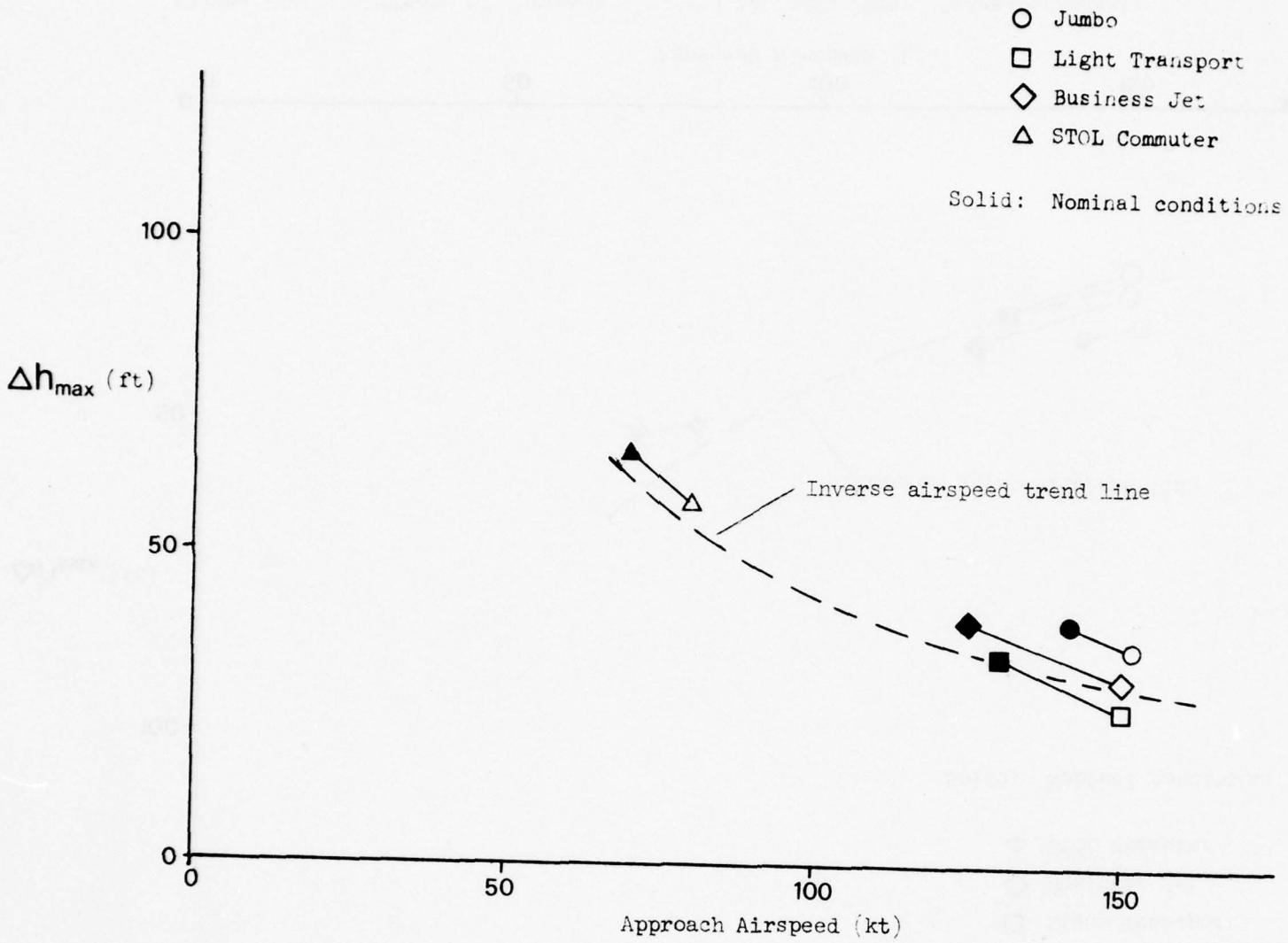

Figure IV-12. Effects of Approach Airspeed in Logan Shear (Altitude-Dependent)

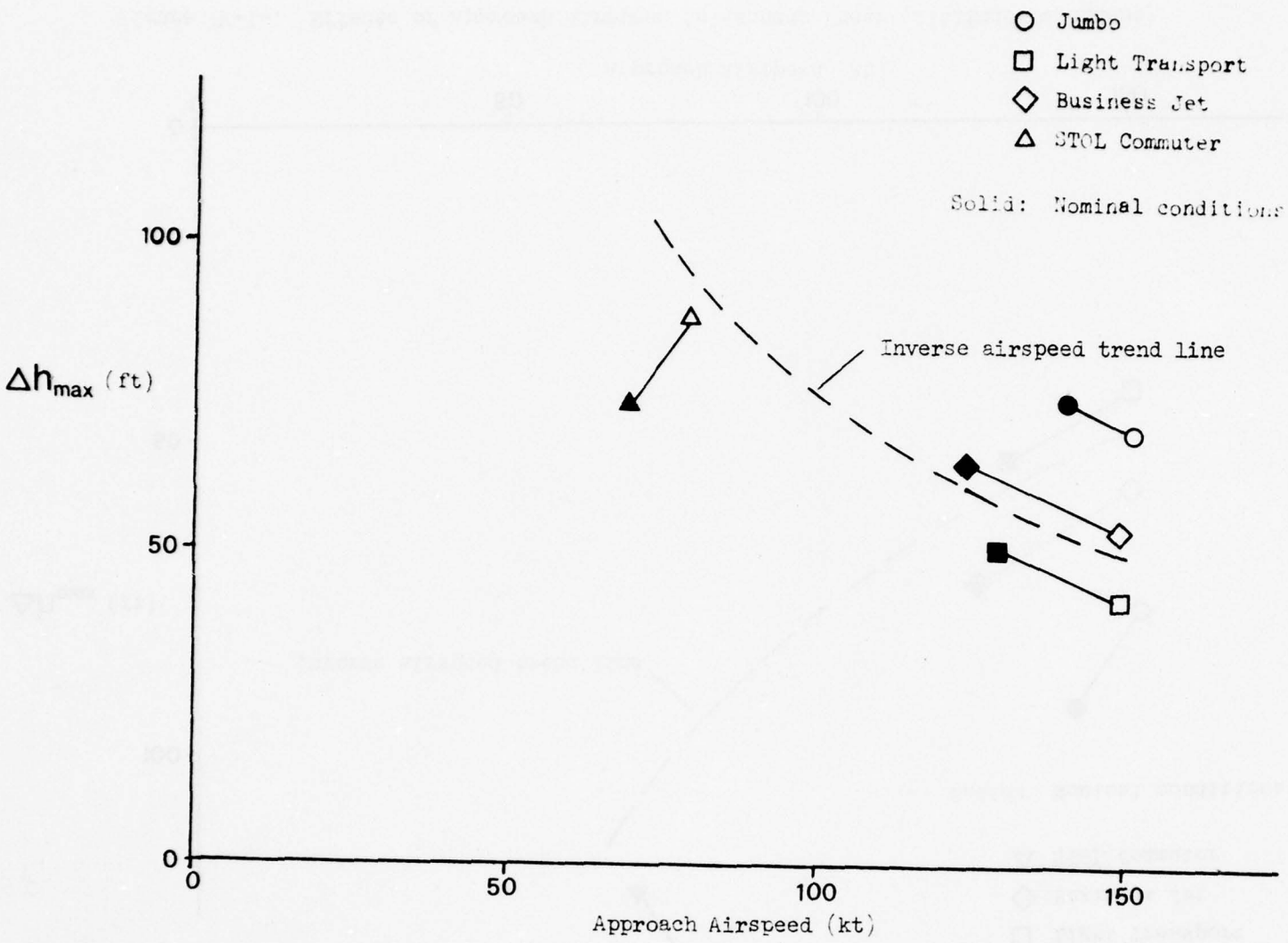

Figure IV-15. Effects of Approach Airspeed in Kennedy Shear (Range-Dependent)

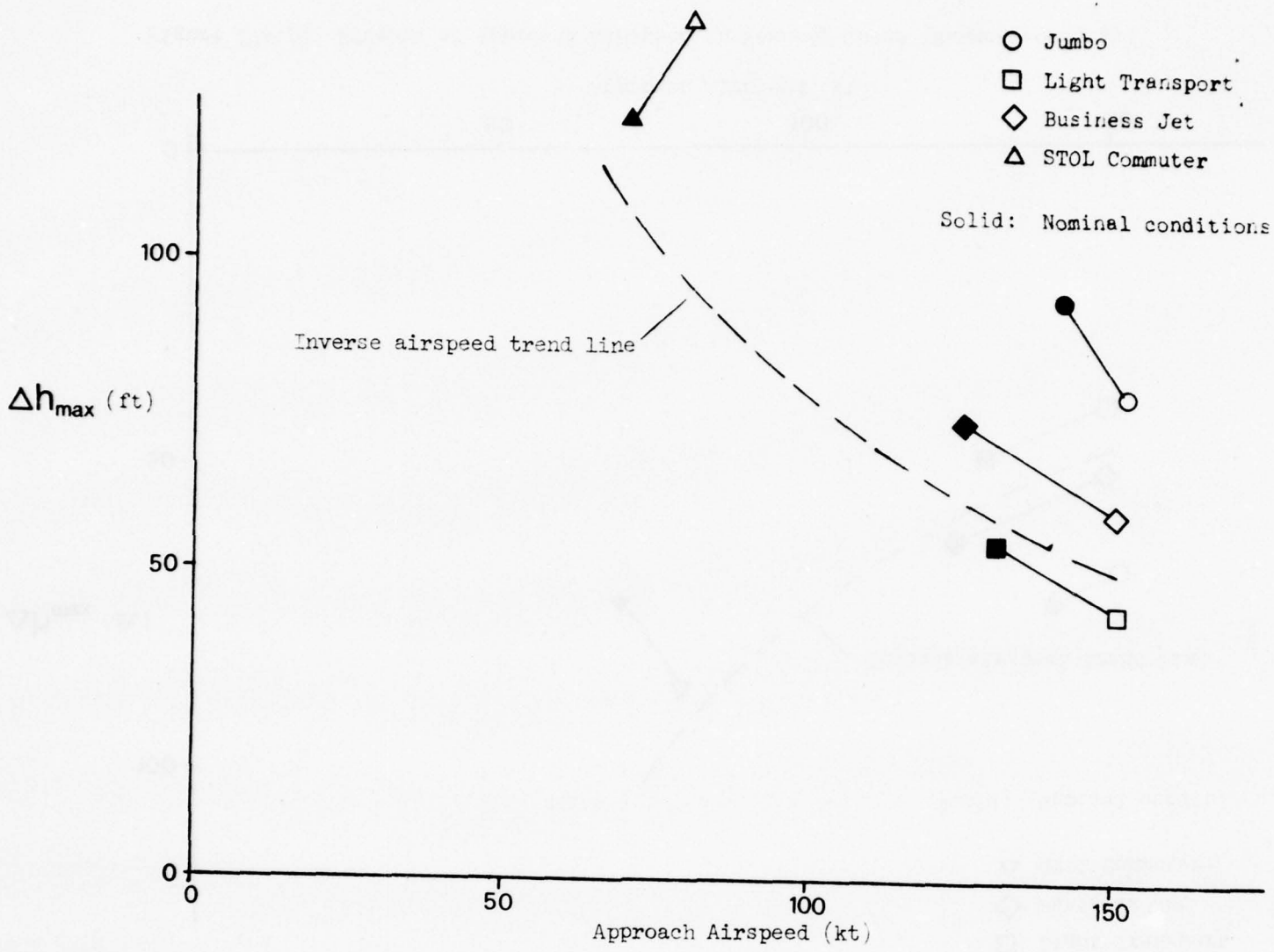

Figure IV-14. Effects of Approach Airspeed in Kennedy Shear (Altitude-Dependent)

explain this phenomenon we can utilize a feature of linear analysis. Recall from the previous section that the stability derivatives which relate incremental normal acceleration to velocity increments of tailwind (u_g) and downdraft (w_g) are Z_u and Z_w, respectively. Considering the sensitivity to horizontal gust components, we should expect to see that the size of an altitude change corresponds to the magnitude of Z_u. This is precisely the trend we obtain since

$$Z_u \doteq -\frac{2g}{V}$$

i.e., Z_u is inversely proportional to airspeed as is the resulting altitude excursion, Δh_{max} for nearly all cases simulated.

The correlation of altitude excursion with airspeed is an important result for it establishes the basic first order effect of a given wind shear on nearly any conventional airplane (which includes the STOL commuter).

The counter example to the general effect of airspeed on shear hazard is the STOL commuter in the Kennedy shear (Figs. IV-13 and IV-14). The source of the anomaly can be traced first to the vertical gust upset which was present in the Kennedy shear and not the Logan shear. In addition, there is an increased sensitivity of the STOL commuter to vertical gusts which is related to a pilot-vehicle interaction.

The STOL commuter pilot-vehicle combination is inherently more sensitive to vertical gusts than the CTOL examples because of a strong flight path-to-airspeed cross coupling quality which produces a low damping ratio oscillatory mode when the flight path loop is closed. This difference is directly related to the effective thrust angle which is 45 deg for the STOL commuter and nearly zero for the CTOL examples. Figure IV-15 shows how the cross coupling effect manifests itself when excited by a step w_g. The altitude excursion is normalized with the closed loop flight path natural frequency (which reflects the precision of the flight path loop closure) and heave damping, Z_w. Thus, the normalized altitude excursion in Fig. IV-15 reflects a direct comparison of flight path-to-airspeed cross coupling and explains the high sensitivity of the STOL commuter to vertical gusts.

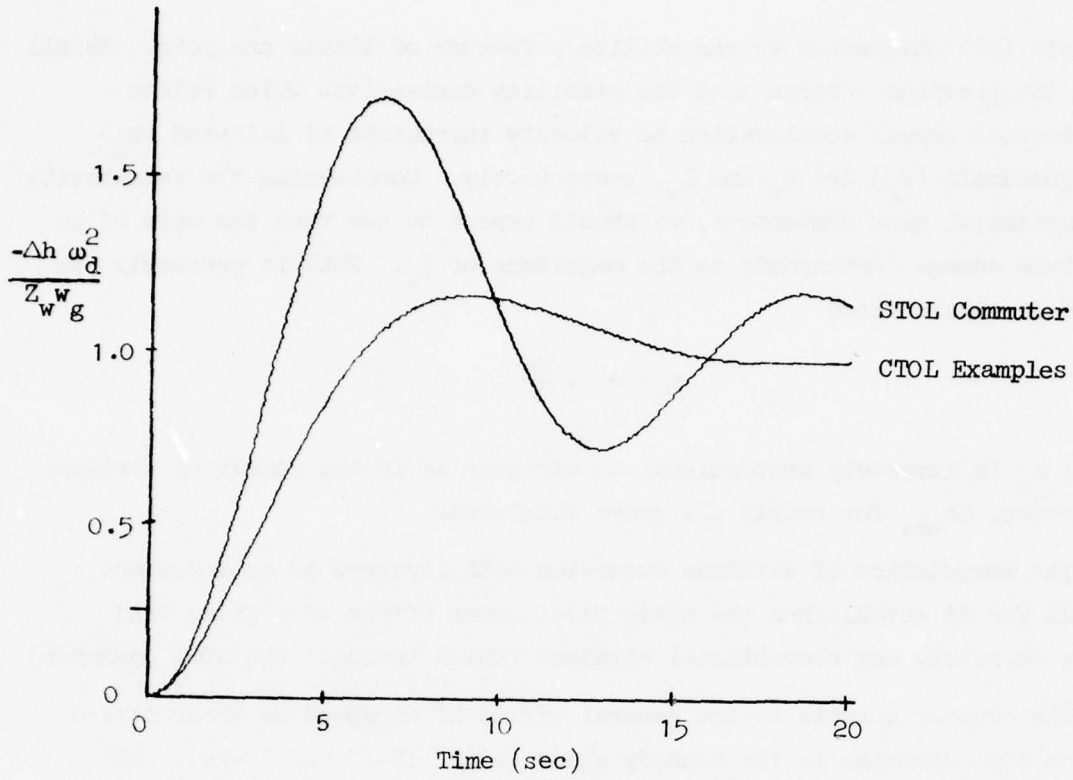

$\omega_d \triangleq$ closed loop flight path mode natural frequency

$Z_w \triangleq$ heave damping stability derivative

Figure IV-15. Normalized Altitude Response of Aircraft to a Vertical Gust Step Function

The reason for the STOL's increased shear hazard at 80 kt is attributable to the increased heave damping, Z_w, which is proportional to airspeed.

To sum up the results, then, the major contributor to wind shear hazard is the horizontal gust sensitivity, Z_u, which is inversely proportional to airspeed. This explains the gross difference in hazard between the slower STOL commuter and the faster CTOL aircraft and the difference for increased approach speeds in the CTOL aircraft alone. However, where a significant vertical gust component is involved, the STOL commuter does not necessarily enjoy the reduction in hazard due to increased airspeed.

b. Effects of Glide Slope Angle on the STOL Commuter Aircraft. The effects of glide slope angle on shear hazard were tested for the STOL commuter aircraft using a three and six deg glide slope. The aircraft model was slightly modified for this series of tests. As we shall discuss shortly, the thrust offset of the STOL commuter appeared unrealistically large and resulted in a large adverse effect on Δh_{max}. In order to prevent thrust offset from dominating the study of glide slope angle, the offset was nulled (by setting the thrust line coincident with the cg).

The data for the Logan shear, both range- and altitude-dependent, are shown in Fig. IV-16 and the data for the Kennedy shear, both range- and altitude-dependent, in Fig. IV-17. The results do not show a consistent trend. In the Logan shear, use of a 3 deg glide slope reduces the shear hazard by a factor of one-half. In the Kennedy shear, the effect of glide slope variation is small compared to the effect of shear dependency.

To explain these results it is useful to refer to the closed loop frequency response plots from Section III (Fig. III- 6). The STOL commuter $\Delta h/u_g$ frequency response is fairly sharply tuned to a frequency of approximately 0.5 rad/sec. For a shear cycle which occurs over a height of, say, 500 ft and an average sink rate of 10 ft/sec, the dominant spectral power would be centered at about $2\pi \cdot \frac{10}{500}$ or 0.12 rad/sec. Therefore, if we were to approach at one-half the sink rate, or 5 ft/sec, the dominant spectral power of the disturbance would shift downward to 0.06 rad/sec. The slope of the $\Delta h/u_g$ frequency response at low frequencies would predict an attenuation of Δh equal to the spectral shift. This is precisely the

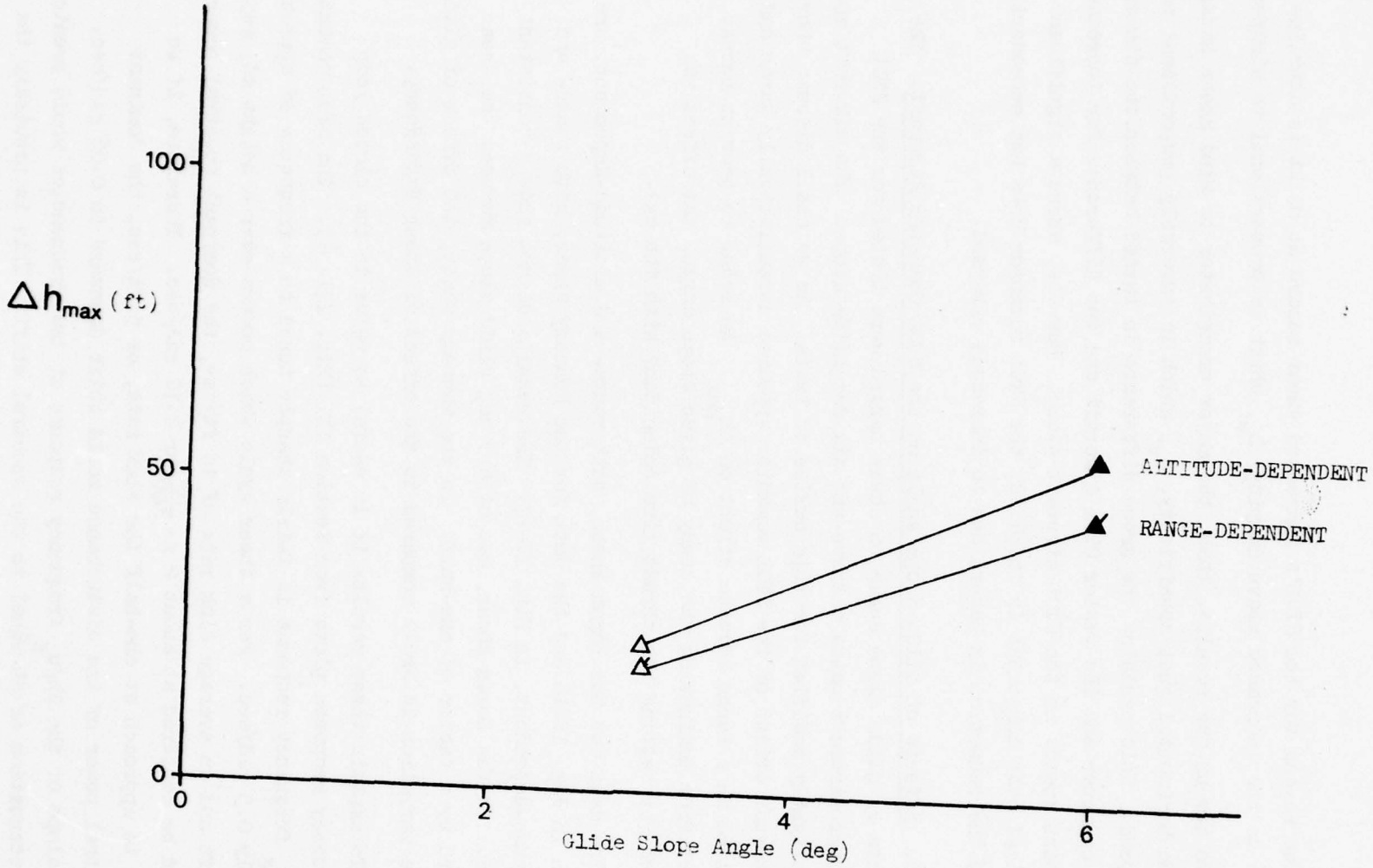

Figure IV-16. Effect of Glide Slope Angle on STOL Commuter in Logan Shear

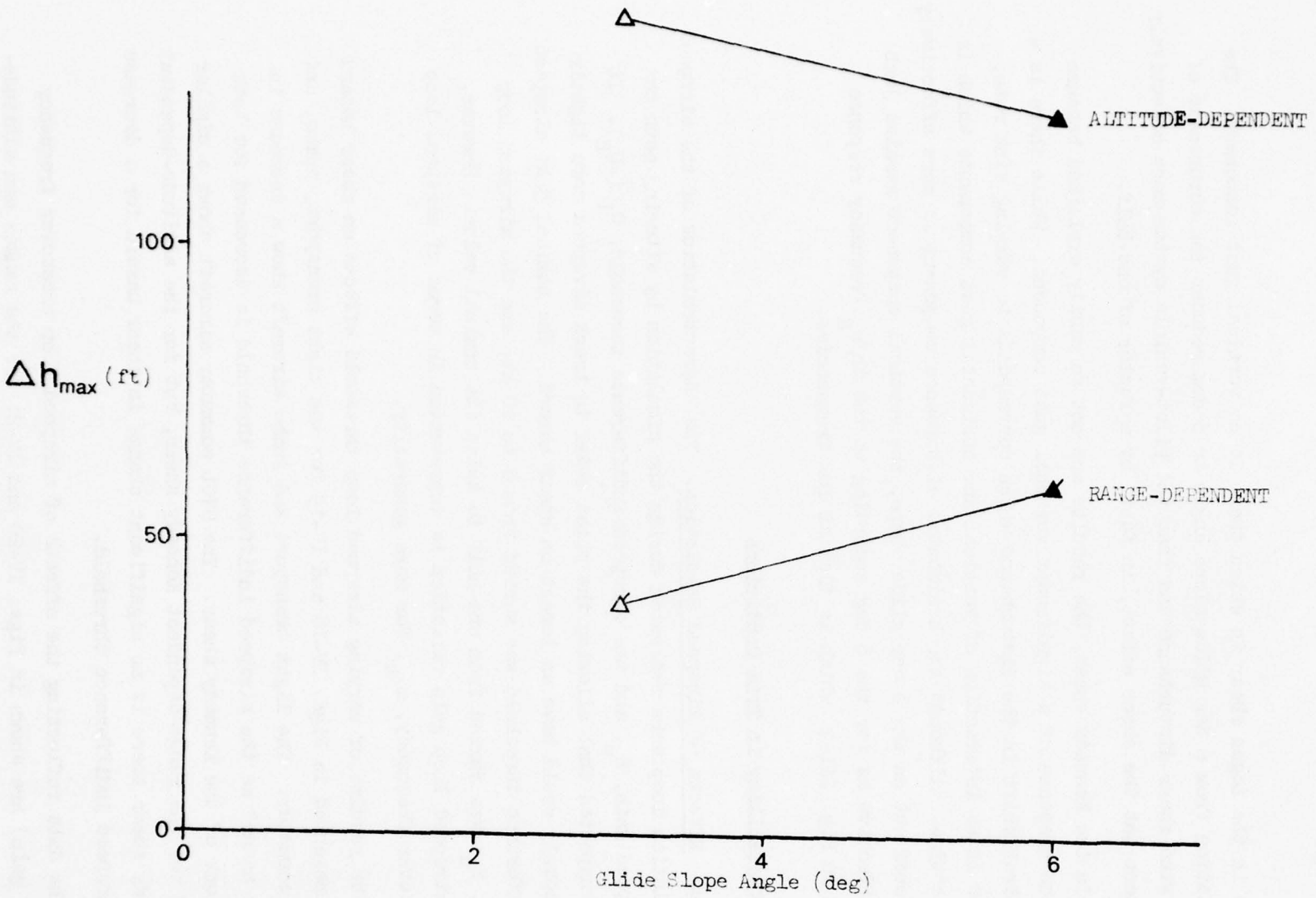

Figure IV-17. Effect of Glide Slope Angle on STOL Commuter in Kennedy Shear

case in the Logan shear in which there is no vertical gust component. The variation from 6 deg glide slope angle to 3 deg reduces the abruptness of the wind shear disturbance and thus the pilot-vehicle system more effectively filters out the shear effect, in fact, by a factor of one-half.

In the Kennedy shear, the results are not so easily explained because of the presence of a significant vertical gust component. While there is a spectral shift in the disturbance which corresponds to varying sink rate, there is an interaction of vertical and horizontal gust components which is offsetting. Although the horizontal disturbance component is more effectively filtered out on the 3 deg glide slope, the vertical component remains just as effective as for the 6 deg according to the $\Delta h/w_g$ frequency response plot in Fig. III-7 which is flat at low frequencies.

2. Variability in Trim Conditions

a. Effects of Airspeed Regulation. The characteristics of the airspeed regulation loop were evaluated during the simulation by altering both the airspeed gain, K_u, and the airspeed indifference threshold, U_L ($=U_H$). It was suspected that allowing the pilot model to track airspeed more tightly or loosely could have an impact on shear hazard. The nominal 5 kt airspeed indifference threshold was varied from 0 to 10 kt, and the airspeed loop gain, K_u, was varied from one-half to twice its nominal value. However, the airspeed loop gain variation is represented in terms of airspeed loop crossover frequency, ω_{c_u}, for more generality.

The results of varying airspeed loop threshold effects on shear hazard are presented in Figs. IV-18 and IV-19 for the light transport, jumbo, and STOL commuter. The light transport and jumbo aircraft show a decrease in shear hazard as the airspeed indifference threshold is decreased for both versions of the Kennedy shear. The STOL commuter aircraft shows a similar trend for the range-dependent Kennedy shear, but for the altitude-dependent Kennedy shear there is no significant change in shear hazard for a decrease in airspeed indifference threshold.

The data reflecting the effects of airspeed loop crossover frequency (loop gain) are shown in Figs. IV-20 and IV-21 for the range- and altitude-dependent versions of the Kennedy shear. Data are shown only for the light

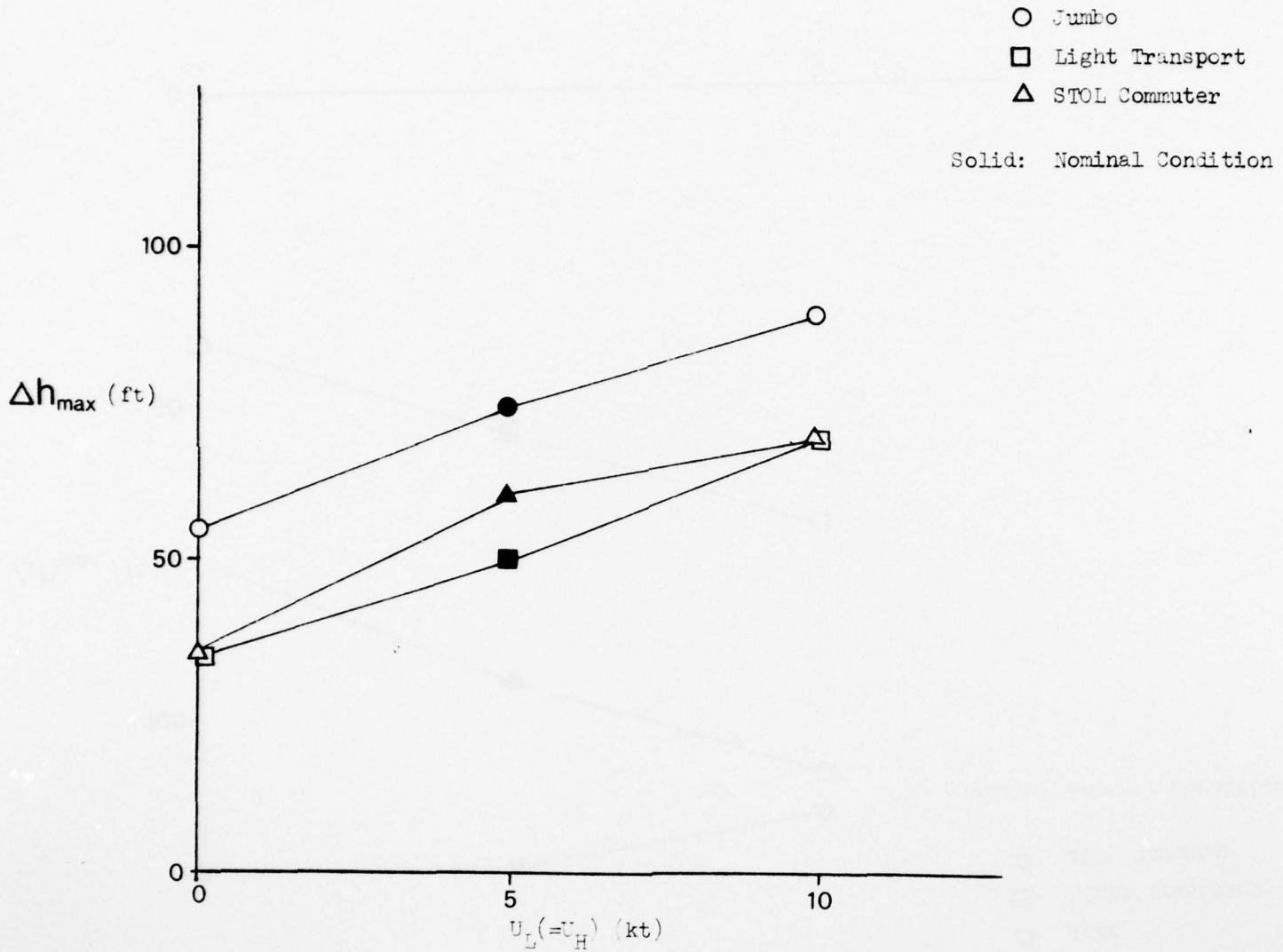

Figure IV-18. Effects of Airspeed Threshold in Kennedy Shear (Range-Dependent)

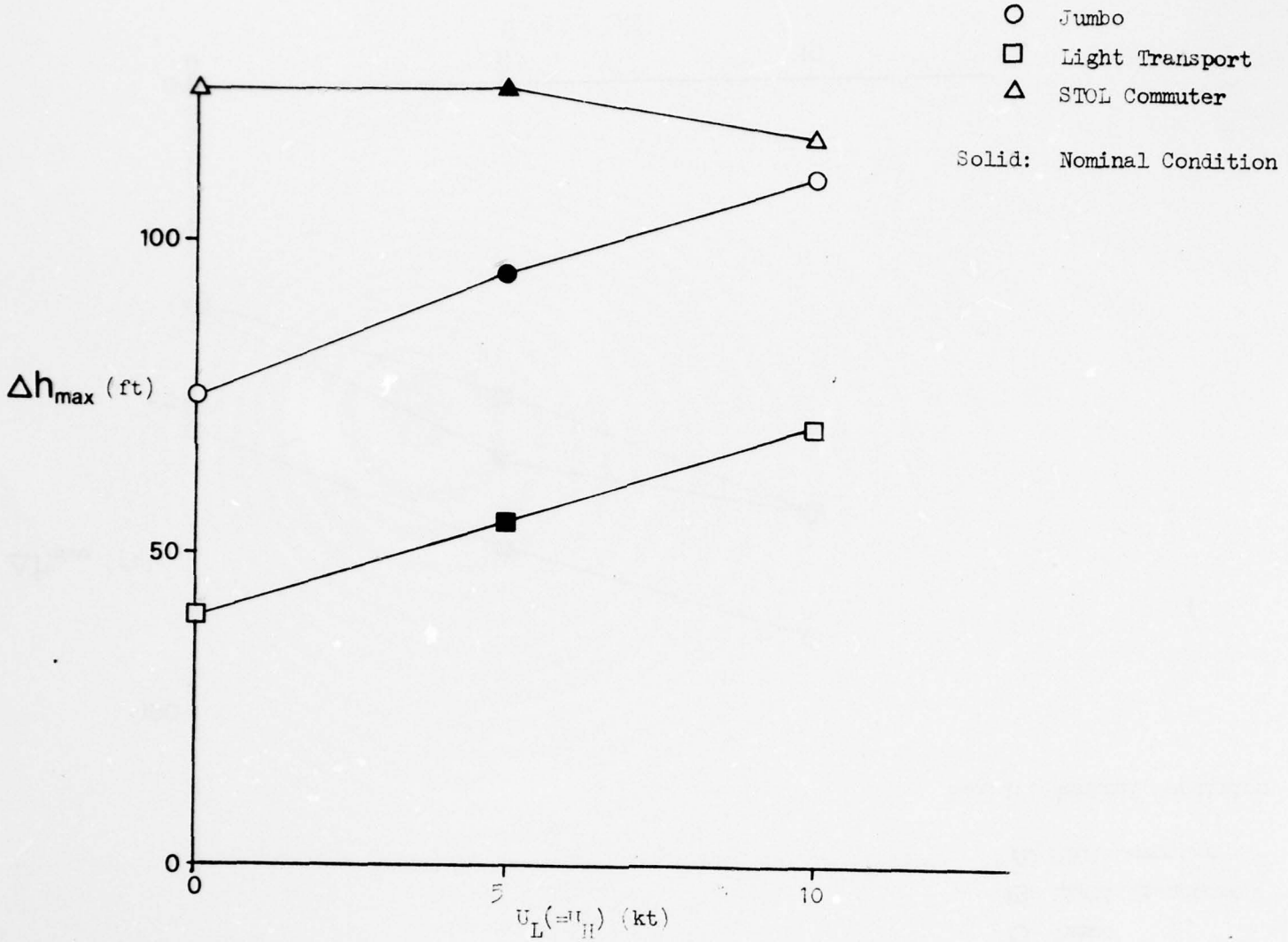

Figure IV-19. Effects of Airspeed Threshold in Kennedy Shear (Altitude-Dependent)

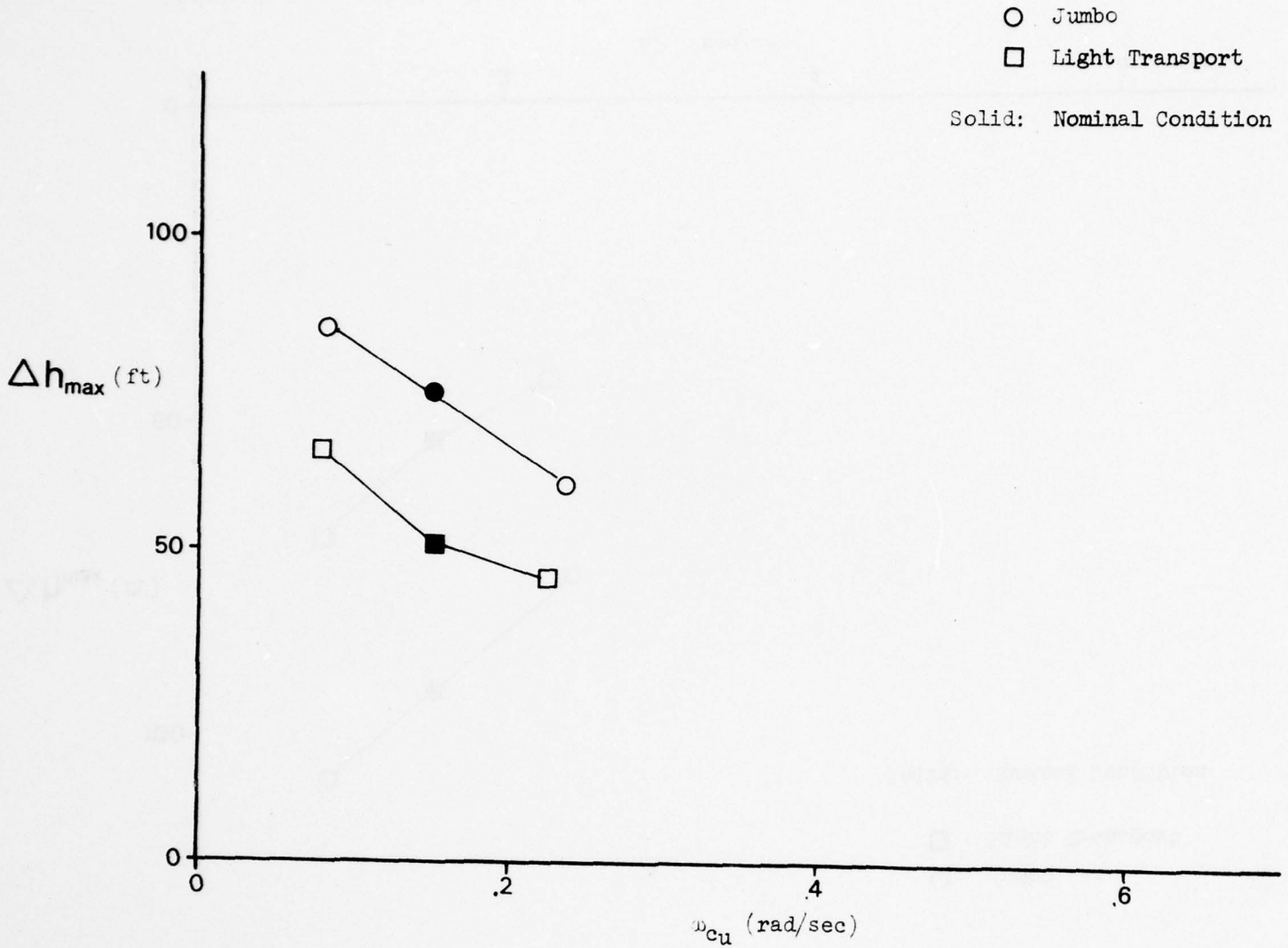

Figure IV-20. Effects of Airspeed Loop Crossover Frequency in Kennedy Shear (Range-Dependent)

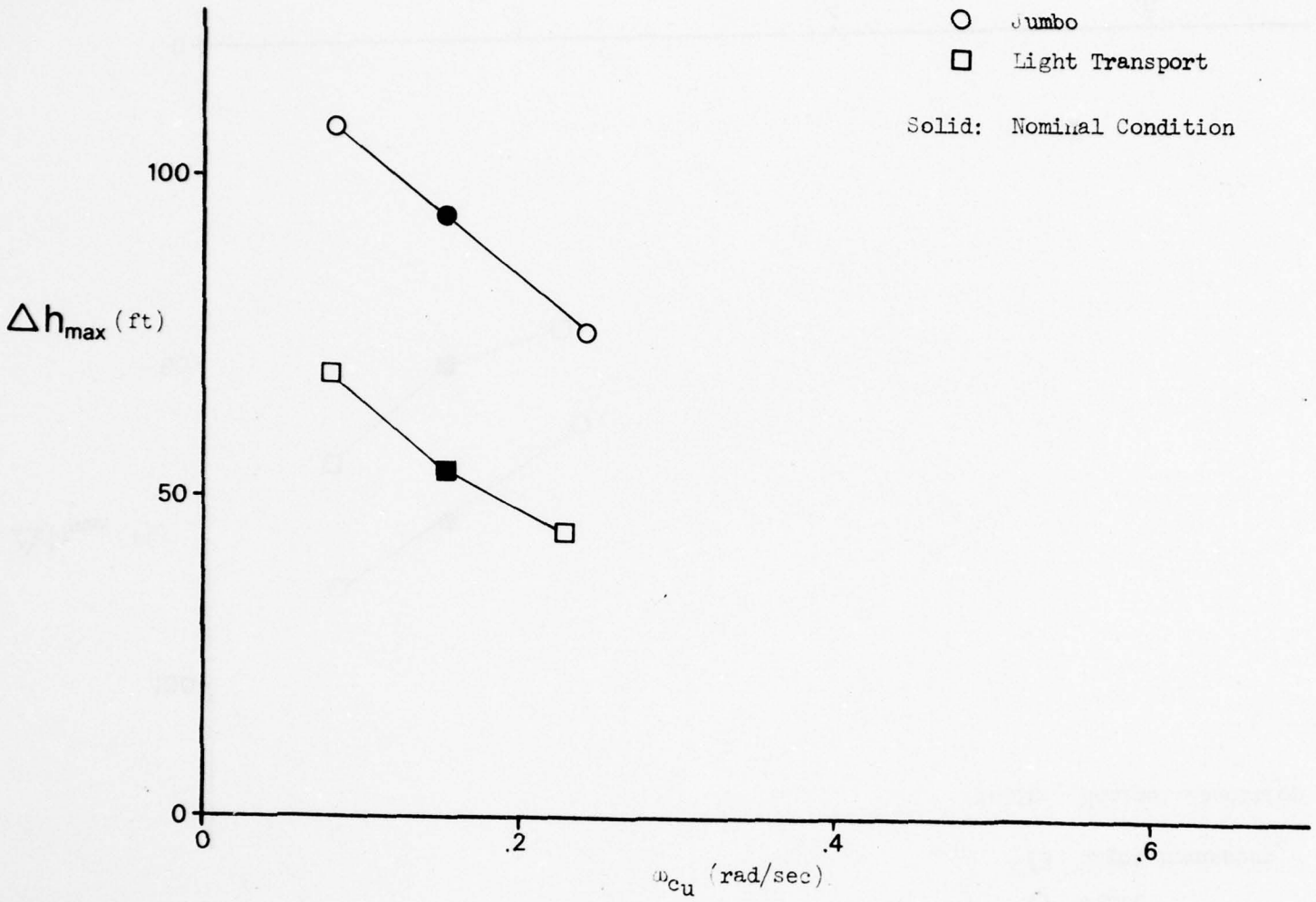

Figure IV-21. Effects of Airspeed Loop Crossover Frequency in Kennedy Shear (Altitude-Dependent)

transport and jumbo aircraft. The STOL commuter airspeed loop dynamics would not permit a simple doubling or halving of the airspeed loop gain without a departure from the loop closure rules adopted, therefore it was dropped in this case. The plotted data in Figs. IV-20 and IV-21 show that for the light transport and jumbo aircraft the precision of speed regulation has a strong effect on shear hazard. With tighter control of airspeed during the shear encounter, less lift is lost, and the subsequent glide slope deviation is reduced.

The data for the effects of airspeed threshold and airspeed loop gain are consistent in that they reflect the fact that an increase in the precision of airspeed regulation results in a reduction of shear hazard for the light transport and jumbo aircraft. It appears that either decreasing the airspeed indifference threshold or increasing the airspeed loop gain are roughly equivalent ways of increasing airspeed regulation although both imply markedly increased concentration of attention (and devotion of workload) to airspeed regulation by a human pilot.

b. Effects of Flight Path Regulation. Since the shear hazard metric used in this study was defined to be aircraft deviation from the glide slope, it is reasonable to expect the shear hazard to vary as a function of how tightly the pilot closes a flight path loop. During the simulation, flight path loop tightness was adjusted by changing the value of the parameter K_d in the flight path loop. The light transport, jumbo, and STOL commuter were flown through range- and altitude-dependent versions of the Kennedy shear with the values of K_d alternatively set to half and twice the nominal values. While K_d was the variable adjusted, it is more generally useful to present the data in terms of flight path loop crossover frequency, ω_{c_d} (i.e., closed loop system bandwidth). The data for the range- and altitude-dependent Kennedy shear is shown in Figs. IV-22 and IV-23, respectively. The higher crossover frequency of 0.5 rad/sec represents a workload increase by a human pilot that, while high, is certainly attainable, especially in later stages of the approach. A crossover frequency of 0.15 rad/sec might be used in early stages of the approach prior to a sensitive glide slope indication.

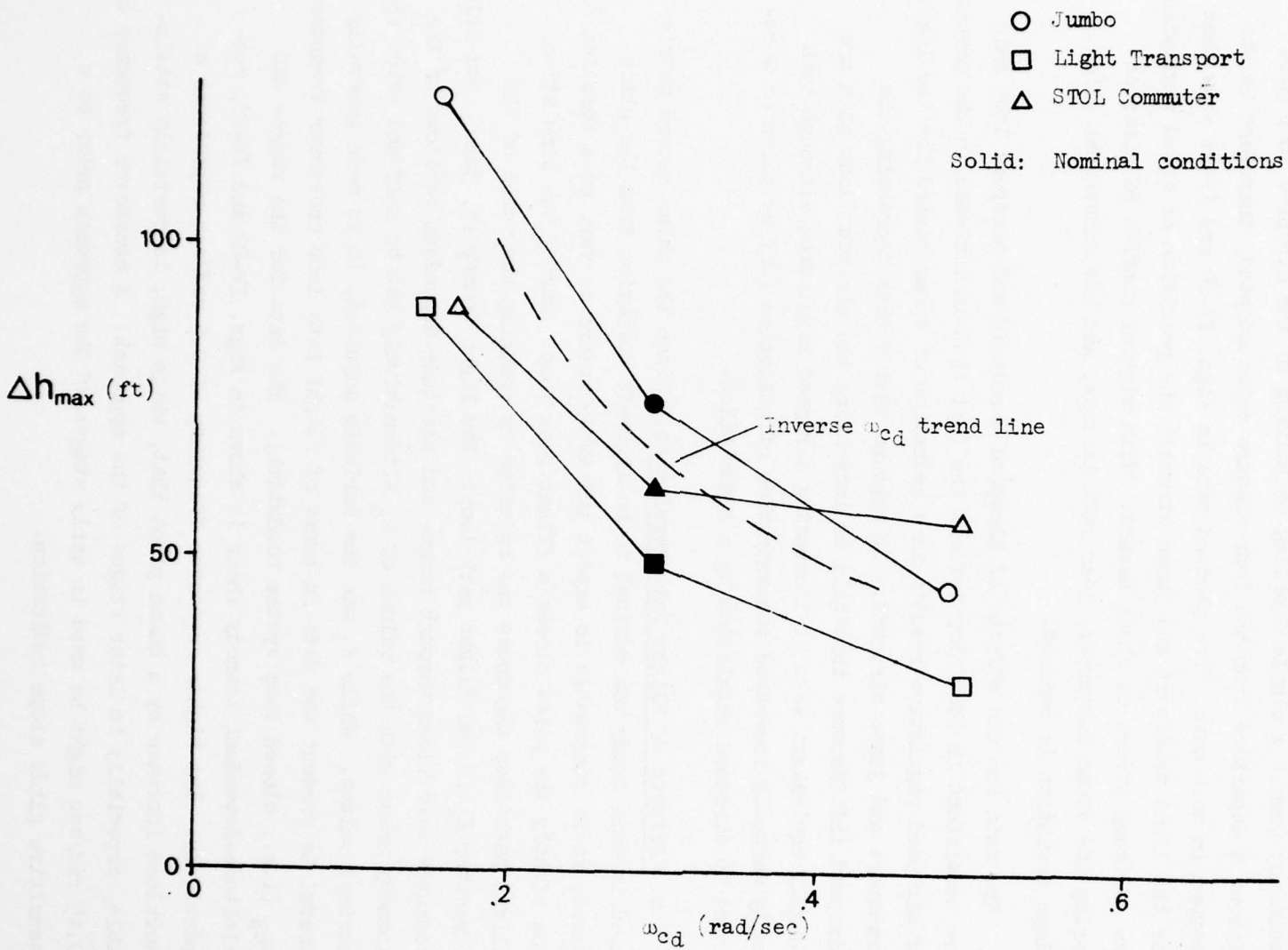

Figure IV-22. Effects of Flight Path Loop Crossover Frequency in Kennedy Shear (Range-Dependent)

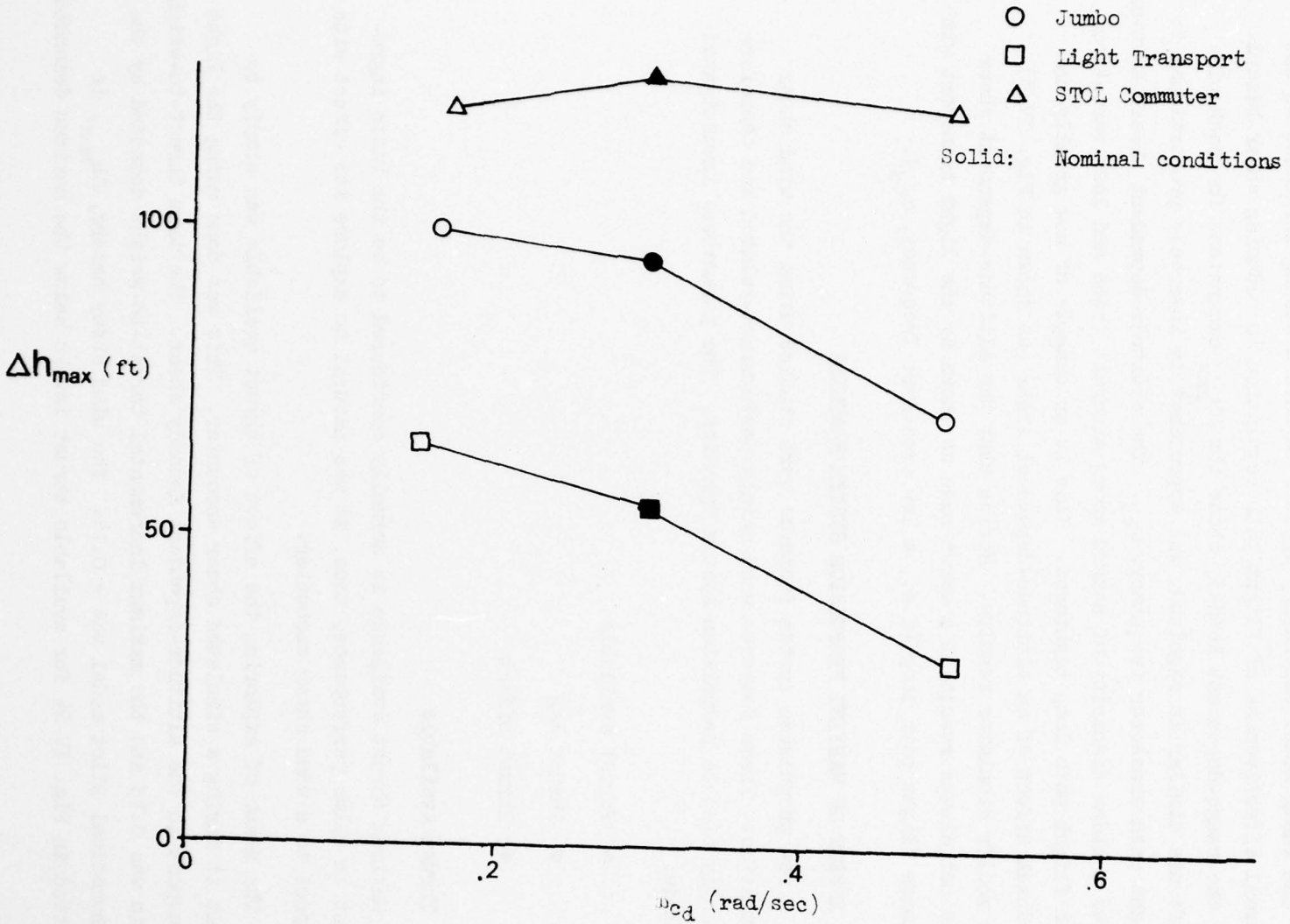

Figure IV-23. Effects of Flight Path Loop Crossover Frequency in Kennedy Shear (Altitude-Dependent)

The shear model dependency appears to have a strong influence on the overall effectiveness of flight path regulation in reducing shear hazard. For the range-dependent Kennedy shear the Δh_{max} excursions for each aircraft are similar in magnitude and approximately inversely proportional to flight path crossover frequency, ω_{cd}. The altitude-dependent shear, however, shows a wider disparity of hazard among aircraft types and less variation with flight path loop tightness. This is an example of how greatly the feedback effect of an altitude-dependent shear (as shown in Fig. IV-3) can modify simulator results. Notice that the altitude-dependent shear does not always result in a worst case as shown by the light transport with a loose flight path loop (i.e., a low crossover frequency, ω_{cd}).

D. EFFECT OF VARYING PROPULSION SYSTEM FEATURES

A few propulsion system features were studied using the wind shear simulation. These features were mainly performance-related and therefore strongly tied to propulsion system dynamics. The parameters investigated include:

- Thrust available
- Thrust lag
- Thrust offset.

1. Thrust Available

Maximum thrust available is normally considered to be the basic ingredient in climb performance, thus, it was natural to explore its effect with respect to a wind shear encounter.

The means of exploring the effect of thrust available was simply to limit it during a simulated shear encounter. This was done using the light transport in the altitude-dependent Kennedy shear. The trim thrust-to-weight ratio was 0.15 and the maximum incremental thrust-to-weight demanded by the mathematical pilot model was + 0.14. The wind shear hazard, Δh_{max}, is plotted in Fig. IV-24 for available thrust levels below the maximum demanded.

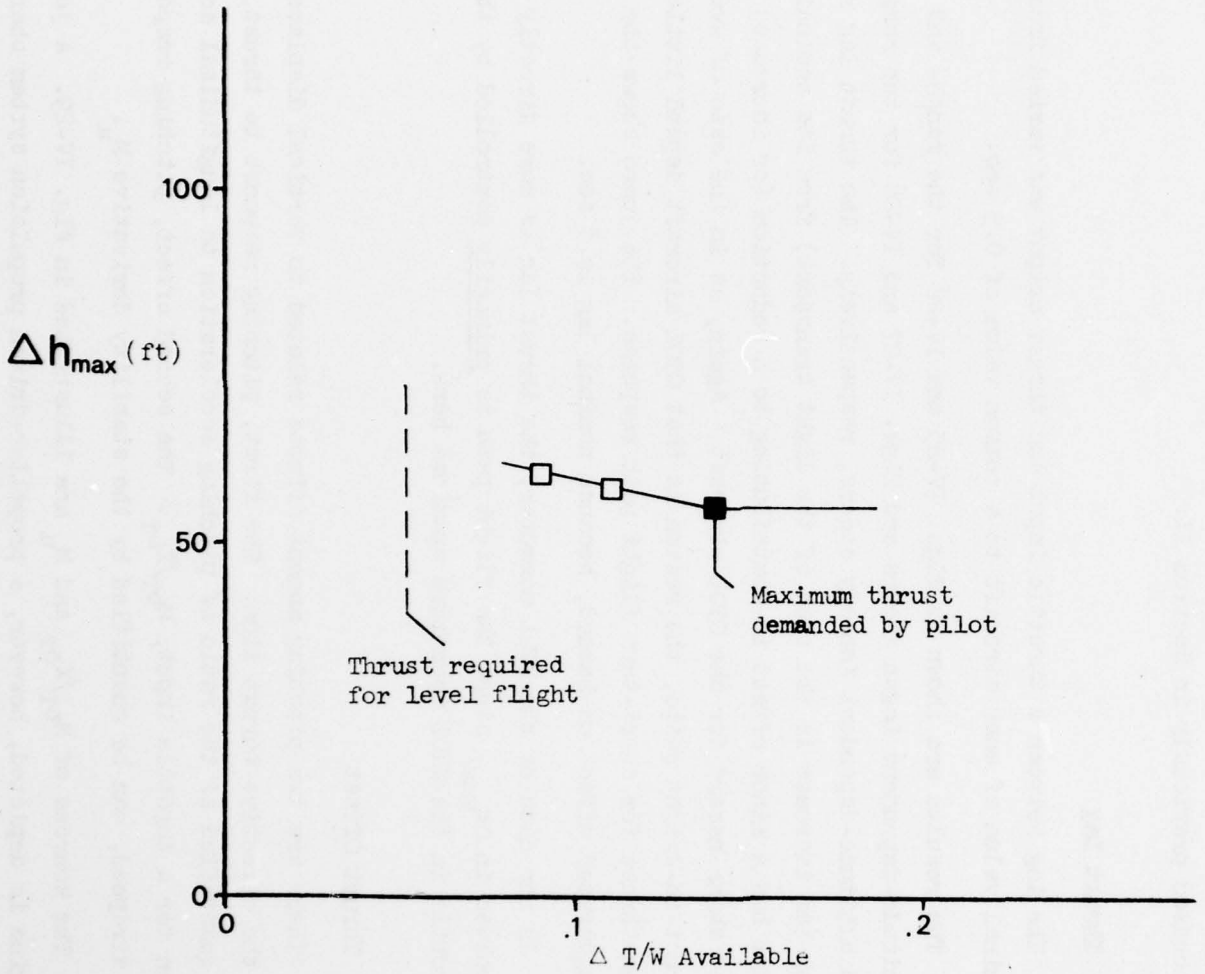

Figure IV-24. Effects of Available Thrust-to-Weight Ratio for Light Transport in Kennedy Shear (Altitude-Dependent)

The results of this investigation show that limited thrust-to-weight ratio has a minor effect in contributing to an increase in wind shear hazard in the case studied. The reason for this is that the CTOL aircraft depend little upon thrust for short-term flight path response. Instead, thrust is modulated in a longer term context to preserve adequate trimmed airspeed and thus to insure effective short term flight path response via attitude control acting through the airspeed-heave damping product $U_o Z_w$ discussed previously in Section II.

2. Thrust Lag

The lag between a throttle input and thrust output was varied from the nominal value of each aircraft to a common value of 0.5 sec.

The results are shown in Figs. IV-25 and IV-26 for the range- and altitude-dependent Logan shears and Figs. IV-27 and IV-28 for the range- and altitude-dependent Kennedy shears, respectively. The thrust lag reduction (or increase in the case of the light transport) from its nominal value has a minor effect in contributing to a reduction (or increase) in wind shear hazard for the CTOL aircraft. Again, as in the case of available thrust-to-weight ratio, the reason is that CTOL aircraft depend little upon thrust for short-term flight path response. The jumbo shows the most exaggerated effect on hazard, because nominal lag is 3 sec.

In the case of the STOL commuter, the thrust lag is more directly involved in Δh_{max}, since the flight path is <u>primarily</u> controlled by the throttle in the STOL technique examined here.

3. Thrust Offset

There are two pitching moment effects related to vertical displacement of the effective thrust line. The first, pitching response to thrust, can be quantified as the ratio of pitching acceleration to longitudinal acceleration for a throttle input, $M_{\delta_T}/X_{\delta_T}$. The second effect, pitching response to airspeed, can be quantified by the stability derivative M_u.

The sources of $M_{\delta_T}/X_{\delta_T}$ and M_u are illustrated in Fig. IV-29. A jet engine is depicted, however, a propeller-driven propulsion system shares

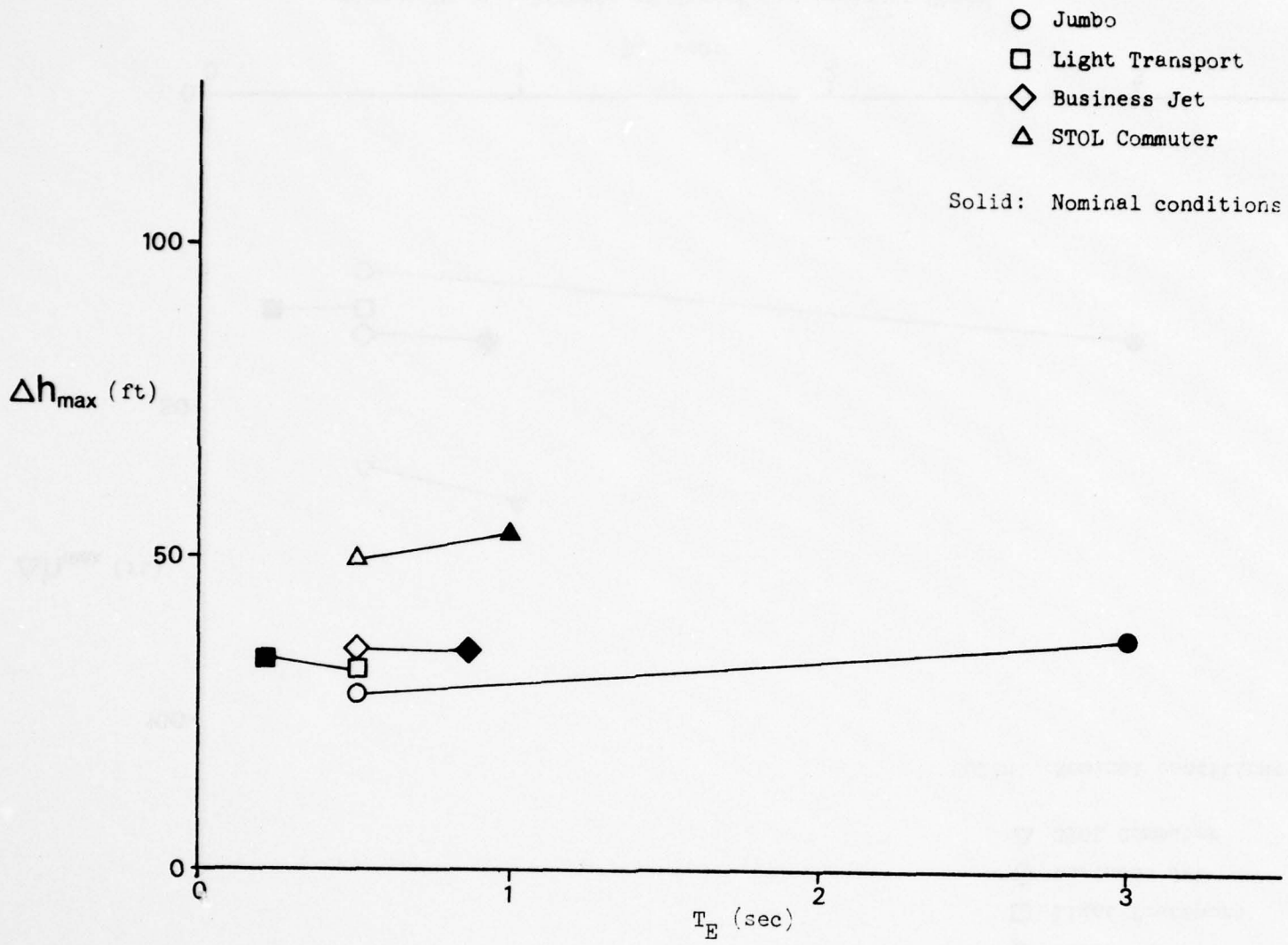

Figure IV-25. Effects of Thrust Lags in Logan Shear (Range-Dependent)

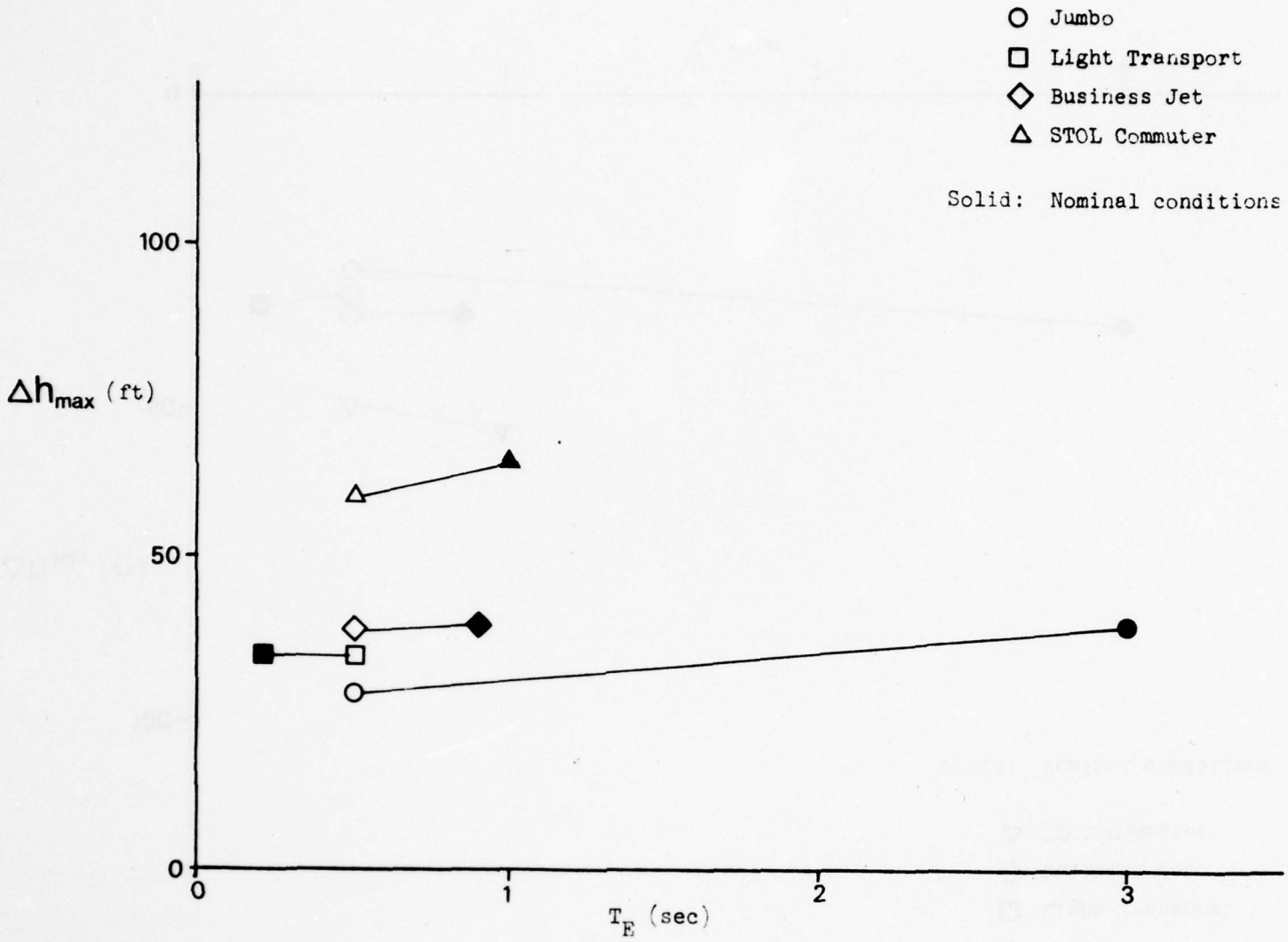

Figure IV-26. Effects of Thrust Lag in Logan Shear (Altitude-Dependent)

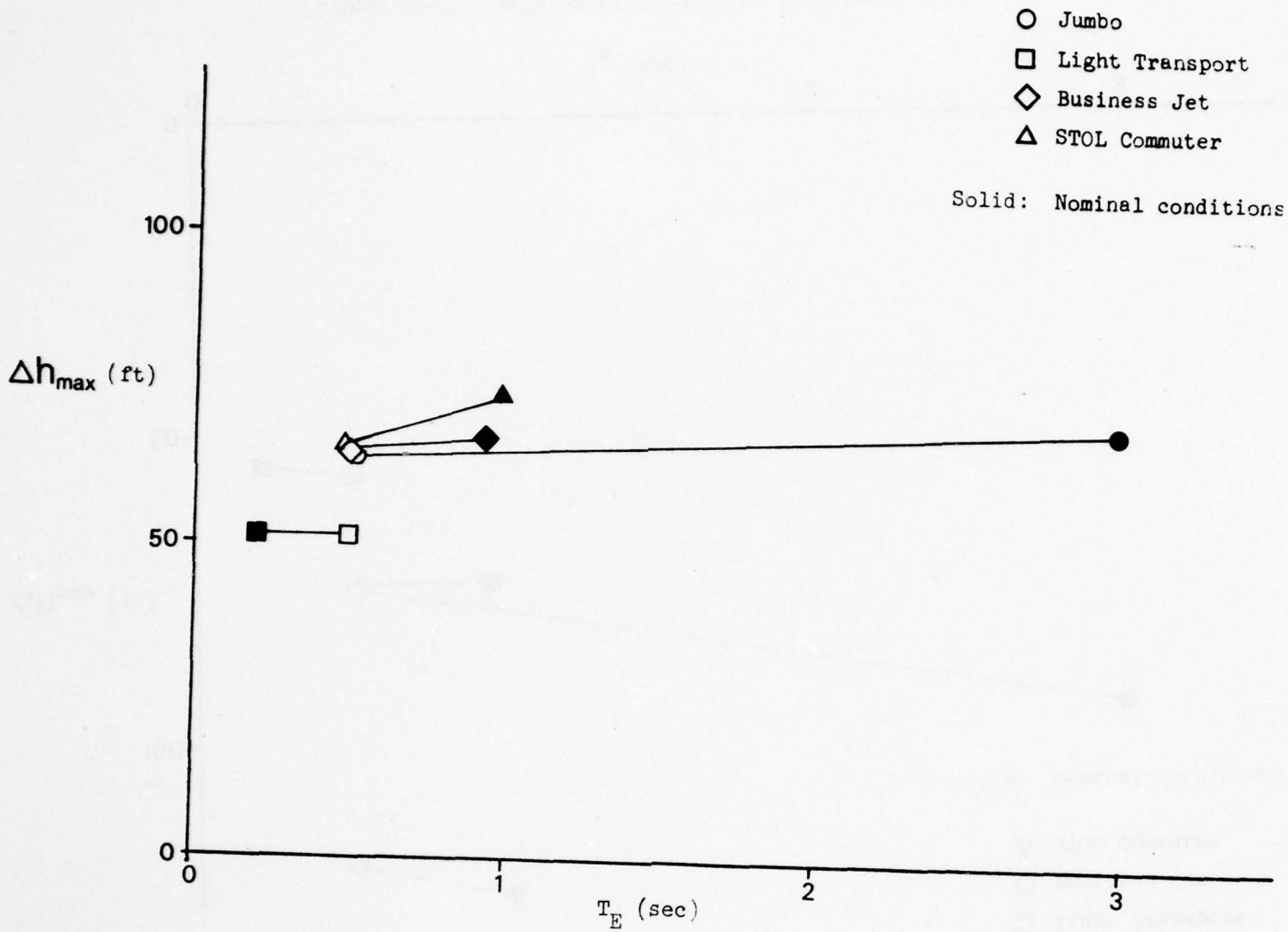

Figure IV-27. Effects of Thrust Lag in Kennedy Shear (Range-Dependent)

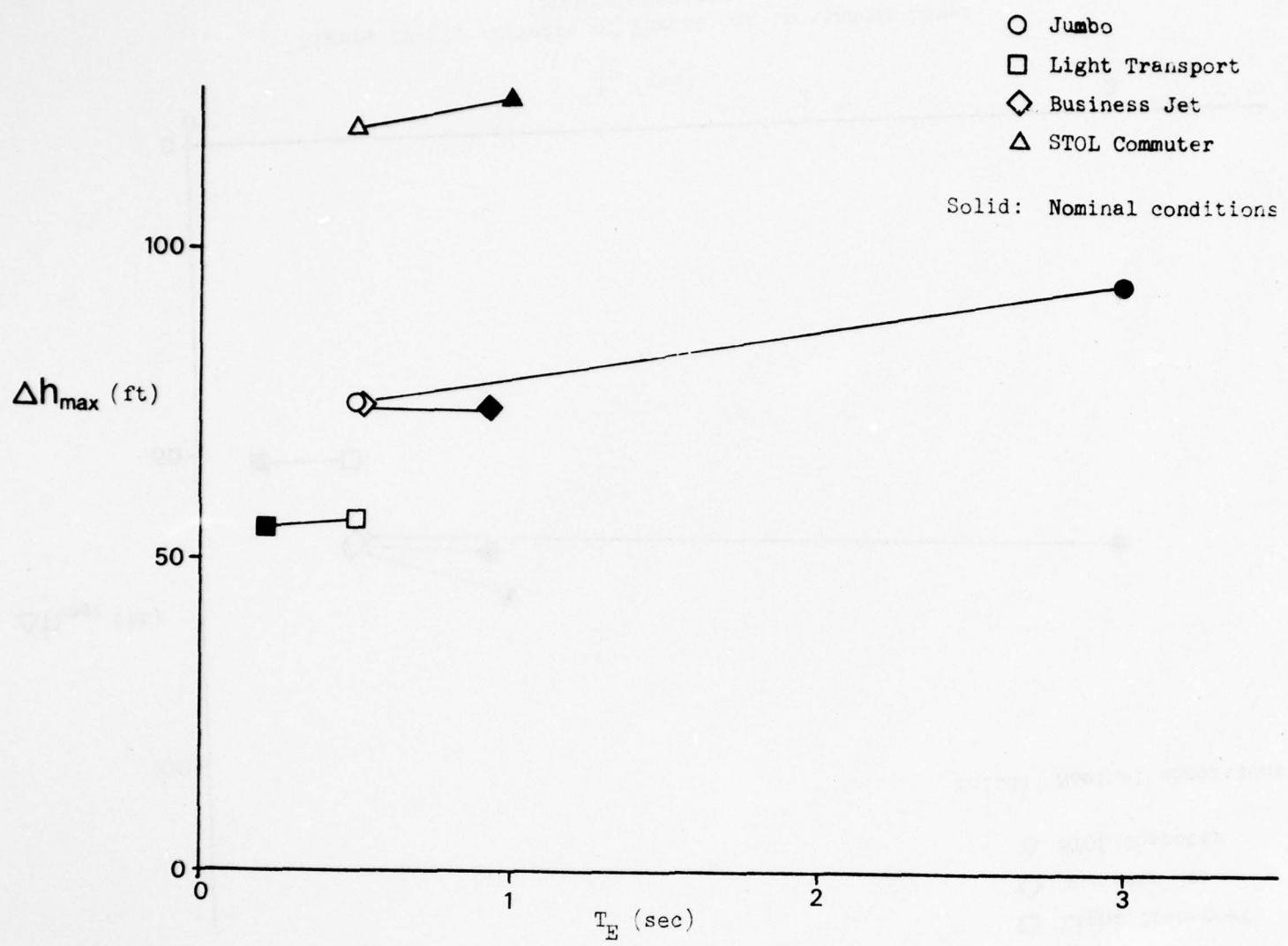

Figure IV-28. Effects of Thrust Lag in Kennedy Shear (Altitude-Dependent)

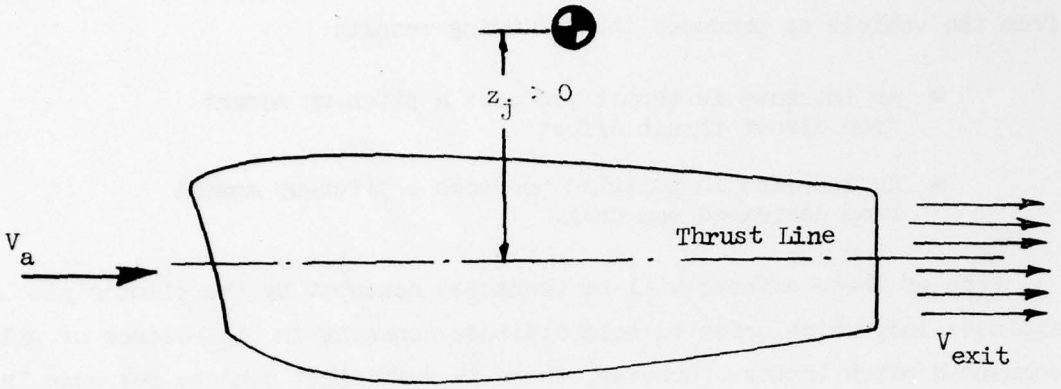

ram drag component

$$\text{Thrust} \doteq \dot{m}_a \, (V_{exit} - V_a)$$

where $\dot{m}_a \triangleq$ air mass flow

$V_{exit} \triangleq$ exit velocity

$$M_{\delta_T} = \frac{z_j}{I_y} \frac{\partial \text{thrust}}{\partial \delta_T}$$

$$X_{\delta_T} = \frac{1}{m} \frac{\partial \text{thrust}}{\partial \delta_T}$$

and $$\frac{M_{\delta_T}}{X_{\delta_T}} = \frac{z_j}{k_y^2}$$

where $k_y^2 = \frac{I_y}{m}$

$$M_u = \frac{z_j}{I_y} \frac{\partial \text{thrust}}{\partial V_a} \doteq \frac{z_j}{I_y} \dot{m}_a$$

Figure IV-29. Contributions of Thrust Offset to Pitching Moment Derivatives

AD-A052 435 SYSTEMS TECHNOLOGY INC MOUNTAIN VIEW CALIF F/G 1/2
SIMULATION AND ANALYSIS OF WIND SHEAR HAZARD.(U)
DEC 77 J M LEHMAN, R K HEFFLEY, W F CLEMENT NAS2-8889

UNCLASSIFIED STI-TR-1063-3 FAA/RD-78/7 NL

2 OF 2
ADA
052435

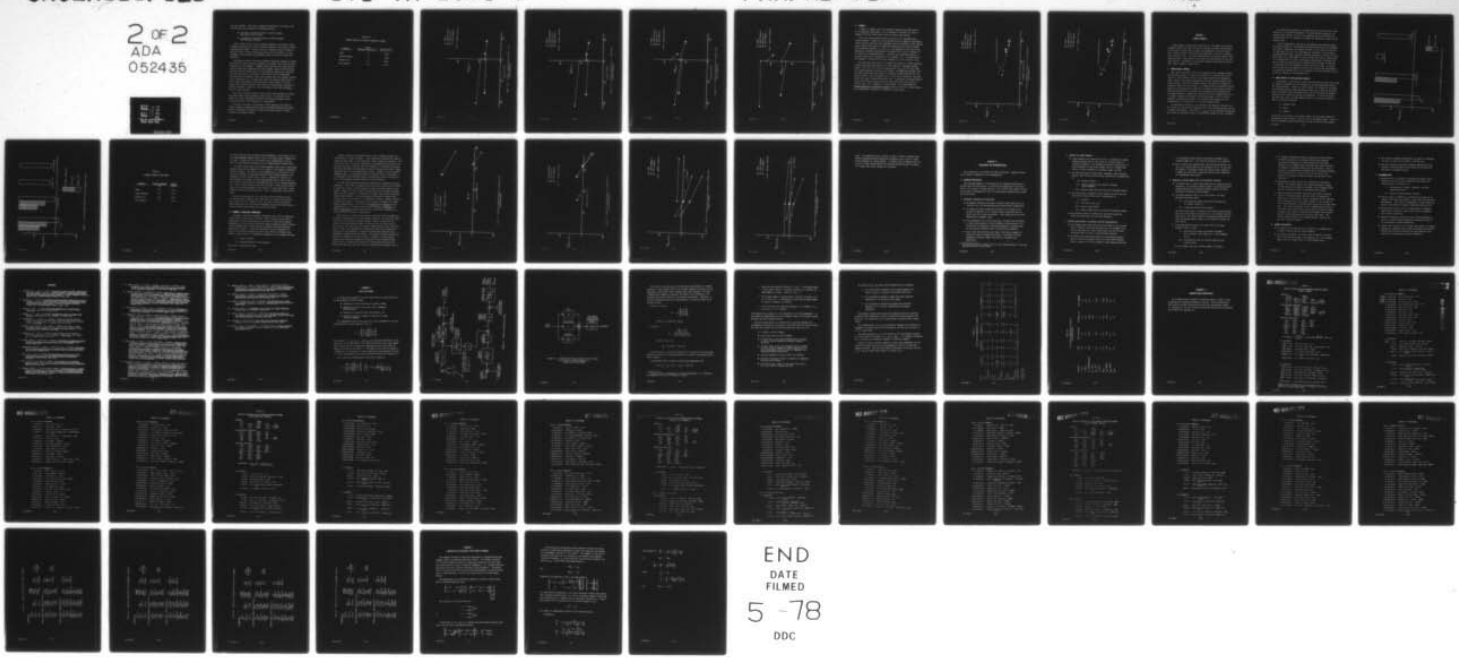

END
DATE
FILMED
5-78
DDC

the same features. Note that a downward displacement of the thrust line from the vehicle cg produces the following results:

- An increase in thrust produces a pitch-up moment from direct thrust effect
- An increase in tailwind produces a pitch-up moment from decreased ram drag.

Both of these effects will be countered somewhat by the pilot's pitch attitude loop which tries to hold attitude constant in the absence of pilot commanded pitch inputs. However, there is sufficient vehicle response in the short term for the M_u and $M_{\delta T}/X_{\delta T}$ effects to be noticeable. As the tightness of the attitude loop increases, these effects will become less noticeable.

Variations in thrust offset were evaluated during the simulation because there was some doubt about the validity of the thrust offsets for the light transport and STOL commuter. Comments from pilots who have flown both the actual aircraft and simulations with these nominal engine offsets indicate that the effective thrust offset for the simulated vehicles was excessive. The effective offset is difficult to estimate and can be considerably different from the geometric offset due to engine flow and downwash effects on the horizontal tail. An additional reason for varying thrust offset is that a pilot could largely cancel the thrust offset effects by using a tighter pitch attitude loop or, more likely, by establishing a throttle-to-elevator crossfeed. Table IV-1 lists the thrust offsets and the $M_{\delta T}/X_{\delta T}$ ratio for each aircraft.

The effects of thrust offset on shear hazard were evaluated by varying the thrust offset from its nominal value to zero. The results for the range- and altitude-dependent versions of the Logan and Kennedy shears are given in Figs. IV-30 through IV-33, respectively.

The trend of the data is consistent in that increasing the pitch-to-thrust coupling by displacing the thrust line downward decreases the shear hazard by producing an immediate favorable pitch-up response to thrust increase and tailwind increase.

TABLE IV-1

THRUST OFFSET AND PITCHING RESPONSE TO THRUST

AIRCRAFT	OFFSET (Positive Below cg) ft	$M_{\delta_T}/X_{\delta_T}$ rad/ft
Jumbo	10	.0055
Light Transport	5	.0169
Business Jet	-1.5	-.0318
STOL Commuter	-2.9	-.0427

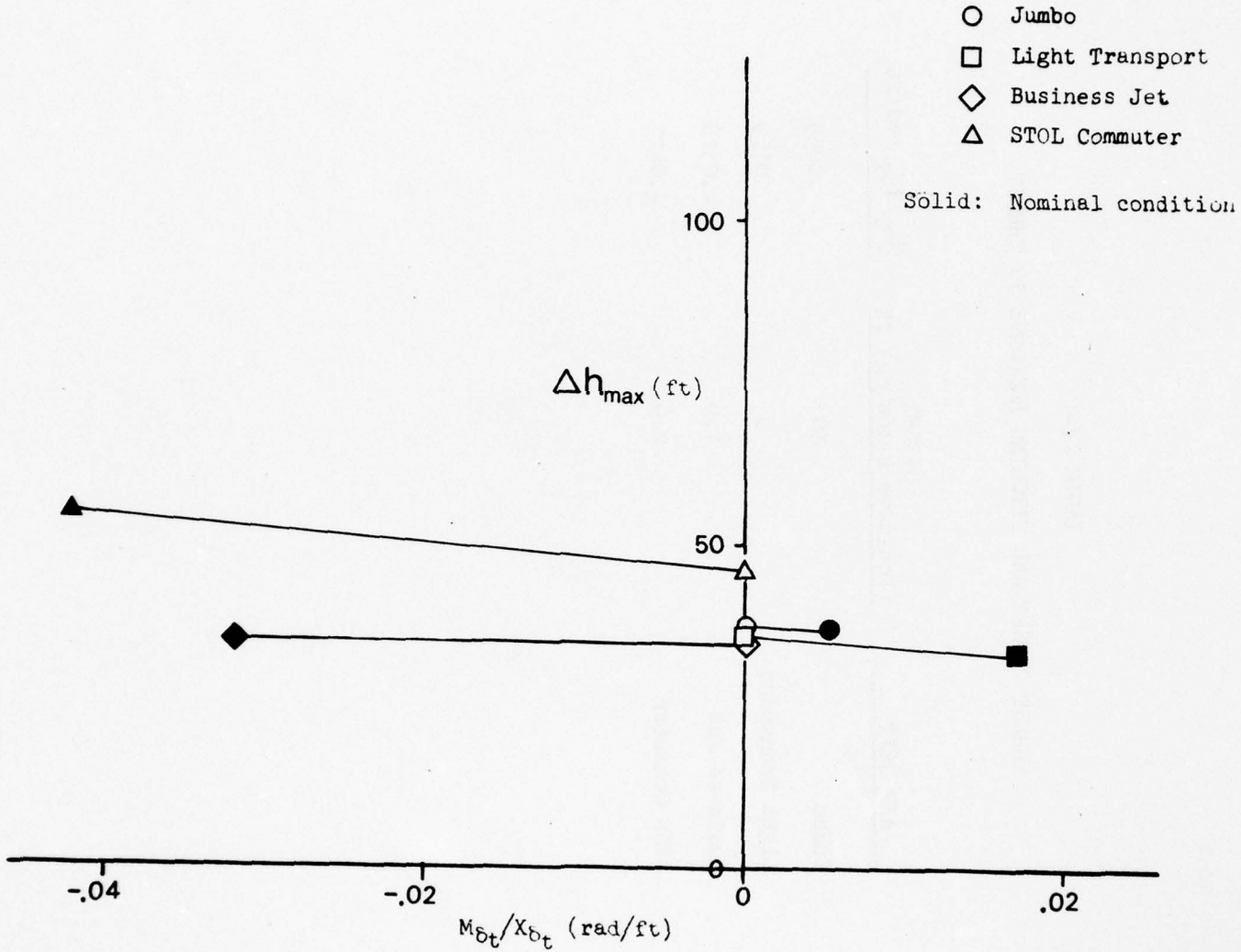

Figure IV-30. Effects of Thrust Offset in Logan Shear (Range-Dependent)

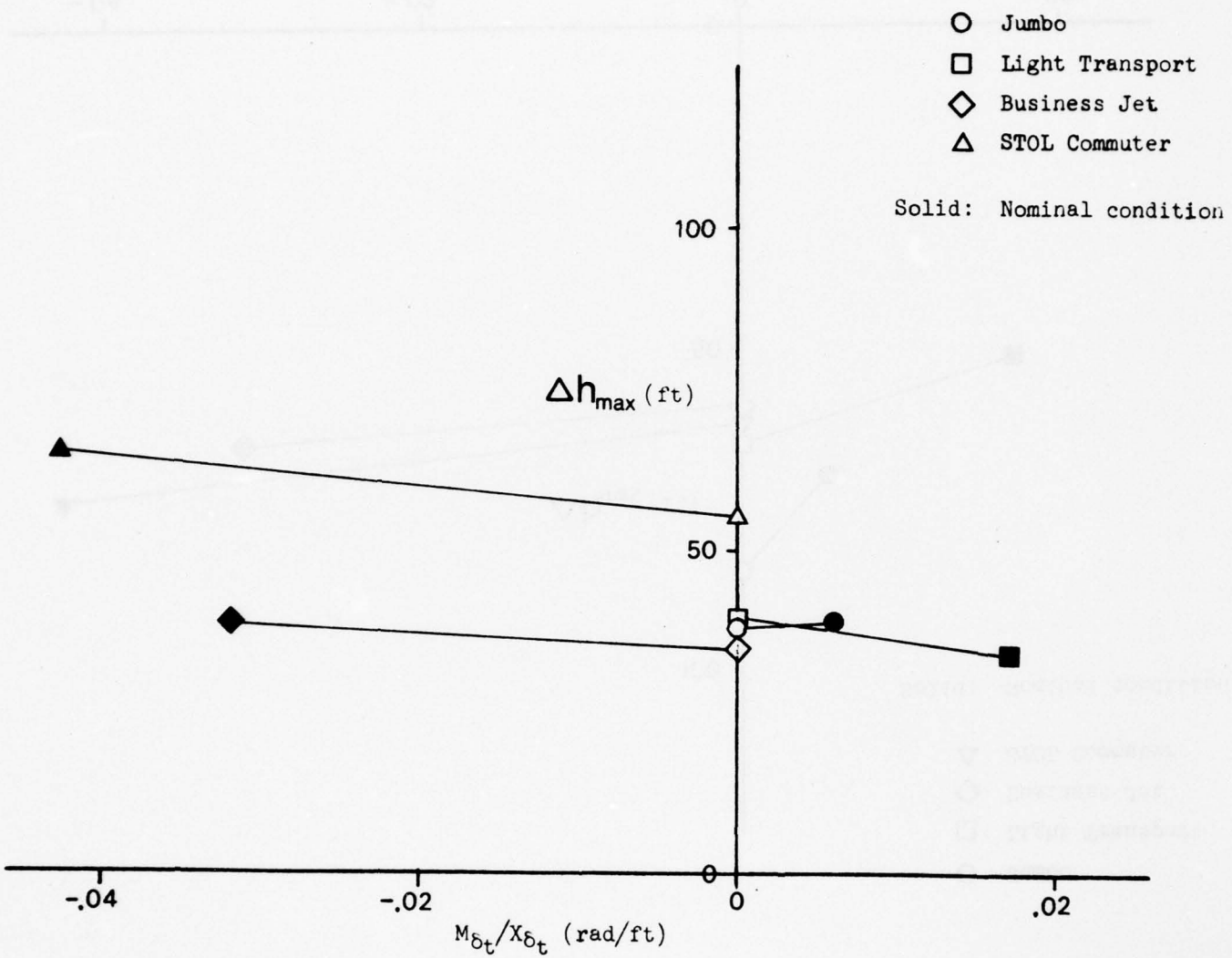

Figure IV-31. Effects of Thrust Offset in Logan Shear (Altitude-Dependent)

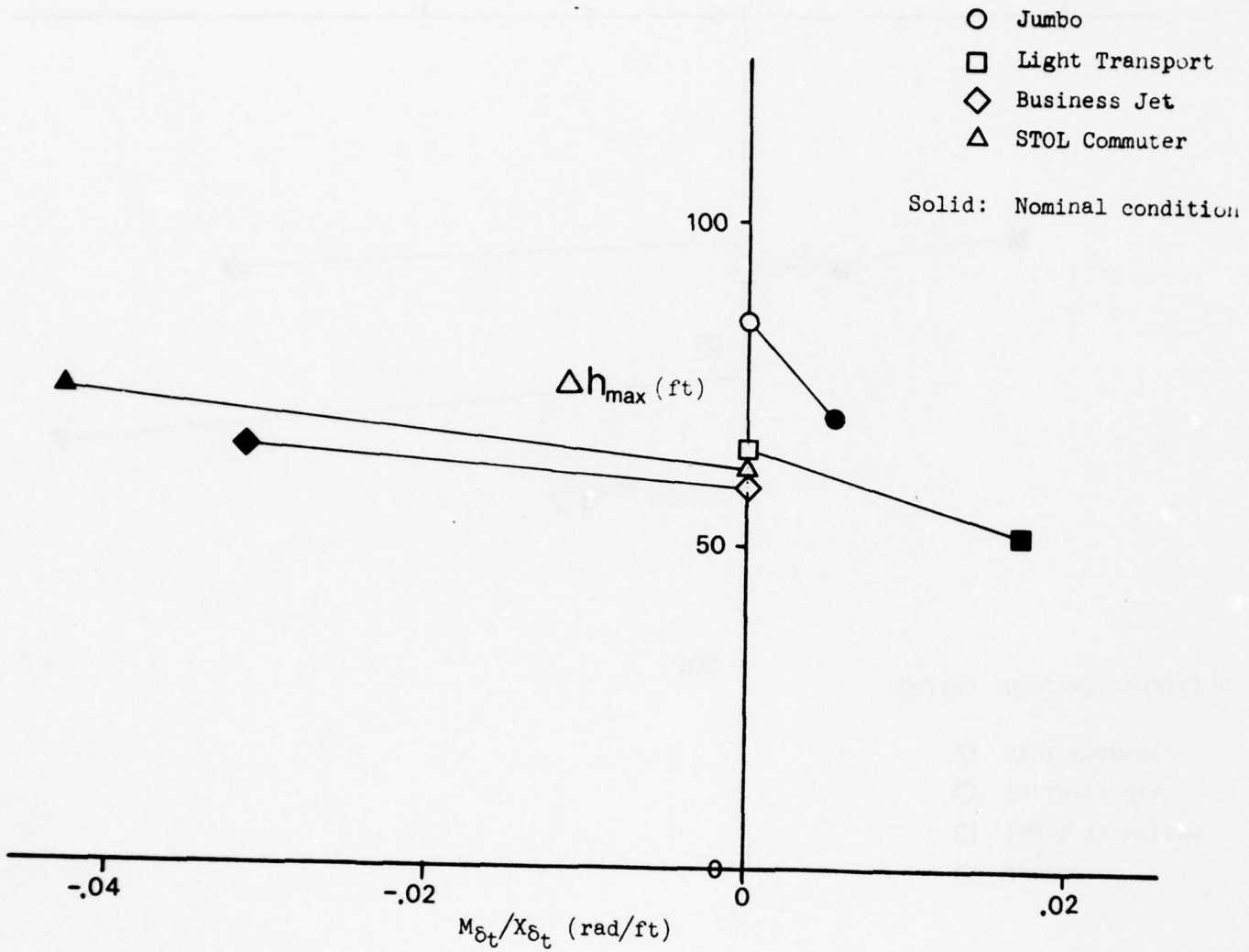

Figure IV-32. Effects of Thrust Offset in Kennedy Shear (Range-Dependent)

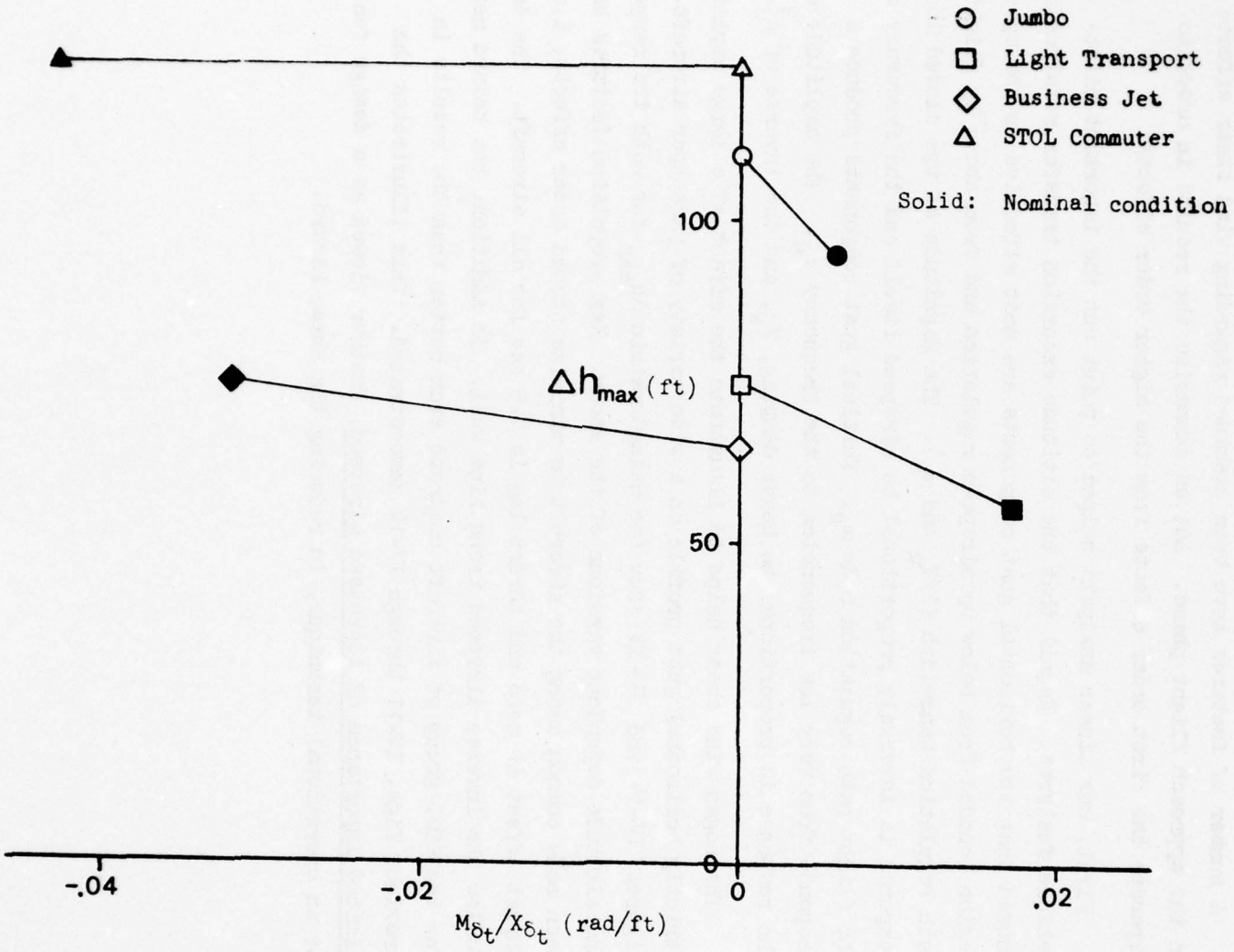

Figure IV-33. Effects of Thrust Offset in Kennedy Shear (Altitude-Dependent)

E. SUMMARY

A number of features have been examined regarding wind shear effects in the approach flight phase. Let us summarize the results in order to separate the first order effects from the higher order effects.

First, our linear analysis helped to point out the important pilot-vehicle features. Recall that the altitude excursion transfer relationships showed that the horizontal gust components are most effective in the spectral region bounded from below by airspeed regulation and from above by flight path regulation bandwidth ($1/T_u$ and ω_d). The magnitude of the closed loop response is inversely proportional to airspeed itself and the frequency of the flight path regulation mode ω_d. Vertical gust components produce a response from very low frequencies to the frequency ω_d. The amplitude of the response is proportional to heave damping, Z_w, and the inverse of ω_d^2.

The Logan wind shear helps to illustrate the effect of a large amplitude, strictly horizontal gust profile on a wide variety of passenger aircraft. Figures IV-34 and IV-35 show the hazard metric Δh_{max} for both the range- and altitude-dependent versions of the shear. Key propulsion features have been made common among the aircraft to minimize second order effects, i.e., thrust offset is zero and thrust lag is 0.5 sec for all aircraft. The data follow the inverse airspeed trend line well. In addition, the hazard metrics for the CTOL group of aircraft coalesce even better than the results in previous Figs. IV-11 through IV-14 demonstrated. This illustrates the limited importance of increased airspeed, whether viewed as a design feature or an operational technique, in reducing the shear hazard.

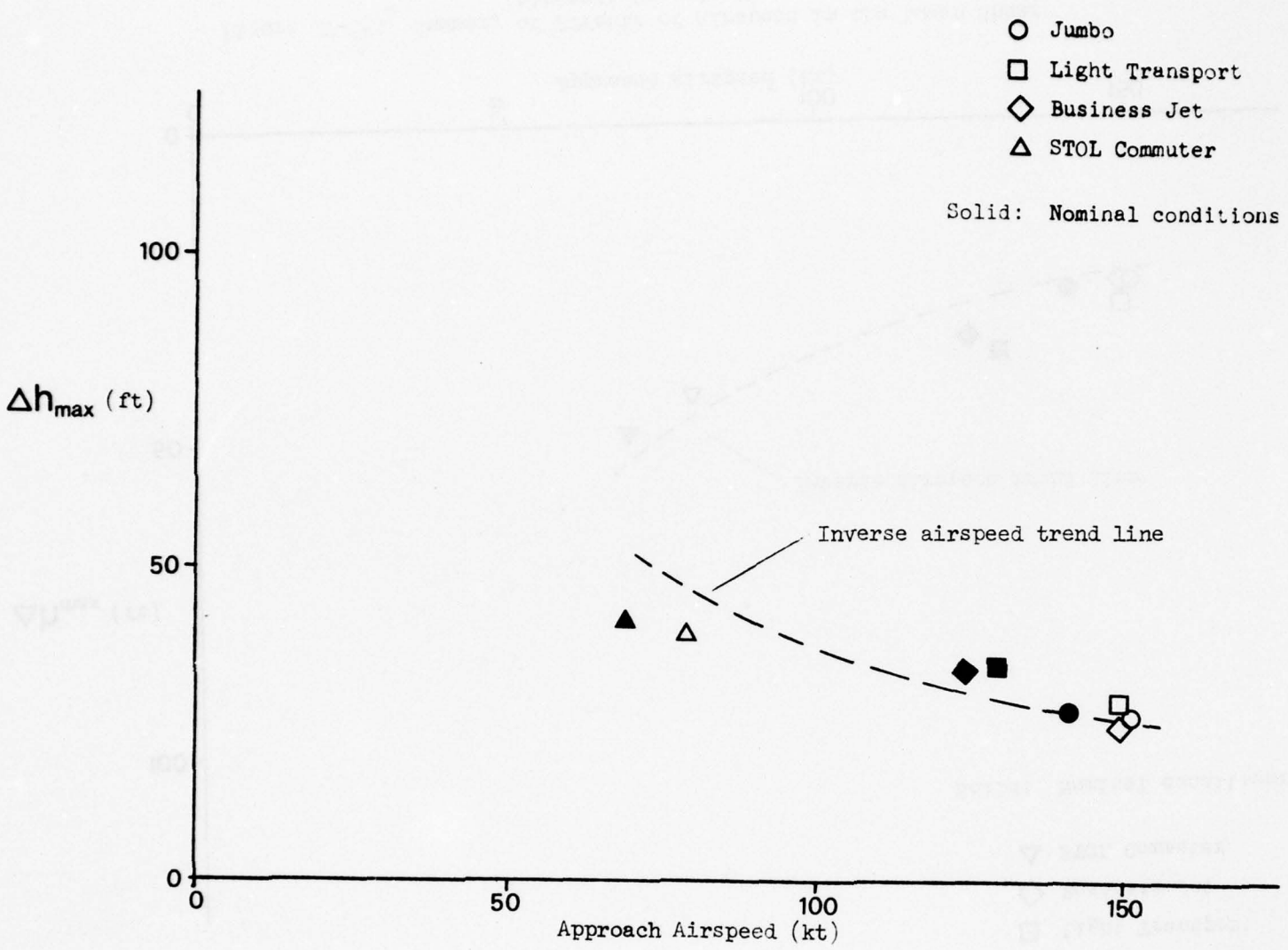

Figure IV-34. Summary of Effects of Airspeed in the Logan Shear (Range-Dependent)

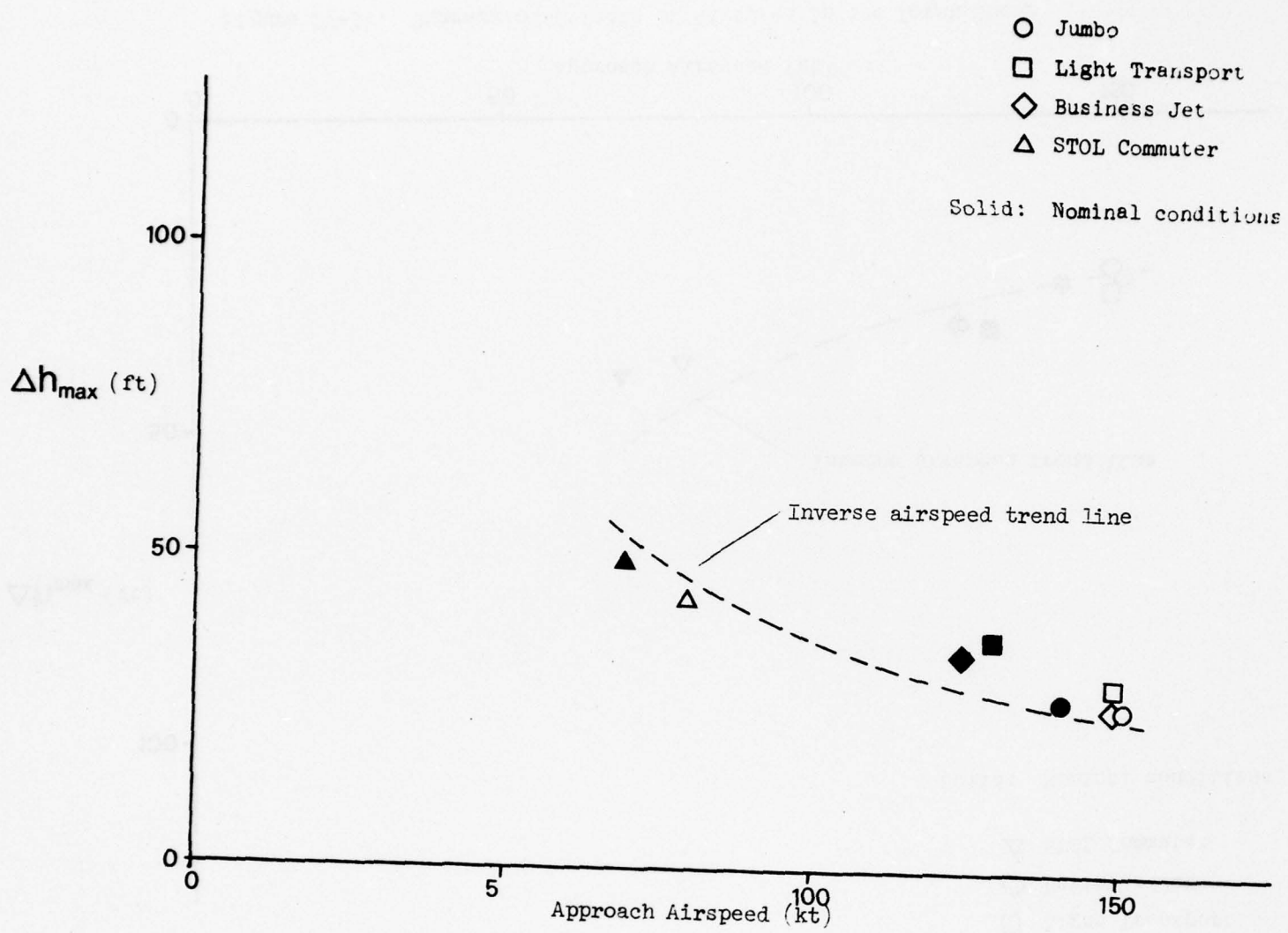

Figure IV-55. Summary of Effects of Airspeed in the Logan Shear (Altitude-Dependent)

SECTION V

TAKEOFF RESULTS

A large number of takeoff cases were tested. The range- and altitude-dependent shears were tested for each of the four aircraft with variations in trim speed, initial rate of climb, and parameters in the pilot model. This section is divided into three subsections each of which is concerned with a specific topic. The first subsection will discuss the takeoff shear hazard criteria. Subsection B will discuss the shear effects for the baseline vehicles. Subsection C will discuss potential operational techniques which have an impact on shear hazard.

A. SHEAR HAZARD CRITERIA

The shear hazard metric used for the approach cases, maximum deviation from the glide slope, is clearly not suitable for a takeoff shear hazard criteria. During takeoff there is not a glide slope for the airplane to track. Rather, the primary tracking task involves airspeed control using pitch attitude. There is no throttle control loop since the aircraft is assumed to remain at takeoff power. The takeoff shear hazard metric decided upon was the minimum rate of climb which resulted from the shear encounter. Another possible metric considered was the minimum speed resulting from the shear encounter. However, the aircraft is not in a trimmed state (i.e., 1 g flight) during the encounter, and the trim angle of attack does not approach a limiting case (stall). Thus minimum speed during the shear encounter was not considered to be a critical hazard metric.

As indicated in Section II, the procedure used during the takeoff tests was to trim the aircraft at a height of 30 ft. The aircraft airspeed was set at either a published V_2 speed or at 1.3 V_{stall} for the takeoff configuration. This shear was oriented so that the aircraft was taking off into a headwind.

The takeoff model utilizes an airspeed-to-pitch attitude control feedback with a 3 kt airspeed threshold. The power remains constant at the takeoff power setting. The rules for adjusting the pitch attitude and airspeed loops are, as indicated in Section II, identical to those for the approach case.

A brief restatement of the problem encountered by an aircraft taking off in the presence of a decreasing headwind shear will help to illuminate the results. Typically, the takeoff aircraft is at or near its best rate of climb speed (V_y) at a 30 ft altitude and, following a loss in speed, the airplane must reduce the pitch attitude (and angle of attack) to accelerate back to V_y. Any attempt to fly at a speed less than V_y would result in a decreased rate of climb. Additionally, any attempt to increase the rate of climb by increasing pitch attitude would only cause the aircraft to decelerate and would ultimately reduce the rate of climb. It should also be noted that the immediate problem of an aircraft upon encountering the decreasing headwind shear is not proximity to stall but rather the loss of rate of climb due to the airspeed loss.

B. SHEAR EFFECTS FOR THE BASELINE VEHICLES

As indicated in the previous section, the shear hazard metric used during the takeoff simulations was the minimum rate of climb encountered during the shear encounter. Figures V-1 and V-2 depict the results for the range- and altitude-dependent Logan and Kennedy shears for the baseline aircraft. Only the severest shear, the Kennedy shear, was tested among all aircraft, because of time limitations during the simulation. It can be seen from the data that, just as for the approach cases, we can rank the shears in terms of increasing severity:

(1) Boundary layer

(2) Logan

(3) Kennedy

It can also be seen that, of the three shears, the only shear capable of reducing the aircraft rate of climb to zero is the Kennedy shear. Table V-1 lists the nominal trimmed takeoff rate of climb for each of the aircraft.

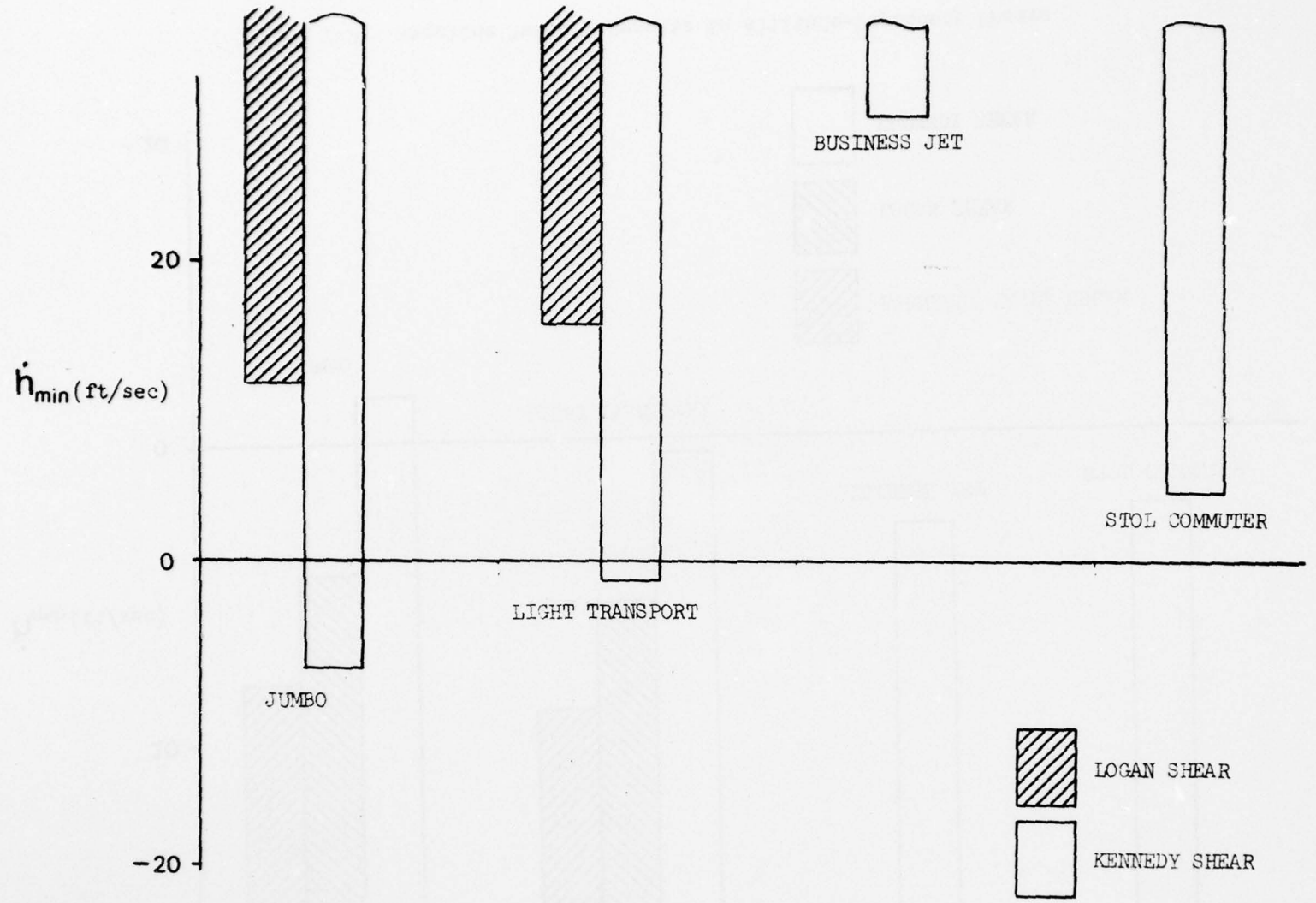

Figure V-1. Baseline Takeoff Results in Range-Dependent Shears

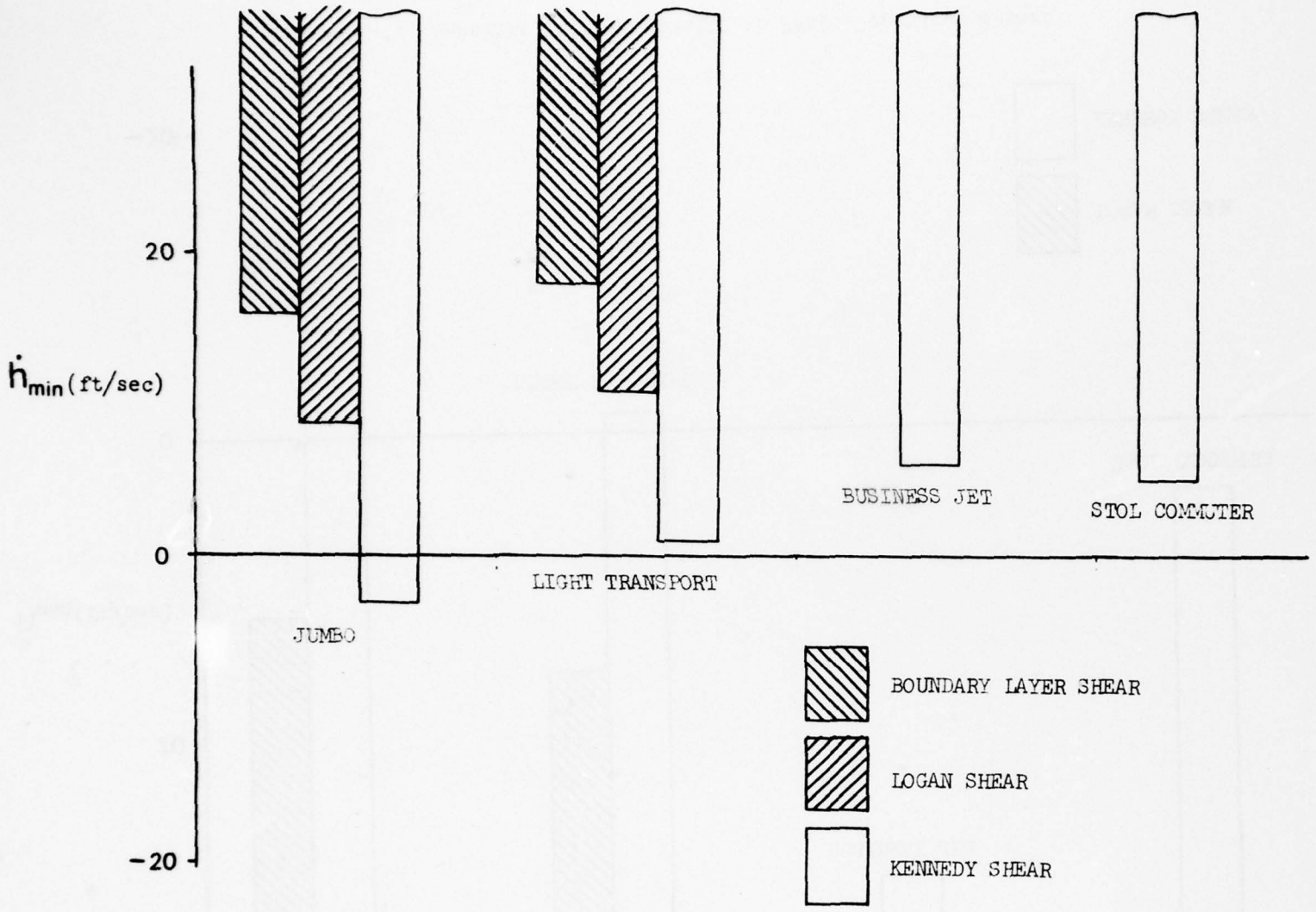

Figure V-2. Baseline Takeoff Results in Altitude-Dependent Shears

TABLE V-1

NOMINAL AIRCRAFT TRIM STATES

AIRCRAFT	TAKEOFF AIRSPEED (kt)	TRIM $\dot{h}$ (ft/sec)
Jumbo	187	38.7
Light Transport	161	37.4
Business Jet	135	62.5
STOL Commuter	78	21.5

It can be seen that the relatively good performance of the business jet in the range-dependent Kennedy shear is due to its large initial trimmed rate of climb. In fact, each of the aircraft loses approximately 30 ft/sec rate of climb during an encounter with the range-dependent Kennedy shear.

It should be noted that the altitude-dependent shears have a shear-pilot-vehicle interaction on takeoff which is similar to the approach interaction discussed earlier. The effect of this interaction is to give most of the aircraft virtually the same shear hazard for the altitude-dependent case regardless of their initial rate of climb. Comparing the business jet shear hazard in the range- and altitude-dependent Kennedy shear cases, we see that this aircraft suffers substantially more for the altitude-dependent case. This is due to the fact that this aircraft's higher initial rate-of-climb in an altitude-dependent shear results in a more rapid rate of shear encounter than for the other aircraft. Thus it experiences a more severe shear.

The main conclusions for the shear effect on the baseline aircraft are that the shears maintain their same order of severity in the takeoff cases as they do in the approach cases, and that a shear-vehicle-pilot interaction exists for the altitude-dependent Kennedy shear which tends to create a uniform shear hazard for the aircraft tested.

C. POTENTIAL OPERATIONAL TECHNIQUES

The number of potential operating techniques which could be employed to reduce takeoff shear hazard is limited. This is because the aircraft is operating at or near its airspeed for best rate of climb during takeoff. Additionally, the takeoff pilot model has only an airspeed-to-pitch attitude control feedback loop, and the possible alternative piloting techniques available are limited. During the simulation, all pilot parameters as well as the aircraft operating conditions were varied to determine their effect on shear hazard. The parameters determined to be of importance were:

(1) Takeoff airspeed

(2) Airspeed regulation characteristics.

These will be discussed in order.

Clearly, decreasing the takeoff speed is not a realistic option for a pilot prior to a shear encounter. It was found that increasing the takeoff speed also has little, if any, beneficial effects during the encounter. This is shown in Figs. V-3 and V-4 which depict the Kennedy shear hazard for the business jet, light transport, and STOL commuter as a function of airspeed. This data indicates that increasing the takeoff airspeed will cause a range-dependent shear to be encountered more quickly. Likewise, for an altitude-dependent shear, the subsequent decrease in initial rate of climb which is a consequence of the increased takeoff airspeed will result in having less rate of climb margin available during the shear encounter.

The only other potential operational technique we examined was airspeed regulation. This showed a significant effect on shear hazard but the effect is opposite to that seen in the landing, because the hazard metric is different. Figures V-5 and V-6 show the shear hazard for the light transport, jumbo, and STOL commuter as a function of airspeed loop crossover frequency (closed loop bandwidth). As in the approach section, the airspeed loop gain was varied by a factor of 2 to determine its effect, however, the data is presented in terms of the airspeed loop crossover frequency for a more general interpretation. We can see that <u>increasing</u> the <u>tightness</u> of the airspeed loop (i.e., increasing the crossover frequency) <u>increases</u> the takeoff <u>shear hazard</u> whereas decreasing the airspeed loop crossover frequency decreases the takeoff shear hazard.

This effect is a result of the actions of the pilot when encountering a decreasing headwind shear. As the airspeed decreases, the pilot will lower the nose of the aircraft to regain airspeed. Thus, not only does the action of the shear tend to reduce the aircraft rate of climb, but also the action of the pilot model in tracking airspeed tends to also reduce the rate of climb. By increasing the airspeed loop crossover frequency (increasing the loop tightness), a larger nose-down pitch change for each increment of airspeed loss will result. This larger pitch-down change will result in a larger loss in rate of climb. Likewise, by decreasing the airspeed loop crossover frequency (decreasing the loop tightness) there will be less of a pitch change during the shear encounter and thus the pilot model will have less of an impact on reducing the aircraft's rate of

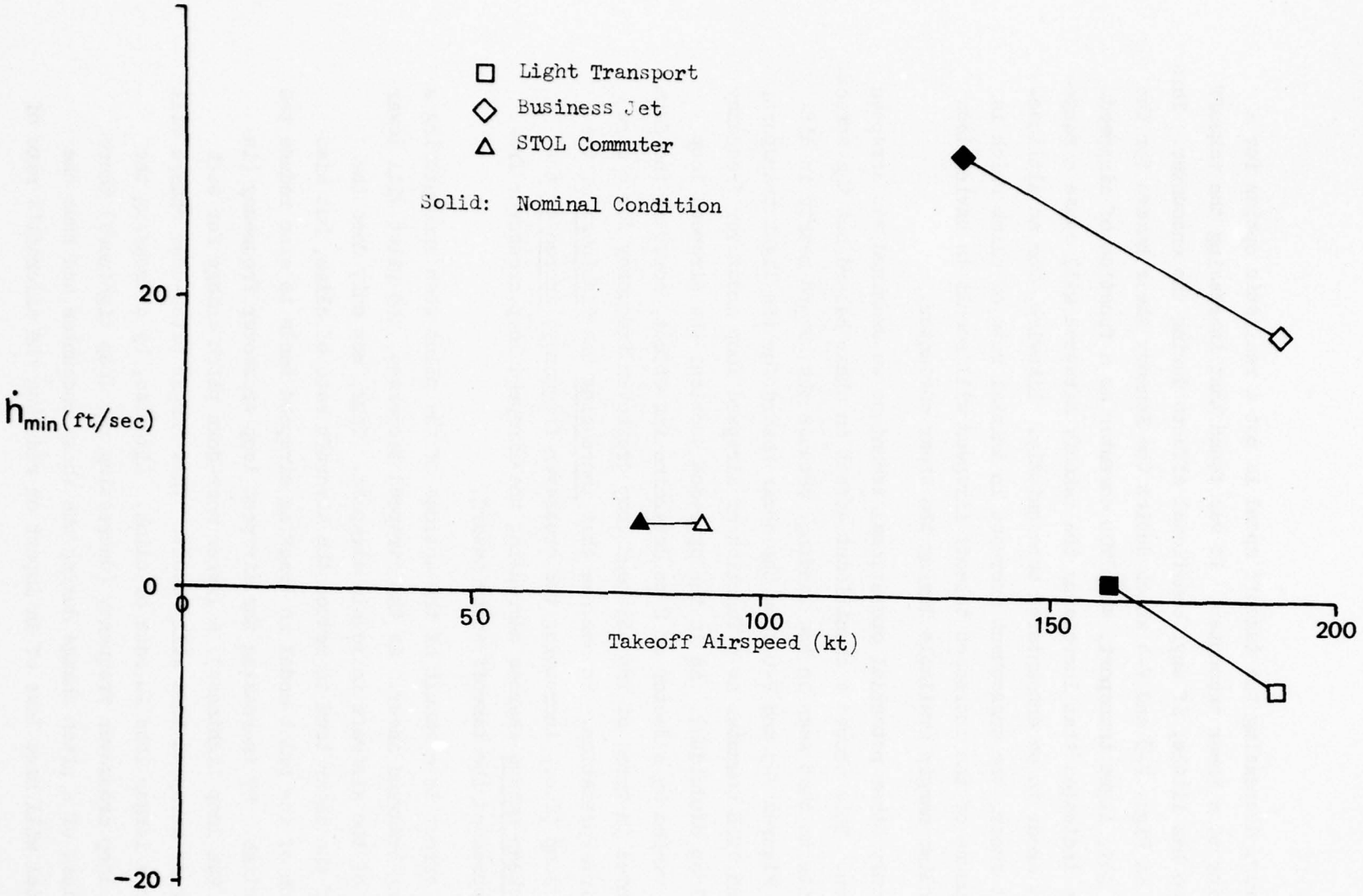

Figure V-3. Effects of Takeoff Airspeed in Kennedy Shear (Range-Dependent)

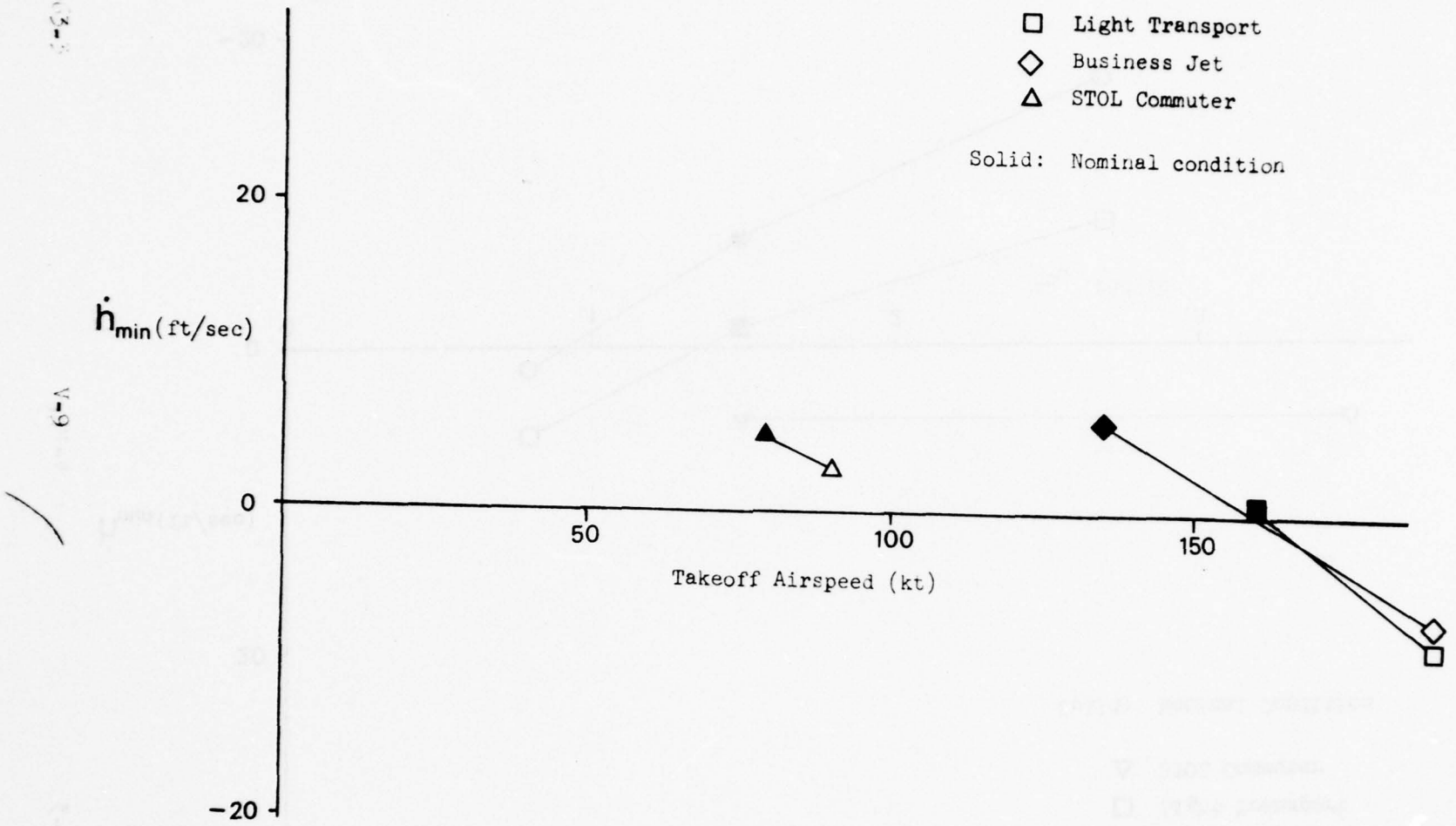

Figure V-4. Effects of Takeoff Airspeed in Kennedy Shear (Altitude-Dependent)

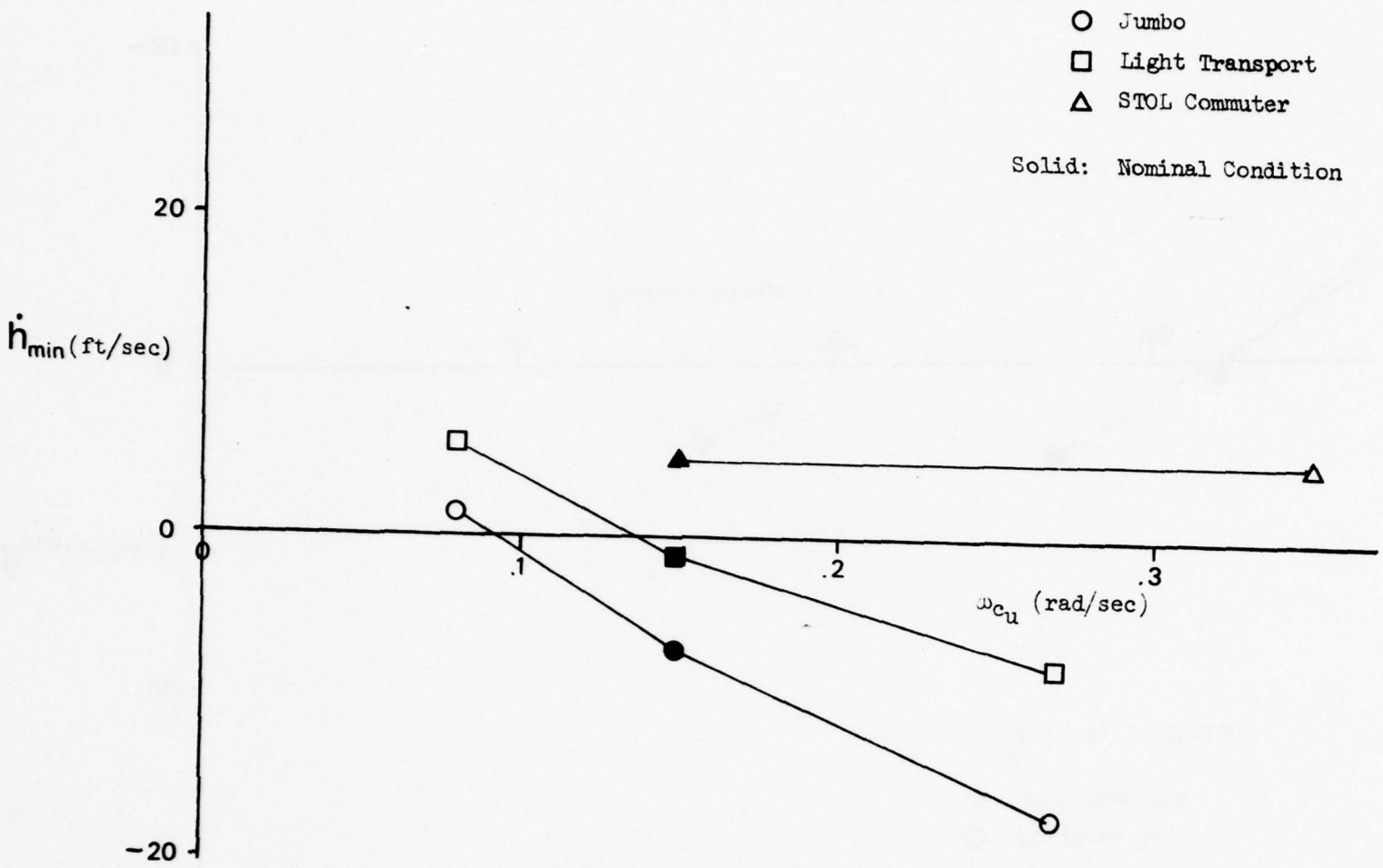

Figure V-5. Effects of Airspeed Loop Crossover Frequency in Kennedy Shear (Range-Dependent)

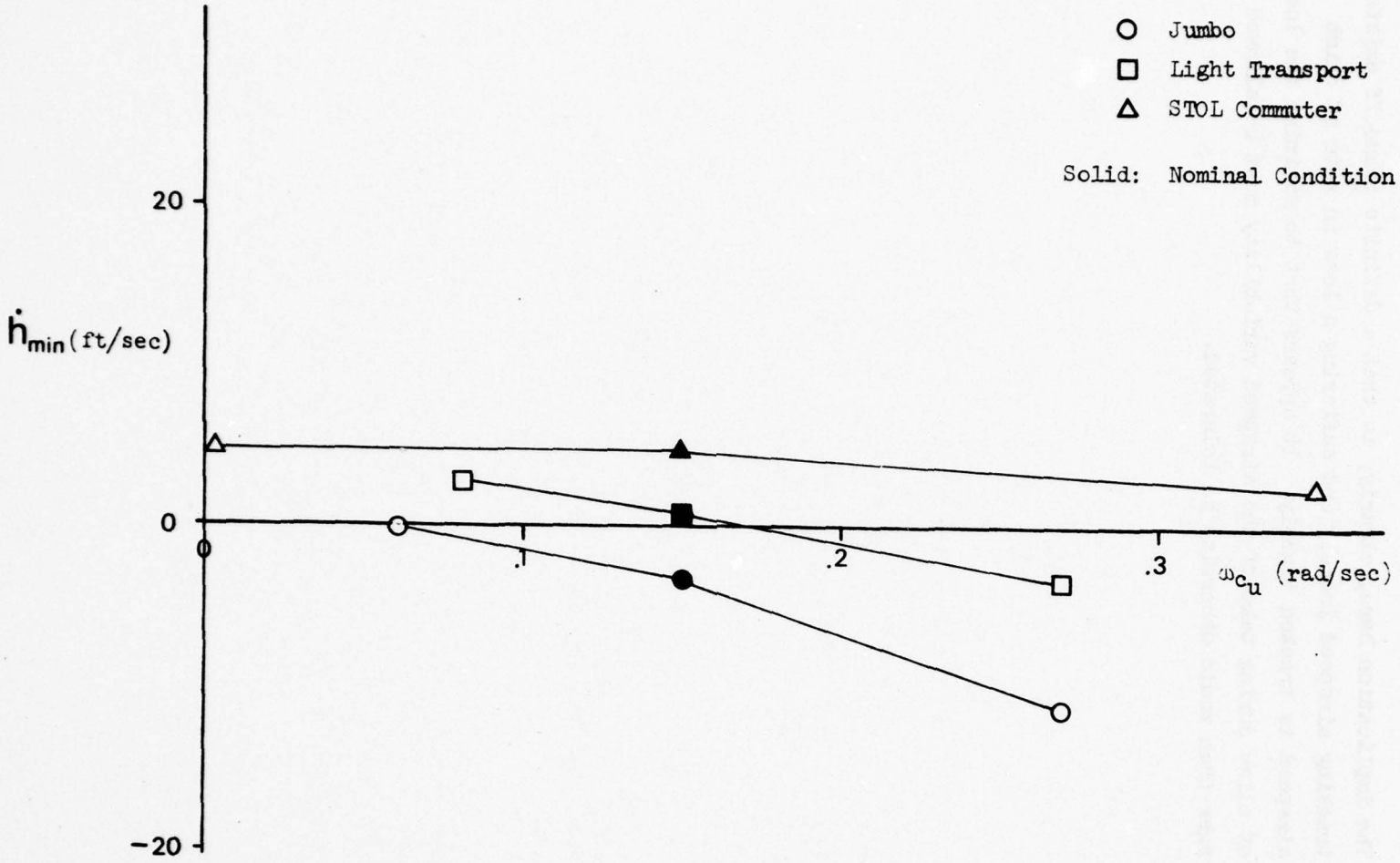

Figure V-6. Effects of Airspeed Loop Crossover Frequency in Kennedy Shear (Altitude-Dependent)

climb. The implication here, clearly, is that a definite tradeoff exists between tracking airspeed loosely and suffering a loss in rate of climb because airspeed is tracked tightly. It appears that to minimize the loss in rate of climb during takeoff the airspeed variability must be allowed to be larger than would otherwise be tolerated.

SECTION VI

CONCLUSIONS AND RECOMMENDATIONS

This section will be divided into three subsections: approach conclusions, takeoff conclusions, and recommendations.

A. APPROACH CONCLUSIONS

The following summary of conclusions for the approach flight phase is divided into four major areas, (i) validity and limitations of the simulation, (ii) results of linear analysis, (iii) results from studies of baseline aircraft configurations,* and (iv) pilot-vehicle features which affect the shear hazard.

1. Simulation Validity and Limitations

- An unmanned simulation utilizing a suitable pilot model can be an effective tool for investigating pilot-vehicle-shear interactions.
- One simple and easily quantifiable measure of the hazard to an aircraft on approach is its maximum vertical deviation from the glide slope due to wind disturbances. This hazard metric was used throughout the approach study.
- Other parameters such as speed and angle of attack were considered as shear hazard metrics but were discarded, either because of insensitivity to variations of aircraft parameters or because they did not approach limiting values as did altitude deviation.
- Shear model characteristics can couple with vehicle dynamics to produce what may be exaggerated results. The effects of shear dependency (altitude, range, time) must be recognized and appreciated.

---

* The baseline aircraft configurations are the unaltered models of the four aircraft involved in this study.

2. Results of Linear Analysis

- Linear analysis was a powerful tool for (i) reducing the complex simulation models used in this study to a minimum number of essential parameters, (ii) showing the specific interrelation of those parameters to wind shear hazard, and (iii) showing some effects of shear dependency on altitude, range, and time.
- For horizontal gust (or wind shear) components linear analysis predicts that the pilot-vehicle-shear sensitivity is proportional to:
  - (i) Inverse airspeed
  - (ii) Inverse airspeed loop crossover frequency (loop tightness)
  - (iii) Inverse flight path loop crossover frequency squared
- For vertical gust components linear analysis predicts that the pilot-vehicle-shear sensitivity is proportional to:
  - (i) Airspeed
  - (ii) Lift curve slope (C_{L_α})
  - (iii) Inverse wing loading
  - (iv) Inverse flight path loop crossover frequency squared
- The spectral regions of interest for wind shear hazard are below the flight path loop crossover frequency.

3. Results From Studies of Baseline Aircraft Configurations

- The boundary layer shear posed the least hazard to all aircraft. This is because it had very low shear rates at altitudes above 200 ft, and below 200 ft the higher shear rates did not have sufficient time to create a large altitude deviation.
- The more severe Logan shear presents a substantially greater hazard to the STOL commuter than to the other three aircraft. This is because of the STOL commuter's lower approach speed and

its consequently higher normal acceleration increment due to airspeed change (i.e., the stability derivative Z_u is greater).

- For the most severe Kennedy shear, the altitude deviations vary over a $\pm$ 15 percent band with an average of 65 ft. In this case the effects of horizontal shears and vertical gusts combine in a complex way such that no single key factor can be identified for determining shear hazard.

4. Reduction in Shear Hazard Due to Pilot-Vehicle Features

- The methods used to reduce shear hazard can be lumped into three categories, (i) increasing approach speed, (ii) increasing pilot tracking precision on flight path and/or airspeed, and (iii) altering the propulsion system dynamics.
- Increasing approach speed has two main effects for range-dependent horizontal shears

  (i) Decreasing the normal acceleration increment due to airspeed change (Z_u)

  (ii) Increasing the shear rate ($\partial u_g/\partial t$)

  The first effect causes a decrease in the vehicle shear response while the second causes an increase, i.e., the effects cancel to some extent. The overall effect of increasing airspeed for the Logan and Kennedy shears, however, was to generally reduce the shear hazard.

- Increasing approach speed has two main effects for range-dependent vertical shears

  (i) Increasing the normal acceleration increment due to vertical speed change (i.e., heave damping or Z_w)

  (ii) Decreasing the time the aircraft spends in the vertical shear

  For the Kennedy shear these effects appeared to cancel.

- For roughly comparable increases in precision, better tracking of flight path results in a greater shear hazard reduction (30 percent reduction in altitude deviation for the light transport in the Kennedy shear) than does more precise tracking of airspeed (18 percent reduction for the same case). This is because (i) airspeed has an indirect effect on altitude deviation while flight path has a direct effect on it, and (ii) the presence of propulsion system lag limits the precision of the speed loop.
- Decreasing the thrust lag was most effective for horizontal shears. For vertical shears, the aircraft undergoes a change in sink rate with no change in airspeed. Thus, changing thrust lag had a negligible effect on the Kennedy shear hazard.
- Positive thrust-to-attitude coupling (in the sense of nose-up pitch with increasing power) has the effect of reducing the hazard for all three shears studied. Reduction of this coupling from its nominal value (5 ft thrust offset) to zero results in an 18 percent increase in Kennedy shear hazard for the light transport. The beneficial results of this coupling result from the fact that as the aircraft gets low and slow an increase in power to regain speed causes an immediate and automatic nose-up pitch which is in the direction to reduce glide slope error. The pilot's pitch-up input, while probably modeled correctly, was not quick enough to compete.

B. TAKEOFF CONCLUSIONS

- A suitable shear hazard metric for takeoff is the minimum rate of climb resulting from the shear encounter.
- For takeoff encounters, the shears could be ranked in the same order of increasing severity as for takeoff, i.e., (i) boundary layer shear, (ii) Logan shear, and (iii) Kennedy shear.

- The altitude-dependent Kennedy shear was capable of reducing the rate of climb for all vehicles to nearly zero.
- The only practical operational technique examined which was capable of reducing takeoff shear hazard was to reduce the precision in tracking airspeed.

C. RECOMMENDATIONS

- Studies should be conducted to determine the generic shear properties which have a major impact on shear hazard for various classes of aircraft, e.g.,
  - (i) Investigation of range-, altitude-, and time-dependency effects
  - (ii) Spectral characterization features.
- Studies should be conducted to develop the real time use of suitable wind shear hazard metrics, given real time wind shear measurements. This could be accomplished, in part, using the generic pilot-aircraft response estimations presented here.
- Consideration should be given to investigation of guidance modifications to minimize shear effects such as asymmetric glide slope sensitivities.
- Unmanned simulations using pilot models should generally be used as a prelude to understanding the important effects to be investigated in manned simulations.
- Further work should be done to refine pilot models for unmanned simulations, especially where large disturbances are involved. Aspects which should be addressed are trim functions (both airspeed and flight path) and pilot inattention.

REFERENCES

1. Gartner, W. B., and A. C. McTee, All-Weather Landing Systems, Engineering Services Support. Task 2 — Head-Up Display. Piloted Flight Simulator Study of Low-Level Wind Shear, Phase 1, Stanford Research Institute, Project 4364, Interim Report (draft), 6 July 1976.

2. Gartner, W. B., et al., All-Weather Landing Systems, Engineering Services Support. Task 2 — Head-Up Display. Piloted Flight Simulator Study of Low-Level Wind Shear, Phase 2, Stanford Research Institute, Project 4364, Interim Report (draft), March 1977.

3. Frost, W., and D. W. Camp, Wind Shear Modeling for Aircraft Hazard Definition, FAA-RD-77-36, March 1977.

4. McRuer, D. T., and E. S. Krendel, Mathematical Models of Human Pilot Behavior, AGARDograph AG-188, Chapter V, January 1974.

5. Stapleford, R. L., and I. L. Ashkenas, "Effects of Manual Altitude Control and Other Factors on Short Period Handling Quality Requirements," J. Aircraft, Vol. 5, Jan-Feb 1968, pp. 41-48.

6. McRuer, Duane, Henry R. Jex, Warren F. Clement, and Dunstan Graham, A Systems Analysis Theory for Displays in Manual Control, Systems Technology, Inc., TR-163-1, June 1968.

7. Clement, W. F., et al., "A Manual Control-Display Theory Applied to Instrument Landings of a Jet Transport," IEEE Trans., Vol. MMS-9, No. 4, December 1968, pp. 93-110.

8. McRuer, Duane T., and Walter A. Johnson, Development of Approach Control System Requirements with Applications to a Jet Transport, NASA CR-2023, May 1972.

9. Stapleford, Robert L., Samuel J. Craig, and Jean A. Tennant, Measurement of Pilot Describing Functions in Single-Controller Multiloop Tasks, NASA CR-1238, January 1969.

10. Weir, D. H., and R. H. Klein, The Measurement and Analysis of Pilot Scanning and Control Behavior During Simulated Instrumented Approaches, NASA CR-1535, June 1970.

11. Weir, David H., and Duane T. McRuer, Pilot Dynamics for Instrument Approach Tasks: Full Panel Multiloop and Flight Director Operations, NASA CR-2019, May 1972.

12. Clement, Warren F., and Lee Gregor Hofmann, A Systems Analysis of Manual Control Techniques and Display Arrangements for Instrument Landing Approaches in Helicopters. Volume I: Speed and Height Regulation, JANAIR Report 690718, July 1969.

13. Craig, Samuel J., Irving L. Ashkenas, and Robert K. Heffley, Pilot Background and Vehicle Parameters Governing Control Technique in STOL Approach Situations, FAA RD-72-69, June 1972.

14. Klein, Richard H., and Warren F. Clement, Application of Manual Control Display Theory to the Development of Flight Director Systems for STOL Aircraft, AFFDL TR-72-152, January 1973; and Clement, Warren F., Lee Gregor Hofmann, and Richard E. Blodgett, Application of Manual Control Display Theory to the Development of Flight Director Systems for STOL Aircraft. Part II: Multi-Axis Sampling, Pilot Workload, and Display Integration, Systems Technology, Inc., TR-1011-2, January 1974.

15. Hoh, Roger H., Richard H. Klein, and Walter A. Johnson, Development of an Integrated Configuration Management/Flight Director System for Piloted STOL Approaches, NASA CR-2883, August 1977.

16. Stapleford, Robert L, Robert K. Heffley, Robert C. Rumold, Charles S. Hynes, and Barry C. Scott, A STOL Airworthiness Investigation Using a Simulation of a Deflected Slipstream Transport. Volume I: Summary of Results and Airworthiness Implications, NASA TM X-62,392 and FAA RD-74-143, I, October 1974; Stapleford, Robert L., Robert K. Heffley, Wayne F. Jewell, John M. Lehman, Charles S. Hynes, and Barry C. Scott, A STOL Airworthiness Investigation Using a Simulation of a Deflected Slipstream Transport. Volume II: Simulation Data and Analysis, NASA TM X-62,393 and FAA RD-74-143, II, October 1974; and Heffley, Robert K., Wayne F. Jewell, Robert L. Stapleford, Samuel J. Craig, Charles S. Hynes, and Barry C. Scott, A STOL Airworthiness Investigation Using a Simulation of a Deflected Slipstream Transport. Volume III: Breguet 941S Simulation Model, NASA TM X-62,394 and FAA RD-74-143, III, October 1974.

17. Hoh, Roger H., Samuel J. Craig, and Irving L. Ashkenas, Identification of Minimum Acceptable Characteristics for Manual STOL Flight Path Control. Volume I: Summary Report, FAA RD-75-123, I, June 1976; Craig, Samuel J., Wayne F. Jewell, and Robert L. Stapleford, Identification of Minimum Acceptable Characteristics for Manual STOL Flight Path Control. Volume II: STOL Aircraft Characteristics and Generic Model, FAA RD-75-123, II, July 1975; and Hoh, Roger H., Samuel J. Craig, and Irving L. Ashkenas, Identification of Minimum Acceptable Characteristics for Manual STOL Flight Path Control. Volume III: Detailed Analyses and Tested Vehicle Characteristics, FAA RD-75-123, III, June 1976.

18. Stapleford, Robert L., Robert K. Heffley, Charles S. Hynes, and Barry C. Scott, A STOL Airworthiness Investigation Using a Simulation of an Augmentor Wing Transport. Volume I: Summary of Results and Airworthiness Implications, NASA TM X-62,395 and FAA RD-74-179, I, October 1974; and Heffley, Robert K., Robert L. Stapleford, Robert C. Rumold, John M. Lehman, Barry C. Scott, and Charles S. Hynes, A STOL Airworthiness Investigation Using a Simulation of an Augmentor Wing Transport. Volume II: Simulation Data and Analysis, NASA TM X-62,396 and FAA RD-74-179, II, October 1974.

19. Rumold, Robert C., John M. Lehman, Robert L. Stapleford, Robert K. Heffley, Barry C. Scott, and Charles S. Hynes, A STOL Airworthiness Investigation Using Simulations of Representative STOL Aircraft, FAA RD-75-197 and NASA TM X-62,498, May 1975.

20. Heffley, Robert K., Robert L. Stapleford, and Robert C. Rumold, Airworthiness Criteria Development for Powered-Lift Aircraft, NASA CR-2791 and FAA RD-76-195, February 1977.

21. Hanke, C. Rodney and Donald R. Nordwall, The Simulation of a Jumbo Jet Transport Aircraft, Volume II: Modeling Data, NASA-CR-114494, Sept. 1970.

22. Spitzer, Robert E., Aerodynamic Data for the 737 Flight Simulator, Boeing Report No. D6-58123, April 1966.

23. Jewell, Wayne F. and Robert L. Stapleford, Mathematical Models of the Lear-23 and Flow Field Out to Wake Vortices, Systems Technology, Inc. Working Paper No. 1025-1R, Jan. 1975.

24. Beyrouty, E. and R. Nemes, DHC-6 Twin Otter Airplane Simulation, Computer Sciences Corporation Report PR-4-74, Feb. 1974.

25. McRuer, Duane, Irving Ashkenas, and Dunstan Graham, Aircraft Dynamics and Automatic Control, Princeton University Press, Princeton, New Jersey, 1973.

APPENDIX A

CTOL PILOT MODEL

An overall block diagram of the CTOL pilot model is given in Fig. A-1, the key features of which include:

- Regulation of pitch attitude with control column,
- Regulation of glide slope error with a commanded, pitch attitude
- Regulation of airspeed error with throttle, and
- Crossfeed from pitch command to throttle for large attitude commands.

The compensation used in the inner pitch loop, designated Y_θ, has the general form of a double lead-lag, that is:

$$Y_\theta = K_\theta \frac{\left(T_{L_1} s+1\right)\left(T_{L_\theta} s+1\right)}{\left(T_2 s+1\right)\left(T_{eff} s+1\right)}$$

The variables K_θ, T_{L_1}, T_{L_θ}, T_2, and T_{eff} are calculated according to rules which will be described later. This particular form of pitch loop compensation is based on the proportional-integral-derivative (PID) model of human pilot behavior, Reference 1. This model states that the output of a human pilot in response to an error signal can be interpreted as the sum of a rate, displacement, and pseudo-integration channel (see Figure A-2).

We can write the relationship between the two forms as

$$Y_\theta = K_\theta \frac{\left(T_{L_1} s+1\right)\left(T_{L_\theta} s+1\right)}{\left(T_2 s+1\right)\left(T_{eff} s+1\right)} = \left[K_R s + K_D + \frac{K_I}{T_2 s+1}\right] \frac{1}{\left(T_{eff} s+1\right)}$$

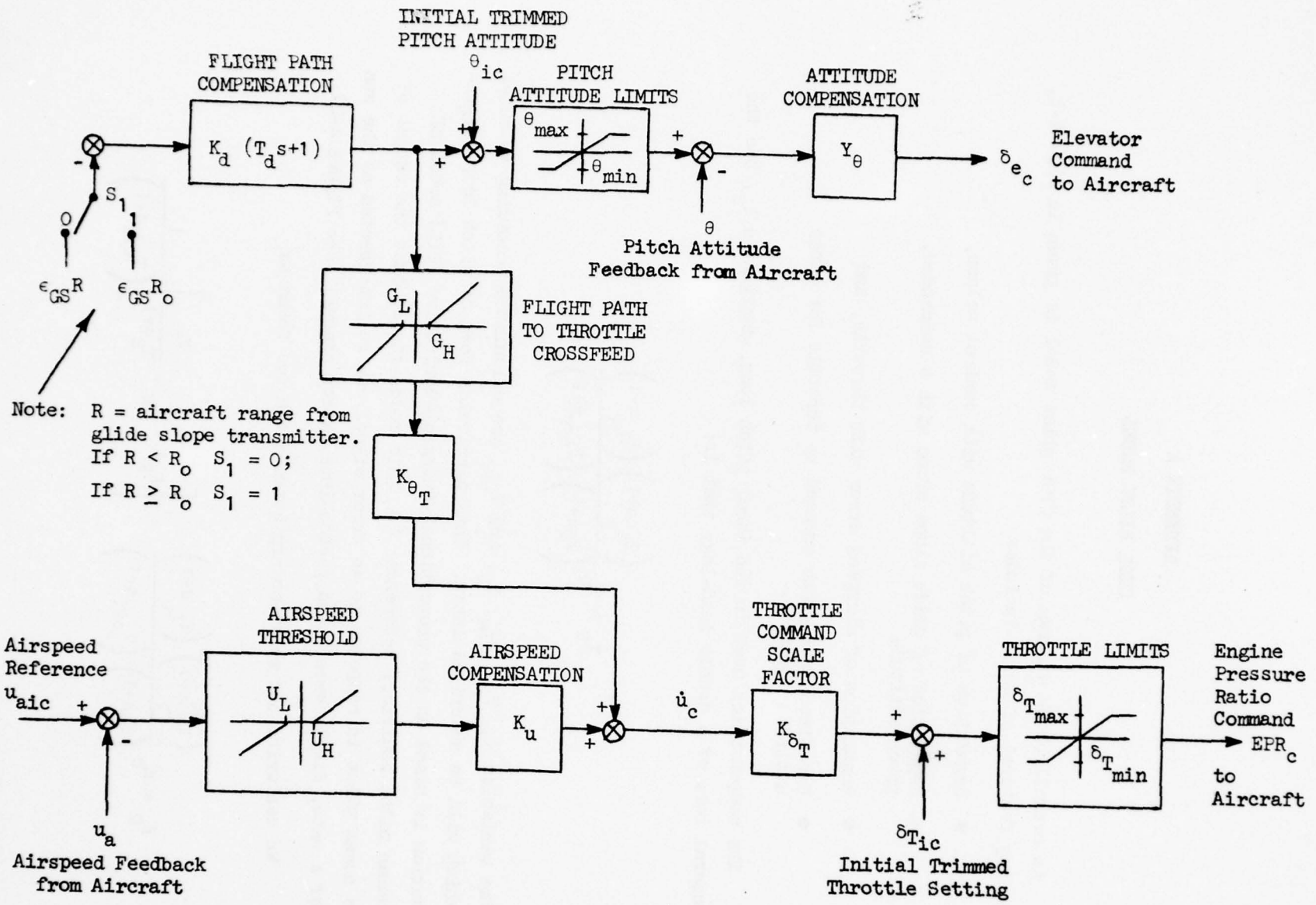

Figure A-1. Details of CTOL Pilot Model

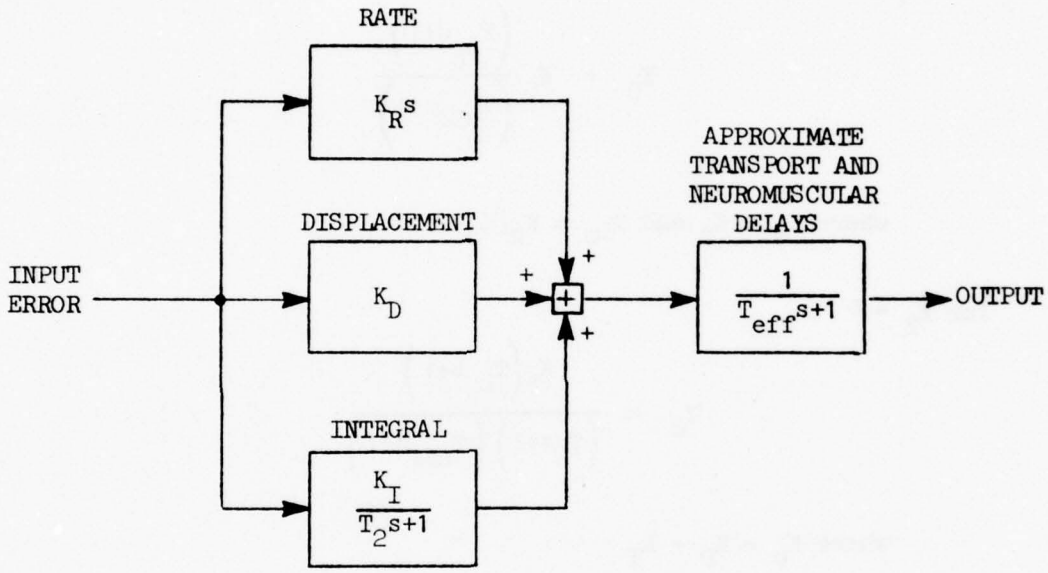

Figure A-2. Proportional-Integral-Derivative (PID) Model for the Pilot's Output Response to a Single Input Error Signal

The effects of K_R and K_I on the system open loop dynamics are roughly opposite, in that K_R adds lead* to the system, increases the phase for all frequencies, and reduces the DC (steady state) gain relative to the high frequency gain, whereas K_I decreases the phase at all frequencies, but increases the DC gain relative to the high frequency gain. Therefore, to achieve satisfactory open loop characteristics, we would use either K_R or K_I but not both.

For $K_I = 0$ we have

$$Y_\theta = K_\theta \frac{\left(T_{L_\theta} s+1\right)}{\left(T_{eff} s+1\right)}$$

where $K_\theta = K_D$ and $T_{L_\theta} = K_R/K_D$

For $K_R \approx 0$

$$Y_\theta = \frac{K_\theta\left(T_{L_1} s+1\right)}{\left(T_2 s+1\right)\left(T_{eff} s+1\right)}$$

where $K_\theta = K_D + K_I$

$$T_{L_1} = K_D T_2/(K_D + K_I) \leq T_2$$

For either case, a crossover frequency of 1.5 rad/sec with 45 deg phase margin was selected as being representative of nominal (not maximum effort) pilot behavior.

The procedure used to adjust the pitch loop compensation was:

1. Set $T_{L_1} = T_{L_\theta} = T_2 = 0$, $T_{eff} = 0.333$ sec

*"Lead" may also be interpreted as pilot anticipation, i.e., detection and feedback of the rate of change of a state.

2. Check the loop transfer function, $Y_\theta \cdot \theta/\delta_e$. If the phase margin is less than 45 deg at 1.5 rad/sec, adjust T_{L_θ} to increase the phase margin to 45 deg. Level $T_2 = T_{L_1} = 0$.

3. If the phase margin is greater than 45 deg at 1.5 rad/sec, set $T_2 = 10$ sec, $T_{L_\theta} = 0$, and adjust T_{L_1} such that the phase margin is equal to 45 deg at 1.5 rad/sec.

4. Set K_θ such that the crossover frequency is 1.5 rad/sec, i.e., $|Y_\theta \cdot \theta/\delta_e| = 1$ at 1.5 rad/sec.

The parameter T_{eff} remains at 0.333 regardless of the other parameters. In this model T_{eff} approximates the low frequency effects of the pilot's neuromuscular and other transport delays.

The pitch loop details, as discussed above, and the procedure for determining the parameters are common to all three forms of the pilot model. The other key features of the CTOL pilot model are (see Fig. A-1):

- A limiter on pitch commands
- Glide slope error to pitch feedback
- At long range, glide slope feedback gain is constant in terms of pitch command per displays (angular) deviation
- At short range, glide slope feedback gain is constant in terms of pitch command per linear deviation, i.e., pilot continually lowers his gain to compensate for increasing display sensitivity
- Airspeed feedback to throttle with 5 kt threshold
- Crossfeed from pitch command to throttle to compensate for large pitch changes
- If the high side θ limit in the glide slope loop is hit, full thrust is applied and held.

The values for K_d, T_d, and K_u were determined by the following:

1. T_d is zero unless required to give a phase margin of at least 30 deg at 0.3 rad/sec in the glide slope loop.

2. K_d is adjusted to provide a glide slope loop crossover frequency of 0.3 rad/sec at short range.

3. K_u is adjusted to provide an airspeed loop crossover frequency of 0.15 rad/sec (neglecting the feedback threshold).

The airspeed feedback and flight path command-to-throttle crossfeed thresholds were determined by review of previous piloted simulation time histories. The values were ± 5 kt airspeed and ± 3 deg path angle, respectively.

The crossfeed gain, K_{θ_T}, is an acceleration command to the throttle to compensate for large pitch attitude excursions, and thus has the value of g, 32.2 ft/sec^2/rad.

The speed loop gain, K_{δ_T}, is the inverse of the x-acceleration derivative with respect to throttle (i.e., $K_{\delta_T} = 1/X_{\delta_T}$). It is simply a convenient way of scaling the acceleration command to a throttle command.

Tables A-1 and A-2 present summaries of pilot model parameters for the three CTOL aircraft used in this investigation as well as for the STOL commuter aircraft. The STOL pilot model is discussed in the text, Section II.A.2, and the takeoff pilot model, in Section II.A.3.

TABLE A-1

PILOT MODEL PARAMETERS FOR APPROACH

Aircraft	JUMBO		LIGHT TRANSPORT		BUSINESS JET		STOL COMMUTER					
V_{kt}	142	152	130	150	125	150	70	70*	70*	70	80	80*
γ (deg)	-3	-3	-3	-3	-3	-3	-3	-3	-6	-6	-6	-6
K_θ (dimensionless)	-3.569	-3.247	-1.454	-1.303	-8.81	-10.069	-5.291	-5.188	-6.554	-6.554	-5.07	-5.006
T_{L_1} (sec)	0	0	0	0	0.7022	0.5543	2.503	2.557	2.038	2.038	2.263	2.293
T_{L_2} (sec)	0.7001	0.6349	0.399	0.2231	0	0	0	0	0	0	0	0
T_2 (sec)	0	0	0	0	10	10	10	10	10	10	10	10
K_d	0.0843 ($\frac{deg}{ft}$)	0.0779	0.0913	0.0743	0.0857	0.069	1.28 ($\frac{percent}{ft}$)	1.27	2.47	1.27	1.517	1.51
T_{L_d} (sec)	0	0	0	0	0	0	0	0	0	0	0	0
K_{δ_T} (EPR/kt/sec)	0.0771	0.0796	0.186	0.207	0.1123	0.1115	← Not Applicable →					
K_u	0.1904/sec	0.186	0.205	0.186	0.1908	0.1778	-.516 ($\frac{deg}{kt}$)	-.521	-.580	-.53	-.349	-.339
θ_{max} (deg)	7	7	7	7	20	20	2	2	2	2	2	2
θ_{min} (deg)	-5	-5	-5	-5	-10	-10	-14	-14	-14	-14	-14	-14
δT_{max}	1.9 (EPR)	1.9	1.8	1.8	100 (percent)	100	100	100	100	100	100	100
δT_{min}	0	0	0	0	0	0	0	0	0	0	0	0
$K_{\dot{V}_T}$ (ft/sec^2-rad)	32.2	32.2	32.2	32.2	32.2	32.2	← Not Applicable →					
K_{δ_c} (dimensionless)	← Not Applicable →						1	1	1	1	1	1

* No thrust offset

TABLE A-2

PILOT MODEL PARAMETERS FOR TAKEOFF
(BASELINE CASES)

Aircraft	JUMBO	LIGHT TRANSPORT	BUSINESS JET	STOL COMMUTER
V (kt)	187	161	135	78
γ (deg)	7.0	7.9	15.9	9.27
K_θ (dimensionless)	-2.55	-1.127	-9.82	-.421
T_{L_1} (sec)	0	0	0.624	0
T_{L_θ} (sec)	0.58	0.353	0	0.136
T_2 (sec)	0	0	10	0
T_{eff}	0.33	0.33	0.33	0.333
K_u (deg/kt)	-.460	-.452	-.523	-.579
θ_{max} (deg)	20	20	20	20
θ_{min}	-10	-10	-10	-10

APPENDIX B

AIRCRAFT MODEL DESCRIPTIONS

The following tables describe the aircraft models in terms of fixed operating point linearized equations of motion. Stability derivatives and transfer function factors are given for the landing cases (Tables B-1 through B-4), and only stability derivatives are given for the takeoff cases (Tables B-5 through B-8).

TABLE B-1

STABILITY DERVIATIVES AND TRANSFER FUNCTION FACTORS
(JUMBO, LANDING)

GEOMETRY:

V_T		GAMMA		
239.8 ft/sec		-3.000 deg		
a_o	RHO(ρ)	MACH	XID	ZJ
1116.5 ft/sec	.002377 $\frac{slug}{ft^3}$	.2148	7.029 ft	9.991 ft
S	C(8)	WEIGHT	IY	ALTITUDE
5500. ft^2	27.31 ft	570000. lb	.3240E+8 $slug\text{-}ft^2$	0.0 ft

NON-DIMENSIONAL DERIVATIVES:

CL (C_L)	CLA (C_{L_α})	CLAD ($C_{L_{\dot\alpha}}$)	CLM (C_{L_m})	
1.4996	5.681/rad	6.700/rad	0.0	
CMA (C_{m_α})	CMAD ($C_{m_{\dot\alpha}}$)	CMQ (C_{m_q})	CMM (C_{m_m})	
-1.5569/rad	-3.200/rad	-21.25/rad	0.0	
CD (C_D)	CDA (C_{D_α})	CDM (C_{D_m})	TM ($\frac{\partial T}{\partial T_r}$)	TDTH ($\frac{\partial T}{\partial \delta_T}$)
.19493	.9406/rad	0.0	15410.	391000.
CDDE ($C_{D_{\delta e}}$)	CLDE ($C_{L_{\delta e}}$)	CMDE ($C_{m_{\delta e}}$)		
0.0	.3495/rad	-1.3808/rad		

DIMENSIONAL DERIVATIVES:

XU	XU $\dot{}$	XW	TU
-.03448	-.03371	.04947	.0007791
ZU	ZU $\dot{}$	ZWD	ZW
-.2654	-.2655	-.03376	-.5199
MU	MU $\dot{}$	MWD	MW
-.00011244	-.00010819	-.0002408	-.002057
MAD	MA	MQ	
-.05774	-.4934	-.3834	
XDE	ZDE	MDE	
0.0	-7.418	-.4376	
XDTH	ZDTH	MDTH	
21.90	-2.700	.12055	

	phugoid		short period	
DENOMINATOR:	[.0432;.1503	.00649;.1502][	.584;.825	.481;.669]
	<.01536>			

DE NUMERATORS:

$(N^u_{\delta e})$	N(U-DE)	-.355(.721)(-25.7) <6.57>
$(N^w_{\delta e})$	N(W-DE)	-7.18(14.53)[.1025;.1862 .01909;.1852] <-3.61>
$(N^\theta_{\delta e})$	N(THE-DE)	-.436(.0649)(.440) <-.01244>
$(N^d_{\delta e})$	N(DD-DE)	7.18(-.01296)(-2.60)(2.61) <.629>
$(N^{a_0}_{\delta e})$	N(AZ-DE)	-7.18(-2.62)(2.62)[-.1270;.0206 -.00262;.0205] <.0210>
$(N^h_{\delta e})$	N(HD-DE)	7.17(-.00581)(-2.61)(2.62) <.284>

DTH NUMERATORS:

$(N^u_{\delta T})$	N(U-DTH)	21.9(-.1337)[.641;.835 .535;.641] <-2.04>
$(N^w_{\delta T})$	N(W-DTH)	-2.61(-8.07)[-.1602;.219 -.0350;.216] <1.007>
$(N^\theta_{\delta T})$	N(THE-DTH)	.1212[.834;.342 .285;.1885] <.01415>
$(N^d_{\delta T})$	N(DD-DTH)	2.61(.1393)[.557;2.56 1.425;2.13] <2.39>
$(N^{a_0}_{\delta T})$	N(AZ-DTH)	-2.61(.01030)(.1078)[.553;2.57 1.423;2.14] <-.0238>
$(N^h_{\delta T})$	N(HD-DTH)	1.462(.1507)[.662;3.36 2.22;2.52] <2.49>

*Numbers enclosed in parenthesis are first order factors, (s+a) = (a). Quadratic factors are enclosed in brackets, $|s^2+2\zeta\omega s+\omega^2| = |\zeta;\omega|$. Other numbers are the transfer function gains.

TABLE B-1 (Continued)

DE DTH COUPLING NUMERATORS:

$(N^{u\,w}_{\ell\ell\ell_T})$ N(U-DE/W-DTH) 157.2(-.0214)(14.56) <-48.9>

$(N^{u\,a}_{\ell\ell\ell_T})$ N(U-DE/THE-DTH) 9.55(.461) <4.40>

$(N^{u\,d}_{\ell\ell\ell_T})$ N(U-DE/DD-DTH) -157.2(2.63)(-2.67) <1104.>

N(U-DE/AZ-DTH) 157.2(.00662)(2.65)(-2.69) <-7.41>

N(U-DE/HD-DTH) -156.9(2.63)(-2.67) <1102.>

N(W-DE/THE-DTH) -2.01(1.251) <-2.51>

N(W-DE/DD-DTH) -482.(1.251) <-603.>

N(W-DE/AZ-DTH) 482.(.00703)(1.251) <4.23>

N(W-DE/HD-DTH) 8.22(1.613)(-45.6) <-604.>

N(THE-DE/DD-DTH) -2.01(1.251) <-2.51>

N(THE-DE/AZ-DTH) 2.01(0.0)(1.251) <2.51>

N(THE-DE/HD-DTH) -1.506(1.513) <-2.28>

N(DD-DE/AZ-DTH) -3.38(1.251) <-4.23>

N(DD-DE/HD-DTH) -8.22(2.63)(-2.67) <57.8>

N(AZ-DE/HD-DTH) 8.22(-.0696)(-2.57)(2.61) <3.84>

UG NUMERATORS:

$(N^{u}_{u_g})$ N(U-UG) .0337(.971)[.254:.685 .1742:.663] <.01536>

N(W-UG) .257(.876E-7)(.001431)(.480) <.759E-11>

N(THE-UG) .464E-4(0.0)(-10.23) <-.000474>

N(DD-UG) -.257(.1863E-8)[.329:.666 .219:.629] <.704E-11>

N(AZ-UG) .257(-.1891E-6)(.00707)[.325:.663 .215:.627] <.330E-12>

N(HD-UG) -.258(.00703)[.328:.665 .218:.628] <-.000804>

WG NUMERATORS:

N(U-WG) -.0479(.1863E-8)[-.0844:.894 -.0755:.891] <-.1302E-9>

N(W-WG) .0327[.0788:.1501 .01183:.1496] [.673:4.57 3.07:3.38] <.01536>

N(THE-WG) -.001366(.373E-8)(.021)(-.856) <-.440E-12>

N(DD-WG) -.0327(.834)(15.38)[-.0295:.1915 -.00565:.1915] <-.01536>

N(AZ-WG) .529(-.559E-8)(.802) [-.0093:.1900 -.00747:.1899] <.880E-12>

N(HD-WG) -.0326(.843)(15.30)[-.0406:.1909 -.00775:.1908] <-.01534>

TABLE B-1 (Continued)

DE /UG COUPLING NUMERATORS:

N(U-DE/W-UG) .242(1.113)(13.42) <3.61>

N(U-DE/THE-UG) .01469(.847) <.01244>

N(U-DE/DD-UG) -.242[-.01131;1.613 -.01823;1.612] <-.629>

N(U-DE/AZ-UG) .242(-.0347)[-.00055;1.580 -.00087;1.580] <-.0210>

N(U-DE/HD-UG) -.242[-.01131;1.613 -.01823;1.612] <-.628>

N(W-DE/THE-UG) .1116(0.0) <.1116>

N(W-DE/DD-UG) 26.8(.259E-9) <.693E-8>

N(W-DE/AZ-UG) -26.8(.444E-10)(.00703) <-.836E-11>

N(W-DE/HD-UG) .01266(.00703)(2130.) <.1891>

N(THE-DE/DD-UG) .1116(-.749E-10) <-.836E-11>

N(THE-DE/AZ-UG) -.1116(0.0)(-.749E-10) <.836E-11>

N(THE-DE/HD-UG) .1122(.00580) <.000651>

N(DD-DE/AZ-UG) .1881(.341E-9) <.642E-10>

N(DD-DE/HD-UG) -.01266[-.01131;1.613 -.01823;1.612] <-.0329>

N(AZ-DE/HD-UG) .01266(.00703)(3.49)(-3.53) <-.001098>

DE /WG COUPLING NUMERATORS:

N(U-DE/W-WG) -.355(-1.350)(13.71) <6.57>

N(U-DE/THE-WG) -.0204(.1382E-8) <-.282E-10>

N(U-DE/DD-WG) .355(3.65)(-5.06) <-6.57>

N(U-DE/AZ-WG) -.355(.1639E-6)(3.66)(-5.08) <-.282E-9>

N(U-DE/HD-WG) .354(3.65)(-5.06) <-6.56>

N(W-DE/THE-WG) .0240(.0608)(8.52) <.01244>

N(W-DE/DD-WG) 5.76(.0608)(8.52) <2.98>

N(W-DE/AZ-WG) -5.76(.00703)(.0608)(8.52) <-.0210>

N(W-DE/HD-WG) 5.74(.0682)(8.50) <3.32>

N(THE-DE/DD-WG) .0240(.0608)(8.52) <.01244>

N(THE-DE/AZ-WG) -.0240(0.0)(.0608)(8.52) <-.01244>

N(THE-DE/HD-WG) .0240(.0611)(8.47) <.01243>

N(DD-DE/AZ-WG) .0405(.0608)(8.52) <.0210>

N(DD-DE/HD-WG) .01858(3.65)(-5.06) <-.344>

N(AZ-DE/HD-WG) -.01858(1.339)[-.312;.918 -.286;.872] <-.0209>

TABLE B-1 (Concluded)

DTH/UG COUPLING NUMERATORS:

N(U-DTH/W-UG) 5.71(-.291)(.606) <-1.007>

N(U-DTH/THE-UG) -.00307(4.61) <-.01415>

N(U-DTH/DD-UG) -5.71[.343:.646 .222:.607] <-2.39>

N(U-DTH/AZ-UG) 5.71(.01008)[.337:.644 .217:.606] <.0238>

N(U-DTH/HD-UG) -5.71[.343:.646 .222:.607] <-2.38>

N(W-DTH/THE-UG) -.0312(0.0) <-.0312>

N(W-DTH/DD-UG) -7.49(.240E-9) <-.1802E-8>

N(W-DTH/AZ-UG) 7.49(-.267E-9)(.00703) <-.1408E-10>

N(W-DTH/HD-UG) .299(.00713)(-24.7) <-.0527>

N(THE-DTH/DD-UG) -.0312(0.0) <-.0312>

N(THE-DTH/AZ-UG) .0312(0.0)(0.0) <.0312>

N(THE-DTH/HD-UG) -.0314(.0236) <-.000741>

N(DD-DTH/AZ-UG) -.0527(-.267E-9) <.1408E-10>

N(DD-DTH/HD-UG) -.299[.343:.646 .222:.607] <-.1249>

N(AZ-DTH/HD-UG) .299(.00706)[.284:.769 .218:.737] <.001248>

DTH/WG COUPLING NUMERATORS:

N(U-DTH/W-WG) .715(-.1937)[.633:4.80 3.04:3.72] <-2.04>

N(U-DTH/THE-WG) -.0299(-.705E-8)(-1.068) <-.225E-9>

N(U-DTH/DD-WG) -.715(-.1937)(.968)(15.22) <2.04>

N(U-DTH/AZ-WG) .715(0.0)(-.1971)(.976)(15.21) <-2.09>

N(U-DTH/HD-WG) -.714(-.1937)(.968)(15.22) <2.04>

N(W-DTH/THE-WG) -.000389(.243)(149.6) <-.01415>

N(W-DTH/DD-WG) -.0933(.243)(149.6) <-3.39>

N(W-DTH/AZ-WG) .0933(.00714)(.243)(149.6) <.0238>

N(W-DTH/HD-WG) .0374(.266)(-17.22)(20.4) <-3.50>

N(THE-DTH/DD-WG) -.000389(.243)(149.6) <-.01415>

N(THE-DTH/AZ-WG) .000389(0.0)(.243)(149.6) <.01415>

N(THE-DTH/HD-WG) -.001954(.252)(28.7) <-.01413>

N(DD-DTH/AZ-WG) -.000656(.243)(149.6) <-.0238>

N(DD-DTH/HD-WG) -.0374(-.1937)(.968)(15.22) <.1067>

N(AZ-DTH/HD-WG) .0374(.853)(15.22)[-.1902:.221 -.0421:.217]
<.0238>

TABLE B-2

STABILITY DERIVATIVES AND TRANSFER FUNCTION FACTORS
(LIGHT TRANSPORT, LANDING)

GEOMETRY:

VT		GAMMA		
219.6		-2.994		
A	RHO	MACH	XID	ZJ
1116.5	.002377	.19667	3.390	4.999
S	C	WEIGHT	IY	ALTITUDE
980.0	11.200	95000.	875100.	0.0

NON-DIMENSIONAL DERIVATIVES:

CL	CLA	CLAD	CLM	
1.6799	7.095	-8.000	0.0	
CMA	CMAD	CMQ	CMM	
-1.4724	-2.400	-24.95	0.0	
CD	CDA	CDM	TM	TDTH
.2508	.7899	0.0	-3520.	26840.
CDDE	CLDE	CMDE		
0.0	.4583	-1.6500		

DIMENSIONAL DERIVATIVES:

XU	XU ◆	XW	TU
-.04345	-.04451	.07708	-.0010676
ZU	ZU ◆	ZWD	ZW
-.2910	-.2909	.017671	-.6362
MU	MU ◆	MWD	MW
-.0004753	-.0004934	-.0002004	-.004820
MAD	MA	MQ	
-.04299	-1.0583	-.4574	
XDE	ZDE	MDE	
0.0	-8.716	-1.1859	
XDTH	ZDTH	MDTH	
9.074	-.5375	.15335	

DENOMINATOR: [.0987;.1614 .01593;.1606]
[.494;1.177 .581;1.023] <.0361>

DE NUMERATORS:

N(U-DE) -.684(1.273)(-26.6) <23.2>

N(W-DE) -8.87(30.3)[.1240;.204 .0253;.203] <-11.24>

N(THE-DE) -1.184(.0875)(.569) <-.0590>

N(DD-DE) 8.87(.01093)(-3.71)(4.77) <-1.716>

N(AZ-DE) -8.87(-3.74)(4.79)[.381;.0250 .00953;.0231]
<.0993>

N(HD-DE) 8.86(.01854)(-3.72)(4.78) <-2.92>

DTH NUMERATORS:

N(U-DTH) 9.07(-.241)[.575;1.206 .693;.986] <-3.18>

N(W-DTH) -.547(-57.2)[-.0314;.217 -.00682;.217] <1.473>

N(THE-DTH) .1535[.994;.344 .342;.0365] <.01811>

N(DD-DTH) .547(.1078)[.326;6.51 2.12;6.16] <2.50>

N(AZ-DTH) -.547(.01282)(.1013)[.323;6.55 2.12;6.20]
<-.0205>

N(HD-DTH) .0725(.1175)[.712;17.69 12.59;12.43] <2.67>

TABLE B-2 (Continued)

DE /DTH COUPLING NUMERATORS:

N(U-DE/W-DTH) 80.5(-.01890)(20.4) <-46.2>

N(U-DE/THE-DTH) 10.75(.598) <6.43>

N(U-DE/DD-DTH) -80.5(-3.77)(4.80) <1457.>

N(U-DE/AZ-DTH) 80.5(.00732)(-3.80)(4.82) <-10.81>

N(U-DE/HD-DTH) -80.4(-3.77)(4.80) <1455.>

N(W-DE/THE-DTH) -2.01(1.611) <-3.24>

N(W-DE/DD-DTH) -441.(1.611) <-711.>

N(W-DE/AZ-DTH) 441.(.00766)(1.611) <5.44>

N(W-DE/HD-DTH) 4.21(2.21)(-76.7) <-712.>

N(THE-DE/DD-DTH) -2.01(1.611) <-3.24>

N(THE-DE/AZ-DTH) 2.01(0.0)(1.611) <3.24>

N(THE-DE/HD-DTH) -1.446(2.00) <-2.90>

N(DD-DE/AZ-DTH) -3.38(1.611) <-5.44>

N(DD-DE/HD-DTH) -4.21(-3.77)(4.80) <76.1>

N(AZ-DE/HD-DTH) 4.21(-.0664)(-3.67)(4.76) <4.87>

UG NUMERATORS:

N(U-UG) .0445(.989)[.372;.905 .337;.840] <.0361>

N(W-UG) .296(-.596E-7)(.00345)(.826) <.671E-10>

N(THE-UG) .000434(0.0)(-2.55) <-.001108>

N(DD-UG) -.296(-.1863E-8)[.280;.908 .254;.872]
<-.296E-10>

N(AZ-UG) .296(-.987E-7)(.00769)[.277;.904 .250;.869]
<-.926E-12>

N(HD-UG) -.298(.00765)[.280;.909 .255;.872] <-.001883>

WG NUMERATORS:

N(U-WG) -.0785(0.0)[.0599;1.209 .0724;1.207] <-.1400E-8>

N(W-WG) -.01799(4.62)(-16.77)[.1447;.1609 .0833;.1592]
<.0361>

N(THE-WG) -.001879(.671E-7)(.0421)(-1.891) <.1852E-11>

N(DD-WG) .01799(.986)(-36.0)[.00703;.238 .001670;.238]
<-.0361

N(AZ-WG) .630(0.0)(1.025)[-.01004;.235 -.00236;.235]
.370E-11>

N(HD-WG) .01796(.999)(-35.8)[-.01104;.237 -.00261;.237]
<-.0360>

TABLE B-2 (Continued)

DE UG COUPLING NUMERATORS:

N(U-DE/W-UG) .395(.970)(29.4) <11.24>

N(U-DE/THE-UG) .0527(1.120) <.0590>

N(U-DE/DD-UG) -.395(-1.632)(2.66) <1.716>

N(U-DE/AZ-UG) .395(.0544)(-1.717)(2.69) <-.0993>

N(U-DE/HD-UG) -.394(-1.632)(2.66) <1.713>

N(W-DE/THE-UG) .347(0.0) <.347>

N(W-DE/DD-UG) 76.2(-.286E-9) <-.218E-7>

N(W-DE/AZ-UG) -76.2(.1206E-9)(.00766) <-.704E-10>

N(W-DE/HD-UG) .0206(.00766)(3720.) <.587>

N(THE-DE/DD-UG) .347(.1068E-10) <.370E-11>

N(THE-DE/AZ-UG) -.347(0.0)(.1068E-10) <-.370E-11>

N(THE-DE/HD-UG) .349(.00883) <.00308>

N(DD-DE/AZ-UG) .583(.1206E-9) <.704E-10>

N(DD-DE/HD-UG) -.0206(-1.632)(2.66) <.0896>

N(AZ-DE/HD-UG) .0206(.00766)(-5.24)(6.26) <-.00518>

DE /WG COUPLING NUMERATORS:

N(U-DE/W-WG) -.684(-1.071)(31.6) <23.2>

N(U-DE/THE-WG) -.0916(-.1617E-8) <.1482E-9>

N(U-DE/DD-WG) .684(-5.28)(6.41) <-23.2>

N(U-DE/AZ-WG) -.684(.291E-6)(-5.30)(6.43) <-.237E-9>

N(U-DE/HD-WG) .683(-5.28)(6.41) <-23.1>

N(W-DE/THE-WG) -.00463(.0814)(-156.7) <.0590>

N(W-DE/DD-WG) -1.016(.0814)(-156.7) <12.96>

N(W-DE/AZ-WG) 1.016(.00760)(.0814)(-156.7) <-.0993>

N(W-DE/HD-WG) -1.051(.0896)(-150.4) <14.15>

N(THE-DE/DD-WG) -.00463(.0814)(-156.7) <.0590>

N(THE-DE/AZ-WG) .00463(0.0)(.0814)(-156.7) <-.0590>

N(THE-DE/HD-WG) -.00462(.0819)(-155.7) <.0589>

N(DD-DE/AZ-WG) -.00779(.0814)(-156.7) <.0993>

N(DD-DE/HD-WG) .0357(-5.28)(6.41) <-1.210>

N(AZ-DE/HD-WG) -.0357(1.787)[-.350:1.246 -.436:1.167] <-.0991>

TABLE B-2 (Concluded)

DTH/UG COUPLING NUMERATORS:

N(U-DTH/W-UG) 2.71(-.617)(.881) <-1.473>

N(U-DTH/THE-UG) -.0028(6.26) <-.01811>

N(U-DTH/DD-UG) -2.71[.259:.961 .249:.928] <-2.50>

N(U-DTH/AZ-UG) 2.71(.01222)[.253:.959 .243:.927] <.0305>

N(U-DTH/HD-UG) -2.71[.259:.961 .249:.928] <-2.50>

N(W-DTH/THE-UG) -.0457(0.0) <-.0457>

N(W-DTH/DD-UG) -10.03(-.1134E-8) <.1138E-7>

N(W-DTH/AZ-UG) 10.03(-.771E-9)(.00766) <-.593E-10>

N(W-DTH/HD-UG) .1416(.00771)(-70.5) <-.0769>

N(THE-DTH/DD-UG) -.0457(-.649E-9) <.296E-10>

N(THE-DTH/AZ-UG) .0457(0.0)(-.649E-9) <-.296E-10>

N(THE-DTH/HD-UG) -.0458(.0207) <-.000946>

N(DD-DTH/AZ-UG) -.0768(.386E-9) <-.296E-10>

N(DD-DTH/HD-UG) -.1416[.259:.961 .249:.928] <-.1308>

N(AZ-DTH/HD-UG) .1416(.00768)[.203:1.210 .245:1.185] <.001591>

DTH/WG COUPLING NUMERATORS:

N(U-DTH/W-WG) -.1632(-.204)(5.54)(-17.23) <-3.18>

N(U-DTH/THE-WG) -.01705(0.0)(-2.60) <.0444>

N(U-DTH/DD-WG) .1632(-.411)(1.327)(-35.7) <3.18>

N(U-DTH/AZ-WG) -.1632(-.286E-4)(-.417)(1.337)(-35.7) <-.474E-9>

N(U-DTH/HD-WG) .1630(-.411)(1.327)(-35.7) <3.18>

N(W-DTH/THE-WG) .00379(.1858)(-25.7) <-.01811>

N(W-DTH/DD-WG) .832(.1858)(-25.7) <-3.98>

N(W-DTH/AZ-WG) -.832(.00767)(.1857)(-25.7) <.0305>

N(W-DTH/HD-WG) -.00853(.201)(-30.7)(-78.9) <-4.14>

N(THE-DTH/DD-WG) .00379(.1858)(-25.7) <-.01811>

N(THE-DTH/AZ-WG) -.00379(0.0)(.1858)(-25.7) <.01811>

N(THE-DTH/HD-WG) .00289(.1906)(-32.8) <-.01809>

N(DD-DTH/AZ-WG) .00637(.1858)(-25.7) <-.0305>

N(DD-DTH/HD-WG) .00853(-.411)(1.327)(-35.7) <.1663>

N(AZ-DTH/HD-WG) -.00853(1.030)(-35.7)[-.1856:.311 -.0578:.306]
.0304>

TABLE B-3

STABILITY DERIVATIVES AND TRANSFER FUNCTION FACTORS
(BUSINESS JET, LANDING)

GEOMETRY:

VT		GAMMA		
211.1		-3.000		
R	RHO	MACH	XIO	ZJ
1116.5	.002377	.18910	8.071	-1.4979
S	C	WEIGHT	IY	ALTITUDE
231.8	7.040	12500.	18701.	0.0

NON-DIMENSIONAL DERIVATIVES:

CL	CLA	CLAD	CLM	
1.0001	4.552	1.7600	0.0	
CMA	CMAD	CMQ	CMM	
-.9969	-4.800	-12.000	0.0	
CD	CDA	CDM	TM	TDTH
.17109	.6165	0.0	0.0	59.00
CDDE	CLDE	CMDE		
0.0	.4406	-1.0886		

DIMENSIONAL DERIVATIVES:

XU	XU *	XW	TU
-.05122	-.05122	.05742	0.0
ZU	ZU *	ZWD	ZW
-.2994	-.2994	-.004393	-.7070
MU	MU *	MWD	MW
.0011081	.0011081	-.017521	-.02183
MAD	MA	MQ	
-.3699	-4.608	-.9248	
XDE	ZDE	MDE	
0.0	-13.924	-5.032	
XDTH	ZDTH	MDTH	
.15037	-.02132	-.004726	

DENOMINATOR: [.1215:.213 .0259:.211][.437:2.28 .998:2.05] <.236>

DE NUMERATORS:

N(U-DE) -.796(1.033)(-126.1) <103.7>

N(W-DE) -13.86(77.2)[.1365:.214 .0293:.212] <-49.2>

N(THE-DE) -5.01(.0820)(.616) <-.253>

N(DD-DE) 13.86(.00628)(-6.49)(7.50) <-4.24>

N(AD-DE) -13.86(-6.54)(7.54)[.297:.0250 .00742:.0239] <.426>

N(HD-DE) 13.84(.01422)(-6.52)(7.52) <-9.66>

125.KT 2.07DEG 24.76% A/C=LEA

DTH NUMERATORS:

N(U-DTH) .1504(.1145)[.395:2.38 .937:2.18] <.0971>

N(W-DTH) -.0212(49.8)[.1478:.209 .0309:.207] <-.0462>

N(THE-DTH) -.00469(-.222)(.832) <.000867>

N(DD-DTH) .0212(-.457)(-3.35)(7.06) <.229>

N(AD-DTH) -.0212(.00641)(-.446)(-3.39)(7.09) <-.001461>

N(HD-DTH) .0133(-.400)(-4.64)(9.04) <.224>

TABLE B-3 (Continued)

```
DE /DTH COUPLING NUMERATORS:

    N(U-DE/W-DTH)   2.08(-.000363)(77.2) (-.0584)

  N(U-DE/THE-DTH)    .753(.644) (.485)

   N(U-DE/DD-DTH)  -2.08(-6.54)(7.50) (102.4)

   N(U-DE/AZ-DTH)   2.08(.00788)(-6.59)(7.54) (-.817)

   N(U-DE/HD-DTH)  -2.08(-6.54)(7.50) (102.2)

  N(W-DE/THE-DTH)  -.0413(5.57) (-.230)

   N(W-DE/DD-DTH)  -8.72(5.57) (-48.6)

   N(W-DE/AZ-DTH)   8.72(.00798)(5.57) (.388)

   N(W-DE/HD-DTH)   .1091(19.83)(-22.4) (-48.5)

 N(THE-DE/DD-DTH)  -.0413(5.57) (-.230)

 N(THE-DE/AZ-DTH)   .0413(0.0)(5.57) (.230)

 N(THE-DE/HD-DTH)  -.001832(111.5) (-.204)

  N(DD-DE/AZ-DTH)  -.0696(5.57) (-.388)

  N(DD-DE/HD-DTH)  -.1091(-6.54)(7.50) (5.36)

  N(AZ-DE/HD-DTH)   .1091(-.0644)(-6.51)(7.53) (.344)


UG  NUMERATORS:

          N(U-UG)   .0512(.919)[.315:2.24  .706:2.13] (.236)

          N(W-UG)   .298(-.871E-7)(-.0350)(.1784) (.1703E-9)

        N(THE-UG)  -.001630(0.0)(4.47) (-.00729)

         N(DD-UG)  -.298(.261E-7)[.286:2.27  .649:2.18] (.927E-9)

         N(AZ-UG)   .298(.611E-6)(.00799)[.284:2.27  .645:2.18]
                        (.1811E-11)

         N(HD-UG)  -.300(.00798)[.286:2.27  .650:2.18] (-.01236)

125.KT  2.07DEG 24.76% A/C=LEA

 WG  NUMERATORS:

          N(U-WG)  -.0572(.233E-7)[.0566:3.24  .1834:3.23]
                        (-.475E-8)

          N(W-WG)   .00437[.1236:.212  .0262:.210]
                        [.513:34.7  17.78:29.7] (.236)

        N(THE-WG)  -.00264(.536E-6)(.0438)(-7.07) (.724E-11)

         N(DD-WG)  -.00437(1.929)(160.9)[-.01266:.417  -.00529:.417]
                        -.236)

         N(AZ-WG)   .712(-.1863E-7)(1.934)
                        [-.0177:.413  -.01555:.412] (-.290E-10)

         N(HD-WG)  -.00437(1.958)(160.2)[-.0385:.415  -.01598:.415]
                        (-.236
```

TABLE B-3 (Continued)

DE /UG COUPLING NUMERATORS:

N(U-DE/W-UG) .710(.907)(76.3) <49.2>

N(U-DE/THE-UG) .256(.986) <.253>

N(U-DE/DD-UG) -.710(-2.01)(2.97) <4.24>

N(U-DE/AZ-UG) .710(.0902)(-2.18)(3.05) <-.426>

N(U-DE/HD-UG) -.709(-2.01)(2.97) <4.23>

N(W-DE/THE-UG) 1.515(0.0) <1.515>

N(W-DE/DD-UG) 320.(.1449E-9) <.464E-7>

N(W-DE/AZ-UG) -320.(.289E-9)(.00798) <-.739E-9>

N(W-DE/HD-UG) .0372(.00798)(8670.) <2.57>

N(THE-DE/DD-UG) 1.515(-.861E-10) <-.1304E-9>

N(THE-DE/AZ-UG) -1.515(0.0)(-.861E-10) <.1304E-9>

N(THE-DE/HD-UG) 1.527(.00867) <.01324>

N(DD-DE/AZ-UG) 2.55(.289E-9) <.739E-9>

N(DD-DE/HD-UG) -.0372(-2.01)(2.97) <.222>

N(AZ-DE/HD-UG) .0372(.00798)(-8.21)(9.16) <-.0223>

DE /WG COUPLING NUMERATORS:

N(U-DE/W-WG) -.796(-1.701)(76.6) <103.7>

N(U-DE/THE-WG) -.284(-.162E-8) <.464E-9>

N(U-DE/DD-WG) .796(11.16)(-11.67) <-103.7>

N(U-DE/AZ-WG) -.796(.611E-6)(11.19)(-11.70) <.232E-9>

N(U-DE/HD-WG) .795(11.16)(-11.67) <-103.5>

N(W-DE/THE-WG) .0584(.0781)(55.4) <.253>

N(W-DE/DD-WG) 12.34(.0781)(55.4) <53.4>

N(W-DE/AZ-WG) -12.34(.00797)(.0781)(55.4) <-.426>

N(W-DE/HD-WG) 12.28(.0865)(55.3) <58.7>

N(THE-DE/DD-WG) .0584(.0781)(55.4) <.253>

N(THE-DE/AZ-WG) -.0584(0.0)(.0781)(55.4) <-.253>

N(THE-DE/HD-WG) .0584(.0785)(55.1) <.253>

N(DD-DE/AZ-WG) .0985(.0781)(55.4) <.426>

N(DD-DE/HD-WG) .0417(11.16)(-11.67) <-5.4>

N(AZ-DE/HD-WG) -.0417(2.97)[-.301:1.856 -.559:1.770] <-.426>

TABLE B-3 (Concluded)

DTH/UG COUPLING NUMERATORS:

N(U-DTH/W-UG) .0459[.63:1.003 .635:.776] <.0462>

N(U-DTH/THE-UG) -.499E-5(173.8) <-.000867>

N(U-DTH/DD-UG) -.0459[.289:2.23 .647:2.14] <-.229>

N(U-DTH/AZ-UG) .0459(.00638)[.288:2.23 .643:2.14] <.001461>

N(U-DTH/HD-UG) -.0459[.289:2.23 .647:2.14] <-.229>

N(W-DTH/THE-UG) .001432(-.632E-9) <-.906E-12>

N(W-DTH/DD-UG) .302(.388E-9) <.1159E-9>

N(W-DTH/AZ-UG) -.302(0.0)(.00798) <-.00241>

N(W-DTH/HD-UG) .00240(.00793)(126.9) <.00242>

N(THE-DTH/DD-UG) .001432(0.0) <.001432>

N(THE-DTH/AZ-UG) -.001432(0.0)(0.0) <-.001432>

N(THE-DTH/HD-UG) .001430(-.0317) <-.454E-4>

N(DD-DTH/AZ-UG) .00241(.375E-9) <.906E-12>

N(DD-DTH/HD-UG) -.00240[.289:2.23 .647:2.14] <-.01200>

N(AZ-DTH/HD-UG) .00240(.00800)[.322:1.99 .643:1.888] <.765E-4>

DTH/WG COUPLING NUMERATORS:

N(U-DTH/W-WG) .000658(.1333)[.504:33.3 16.78:28.7] <.0971>

N(U-DTH/THE-WG) -.000396(0.0)(-6.41) <.00254>

N(U-DTH/DD-WG) -.000658(159.1)[.966:.964 .930:.250] <-.0971>

N(U-DTH/AZ-WG) .000658(-.000609)(159.1)[.991:.943 .934:.1266] <.580E-10>

N(U-DTH/HD-WG) -.000657(159.1)[.966:.964 .930:.250] <-.0970>

N(W-DTH/THE-WG) .765E-4(-.288)(39.3) <-.000867>

N(W-DTH/DD-WG) .01614(-.288)(39.3) <-.1830>

N(W-DTH/AZ-WG) -.01614(.00799)(-.288)(39.3) <.001461>

N(W-DTH/HD-WG) .344E-4(-.264)(42.5)(460.) <-.1776>

N(THE-DTH/DD-WG) .765E-4(-.288)(39.3) <-.000867>

N(THE-DTH/AZ-WG) -.765E-4(0.0)(-.288)(39.3) <.000867>

N(THE-DTH/HD-WG) .556E-4(-.277)(56.3) <-.000866>

N(DD-DTH/AZ-WG) .0001289(-.288)(39.3) <-.001461>

N(DD-DTH/HD-WG) -.344E-4(159.1)[.966:.964 .930:.250] <-.00508>

N(AZ-DTH/HD-WG) .344E-4(1.937)(159.1)[-.1176:.371 -.0436:.368] <.001459>

TABLE B-4

STABILITY DERIVATIVES AND TRANSFER FUNCTION FACTORS
(STOL COMMUTER, LANDING)

GEOMETRY:

VT		GAMMA		
118.23		-5.998		
A	RHO	MACH	XIO	ZJ
1116.5	.002377	.10590	45.20	-2.043
S	C	WEIGHT	IY	ALTITUDE
420.0	6.500	11001.	23470.	0.0

NON-DIMENSIONAL DERIVATIVES:

CL	CLA	CLAD	CLM	
1.5604	5.251	-8.180	0.0	
CMA	CMAD	CMQ	CMM	
-1.4861	-6.060	-32.84	0.0	
CD	CDA	CDM	TM	TDTH
.17212	.4984	0.0	-8320.	42.07
CDDE	CLDE	CMDE		
0.0	.4870	-1.8219		

DIMENSIONAL DERIVATIVES:

XU	XU *	XW	TU
-.05942	-.07478	.18831	-.02180
ZU	ZU *	ZWD	ZW
-.5387	-.5232	.03881	-.9361
MU	MU *	MWD	MW
.00010586	.0007546	-.002722	-.02429
MAD	MA	MQ	
-.3219	-2.871	-1.7443	
XDE	ZDE	MDE	
0.0	-9.939	-3.520	
XDTH	ZDTH	MDTH	
.08670	-.08731	-.003662	

DENOMINATOR: [.1271±.311 .0395±.308][.704±2.16 1.524±1.537]
<.453>

DE NUMERATORS:

N(U-DE) -1.895(2.88)(-18.25) <99.5>

N(W-DE) -10.34(43.6)[.1329±.372 .0495±.369] <-62.5>

N(THE-DE) -3.49(.222)(.763) <-.590>

N(DD-DE) 10.34(.0201)(-4.33)(8.07) <-7.25>

N(AZ-DE) -10.34(-4.44)(8.15)[.349±.0728 .0254±.0683]
<1.986>

N(HD-DE) 10.28(.0485)(-4.36)(8.10) <-17.61>

DTH NUMERATORS:

N(U-DTH) .0867(.1299)[.657±2.08 1.366±1.565] <.0486>

N(W-DTH) -.0908(7.11)[.297±.322 .0954±.307] <-.0668>

N(THE-DTH) -.00342(-.299)(.715) <.000730>

N(DD-DTH) .0908(3.15)[-.201±.732 -.1472±.717] <.1531>

N(AZ-DTH) -.0908(.01647)(.18)[-.237±.719 -.1701±.699]
-.00246

N(HD-DTH) .0813(3.31)[-.307±.740 -.227±.704] <.1472>

TABLE B-4 (Continued)

DE /DTH COUPLING NUMERATORS:

N(U-DE/W-DTH) .896(-.203)(43.8) <-7.96>

N(U-DE/THE-DTH) .30?(.739) <.224>

N(U-DE/DD-DTH) -.896(-4.62)(8.31) <34.4>

N(U-DE/AZ-DTH) .896(.0212)(-4.72)(8.39) <-.753>

N(U-DE/HD-DTH) -.892(-4.62)(8.31) <34.2>

N(W-DE/THE-DTH) -.282(.667) <-.1879>

N(W-DE/DD-DTH) -33.3(.667) <-22.2>

N(W-DE/AZ-DTH) 33.3(.0285)(.667) <.632>

N(W-DE/HD-DTH) .0937(.787)(-311.) <-22.9>

N(THE-DE/DD-DTH) -.282(.667) <-.1879>

N(THE-DE/AZ-DTH) .282(0.0)(.667) <.1879>

N(THE-DE/HD-DTH) -.249(.657) <-.1635>

N(DD-DE/AZ-DTH) -.948(.667) <-.632>

N(DD-DE/HD-DTH) -.0937(-4.62)(8.31) <3.60>

N(AZ-DE/HD-DTH) .0937(-.205)(-3.75)(7.65) <.550>

UG NUMERATORS:

N(U-UG) .0748(2.04)[.681?1.722 1.172?1.261] <.453>

N(W-UG) .544(-.283E-6)(-.00308)(1.577) <.587E-10>

N(THE-UG) -.00224(0.0)(6.24) <-.01396>

N(DD-UG) -.544(-.745E-8)[.592?1.740 1.030?1.402] <-.575E-9>

N(AZ-UG) .544(.671E-7)(.0289)[.588?1.727 1.015?1.397] <-.454E-10>

N(HD-UG) -.549(.0284)[.592?1.742 1.032?1.403] <-.0473>

WG NUMERATORS:

N(U-WG) -.1907(-.373E-8)[.542?1.371 .743?1.152] <-.1211E-9>

N(W-WG) -.0404(-5.86)(20.1)[.1477?.309 .0456?.305] <.453>

N(THE-WG) -.01192(0.0)(-.0896)(-.750) <-.000801>

N(DD-WG) .0404(3.52)(-24.2)[.1457?.363 .0529?.359] <-.453>

N(AZ-WG) .830(0.0)(4.19)[.1315?.362 .0476?.359] <.455>

N(HD-WG) .0402(3.57)(-23.7)[.1318?.364 .0480?.361] <-.450>

TABLE B-4 (Continued)

DE /UG COUPLING NUMERATORS:

N(U-DE/W-UG) .773(1.940)(41.7) (62.5)

N(U-DE/THE-UG) .261(2.26) (.590)

N(U-DE/DD-UG) -.773(-1.730)(5.42) (7.25)

N(U-DE/AZ-UG) .773(.227)(-2.05)(5.51) (-1.986)

N(U-DE/HD-UG) -.769(-1.730)(5.42) (7.21)

N(W-DE/THE-UG) 1.924(0.0) (1.924)

N(W-DE/DD-UG) 227.(-.1619E-9) (-.368E-7)

N(W-DE/AZ-UG) -227.(.489E-9)(.0285) (-.316E-8)

N(W-DE/HD-UG) .0808(.0284)(2840.) (6.53)

N(THE-DE/DD-UG) 1.924(.622E-9) (.1196E-8)

N(THE-DE/AZ-UG) -1.924(0.0)(.622E-9) (-.1196E-8)

N(THE-DE/HD-UG) 1.941(.0318) (.0617)

N(DD-DE/AZ-UG) 6.47(-.709E-9) (-.459E-8)

N(DD-DE/HD-UG) -.0808(-1.730)(5.42) (.758)

N(AZ-DE/HD-UG) .0808(.0284)(-7.85)(11.51) (-.208)

DE /WG COUPLING NUMERATORS:

N(U-DE/W-WG) -1.895(-1.164)(45.1) (99.5)

N(U-DE/THE-WG) -.643(0.0) (-.643)

N(U-DE/DD-WG) 1.895(-5.59)(9.38) (-99.5)

N(U-DE/AZ-WG) -1.895(.611E-6)(-5.67)(9.46) (.213E-7)

N(U-DE/HD-WG) 1.885(-5.59)(9.38) (-98.9)

N(W-DE/THE-WG) -.01776(.1857)(-179.1) (.590)

N(W-DE/DD-WG) -2.10(.1857)(-179.1) (69.8)

N(W-DE/AZ-WG) 2.10(.0282)(.1859)(-179.1) (-1.986)

N(W-DE/HD-WG) -2.29(.218)(-159.8) (79.8)

N(THE-DE/DD-WG) -.01776(.1857)(-179.1) (.590)

N(THE-DE/AZ-WG) .01776(0.0)(.1857)(-179.1) (-.590)

N(THE-DE/HD-WG) -.01766(.1897)(-175.3) (.587)

N(DD-DE/AZ-WG) -.0597(.1857)(-179.1) (1.986)

N(DD-DE/HD-WG) .1980(-5.59)(9.38) (-10.40)

N(AZ-DE/HD-WG) -.1980(4.08)[-.1894:1.563 -.296:1.535] (-1.975)

TABLE B-4 (Concluded)

DTH/UG COUPLING NUMERATORS:

N(U-DTH/W-UG) .0540[.998;1.112 1.110;.0744] <.0668>

N(U-DTH/THE-UG) .615E-4(-11.88) <-.000730>

N(U-DTH/DD-UG) -.0540[.619;1.684 1.042;1.323] <-.1531>

N(U-DTH/AZ-UG) .0540(.01626)[.618;1.673 1.034;1.315] <.00246>

N(U-DTH/HD-UG) -.0537[.619;1.684 1.042;1.323] <-.1523>

N(W-DTH/THE-UG) .00206(0.0) <.00206>

N(W-DTH/DD-UG) .244(.994E-9) <.242E-9>

N(W-DTH/AZ-UG) -.244(.546E-9)(.0285) <-.379E-11>

N(W-DTH/HD-UG) .00564(.0274)(45.2) <.00698>

N(THE-DTH/DD-UG) .00206(.459E-9) <.946E-12>

N(THE-DTH/AZ-UG) -.00206(0.0)(.459E-9) <-.946E-12>

N(THE-DTH/HD-UG) .00206(-.0371) <-.763E-4>

N(DD-DTH/AZ-UG) .00694(-.273E-9) <-.1893E-11>

N(DD-DTH/HD-UG) -.00564[.619;1.684 1.042;1.323] <-.01600>

N(AZ-DTH/HD-UG) .00564(.0294)[.826;1.244 1.028;.702] <.000257>

DTH/W6 COUPLING NUMERATORS:

N(U-DTH/W-WG) -.00350(.1468)(-4.11)(23.0) <.0486>

N(U-DTH/THE-WG) -.001034(.615E-7)(-.476) <.303E-10>

N(U-DTH/DD-WG) .00350(.1926)(3.65)(-19.72) <-.0486>

N(U-DTH/AZ-WG) -.00350(0.0)(.1832)(3.70)(-19.76) <.0469>

N(U-DTH/HD-WG) .00348(.1926)(3.65)(-19.72) <-.0483>

N(W-DTH/THE-WG) .000945(-.317)(2.44) <-.000730>

N(W-DTH/DD-WG) .1117(-.317)(2.44) <-.0863>

N(W-DTH/AZ-WG) -.1117(.0285)(-.317)(2.44) <.00246>

N(W-DTH/HD-WG) -.000366(-.272)(2.83)(-287.) <-.0808>

N(THE-DTH/DD-WG) .000945(-.317)(2.44) <-.000730>

N(THE-DTH/AZ-WG) -.000945(0.0)(-.317)(2.44) <.000730>

N(THE-DTH/HD-WG) .000832(-.315)(2.77) <-.000726>

N(DD-DTH/AZ-WG) .00318(-.317)(2.44) <-.00246>

N(DD-DTH/HD-WG) .000766(.1926)(3.65)(-19.72) <-.00508>

N(AZ-DTH/HD-WG) -.00036(3.57)(-19.35)[-.1497;.311 -.0465;.307] <.00244>

TABLE B-5. STABILITY DERIVATIVES (JUMBO, TAKEOFF)

GEOMETRY:

VT		GAMMA		
315.8		7.025		
A	RHO	MACH	XIO	ZJ
1116.5	.002377	.2829	10.093	9.991
S	C	WEIGHT	IY	ALTITUDE
5500.	27.31	733000.	.3520E+8	0.0

NON-DIMENSIONAL DERIVATIVES:

CL	CLA	CLAD	CLM	
1.0757	5.295	-6.700	0.0	
CMA	CMAD	CMQ	CMM	
-1.3436	-3.170	-20.50	0.0	
CD	CDA	CDM	TM	TDTH
.08712	.6812	0.0	-80000.	187720.
CDDE	CLDE	CMDE		
0.0	.3254	-1.2834		

DIMENSIONAL DERIVATIVES:

XU	XU ◆	XW	TU
-.015789	-.018885	.03575	-.003145
ZU	ZU ◆	ZWD	ZW
-.19496	-.19440	.02625	-.4877
MU	MU ◆	MWD	MW
-.0002675	-.0002878	-.0002195	-.002152
MAD	MA	MQ	
-.06933	-.6797	-.4484	
XDE	ZDE	MDE	
0.0	-9.314	-.6493	
XDTH	ZDTH	MDTH	
8.112	-1.4439	.05328	

TABLE B-6. STABILITY DERIVATIVES (LIGHT TRANSPORT, TAKEOFF)

GEOMETRY:

VT		GAMMA		
271.9		7.899		
A	RHO	MACH	XIO	ZJ
1116.5	.002377	.2436	8.928	4.999
S	C	WEIGHT	IY	ALTITUDE
980.0	11.200	110010.	875100.	0.0

NON-DIMENSIONAL DERIVATIVES:

CL	CLA	CLAD	CLM	
1.2241	6.427	-8.000	0.0	
CMA	CMAD	CMQ	CMM	
-.9218	-2.400	-24.90	0.0	
CD	CDA	CDM	TM	TDTH
.08529	.5668	0.0	-7750.	21720.
CDDE	CLDE	CMDE		
0.0	.4526	-1.6214		

DIMENSIONAL DERIVATIVES:

XU	XU ◆	XW	TU
-.015801	-.017806	.06089	-.002030
ZU	ZU ◆	ZWD	ZW
-.2268	-.2265	.015262	-.6038
MU	MU ◆	MWD	MW
-.0009560	-.0009957	-.0002004	-.003737
MAD	MA	MQ	
-.05449	-1.0162	-.5653	
XDE	ZDE	MDE	
0.0	-11.402	-1.7874	
XDTH	ZDTH	MDTH	
6.275	-.9859	.12408	

TABLE B-7. STABILITY DERIVATIVES (BUSINESS JET, TAKEOFF)

GEOMETRY:

VT		GAMMA		
228.0		15.896		
A	RHO	MACH	XID	ZJ
1116.5	.002377	2042	7.932	-1.5179
S	C	WEIGHT	IY	ALTITUDE
231.8	7.040	12500.	18701.	0.0

NON-DIMENSIONAL DERIVATIVES:

CL	CLA	CLAD	CLM	
.7939	4.647	1.7600	0.0	
CMA	CMAD	CMQ	CMM	
-1.0313	-4.800	-12.000	0.0	
CD	CDA	CDM	TM	TDTH
.09739	.5156	0.0	0.0	59.00
CDDE	CLDE	CMDE		
0.0	.4406	-1.0886		

DIMENSIONAL DERIVATIVES:

XU	XU ◆	XW	TU
-.02826	-.02826	.04499	0.0
ZU	ZU ◆	ZWD	ZW
-.2567	-.2567	-.004393	-.7654
MU	MU ◆	MWD	MW
.003363	.003363.	-.0017521	-.02438
MAD	MA	MQ	
-.3995	-5.560	-.9987	
XDE	ZDE	MDE	
0.0	-16.241	-5.869	
XDTH	ZDTH	MDTH	
.15042	-.02096	-.004789	

TABLE B-8. STABILITY DERIVATIVES (STOL COMMUTER, TAKEOFF)

GEOMETRY:

VT		GAMMA		
131.74		9.268		
A	RHO	MACH	XIO	ZJ
1116.5	.002377	.11800	32.60	0.0
S	C	WEIGHT	IY	ALTITUDE
420.0	6.500	11580.	24000.	0.0

NON-DIMENSIONAL DERIVATIVES:

CL	CLA	CLAD	CLM	
1.1146	7.921	2.820	0.0	
CMA	CMAD	CMQ	CMM	
-.6961	-11.140	-23.95	0.0	
CD	CDA	CDM	TM	TDTH
.10440	.7305	0.0	-12516.	20.72
CDDE	CLDE	CMDE		
0.0	.4526	-1.7761		

DIMENSIONAL DERIVATIVES:

XU	XU ◆	XW	TU
-.03815	-.06439	.07018	-.03115
ZU	ZU ◆	ZWD	ZW
-.4073	-.3905	-.012712	-1.4664
MU	MU ◆	MWD	MW
0.0	0.0	-.004895	-.012398
MAD	MA	MQ	
-.6448	-1.6332	-1.3861	
XDE	ZDE	MDE	
0.0	-10.895	-4.167	
XDTH	ZDTH	MDTH	
.04849	-.03101	0.0	

APPENDIX C

DERIVATION OF SIMPLIFIED PILOT-VEHICLE DYNAMICS

This appendix develops a simplified description of airspeed-flight path dynamics useful for analyzing wind shear effects. The ultimate objective is to directly express airspeed and flight path excursions for the closed loop pilot-vehicle in terms of essential parameters, i.e., aircraft stability derivatives and pilot crossover frequencies (loop tightness). The general form is set up for both CTOL and STOL piloting techniques, but only the CTOL case is fully developed. The STOL case would follow in the same manner, however.

The approximate pitch-constrained equations of motion, without flight path or airspeed regulation, are:

$$\begin{bmatrix} s - X_u & X_w s \\ Z_u & s(s - Z_w) \end{bmatrix} \begin{bmatrix} u_a \\ \Delta h \end{bmatrix} = \begin{bmatrix} (X_\alpha - g) & X_{\delta_T} & -s & -X_w \\ -Z_\alpha & -Z_{\delta_T} & 0 & Z_w \end{bmatrix} \begin{bmatrix} \theta \\ \delta_T \\ u_g \\ w_g \end{bmatrix}$$

The elements of the pilot model are:

$$\left.\begin{aligned} \delta_T &= -K_u u_a \\ \theta &= -K_d \Delta h \end{aligned}\right\} \text{CTOL}$$

or

$$\left.\begin{aligned} \delta_T &= -K_d \Delta h \\ \theta &= -K_u u_a \end{aligned}\right\} \text{STOL}$$

Considering the CTOL case as an example and substituting the above pilot model into the pitch constrained equations:

$$\begin{bmatrix} \left[s - X_u + K_u X_{\delta_T}\right] & \left[X_w s + K_d (X_\alpha - g)\right] \\ (Z_u - K_u \cancel{Z_{\delta_T}}) & \left[s - Z_w s - K_d Z_\alpha\right] \end{bmatrix} \begin{matrix} u_a \\ \Delta h \end{matrix} = \begin{bmatrix} s & -X_w \\ 0 & Z_w \end{bmatrix} \begin{matrix} u_g \\ w_h \end{matrix}$$

(small)

The airspeed and altitude-due-to-gust transfer functions are easily obtained by substituting appropriate columns in the matrices and solving for determinants (see Ref. 25 for details). For example, in the case of altitude, pilot gains are set according to an airspeed loop tightness (crossover frequency, ω_{c_u}) and flight path loop tightness (crossover frequency, ω_{c_d}). A good first order approximation is

$$-K_d Z_\alpha \doteq \omega_{c_d}$$

and

$$K_u X_{\delta_T} \doteq \omega_{c_u}$$

Therefore, the equations of motion are approximately;

$$\begin{bmatrix} (s - X_u + \omega_{c_u}) & \left[X_w s - \dfrac{\omega_{c_d}^2 (X_\alpha - g)}{Z_\alpha}\right] \\ Z_u & s^2 - Z_w s + \omega_{c_d}^2 \end{bmatrix} \begin{bmatrix} u_a \\ \Delta h \end{bmatrix} = \begin{bmatrix} -s & -X_w \\ 0 & Z_w \end{bmatrix} \begin{bmatrix} u_g \\ w_g \end{bmatrix}$$

The characteristic determinant of the above equations of motion will factor into a dominant airspeed mode, $1/T_u$, and an oscillatory dominant flight path mode characterized by a damping ratio ζ_d and natural frequency ω_d. A good approximation for the speed mode of CTOL aircraft appears to be:

$$\frac{1}{T_u} \doteq \omega_{c_u}$$

This permits an approximate solution of the flight path mode.

To summarize,

$$\frac{\Delta h}{u_g} \doteq \frac{Z_u s}{(s + \frac{1}{T_u})(s^2 + 2\zeta_d \omega_d s + \omega_d^2)}$$

$$\frac{\Delta h}{w_g} \doteq \frac{Z_w (s + \frac{1}{T_u} - X_u + \frac{X_w}{Z_w} Z_u)}{(s + \frac{1}{T_u})(s^2 + 2\zeta_d \omega_d s + \omega_d^2)}$$

which reduces to $$\frac{\Delta h}{w_g} \doteq \frac{Z_w}{(s^2 + 2\zeta_d\omega_d s + \omega_d^2)}$$

if $$X_u Z_w \doteq X_w Z_u$$

$$\left(\text{i.e., } \frac{C_L}{C_D} = \frac{2C_{L_\alpha}}{C_{D_\alpha} - C_L}\right)$$

where $$\frac{1}{T_u} = \omega_{c_u}$$

$$\omega_d^2 \doteq \left[1 + \frac{Z_u(X_\alpha - g)}{\omega_{c_u} Z_\alpha}\right] \omega_{c_d}^2$$

and $$2\zeta_d\omega_d \doteq -X_u - Z_u$$